A Thesis

For the Degree of Doctor of Philosophy

Anti-diabetic and Anti-obesity effects of Flavonoids in Premature citrus extract

GRADUATE SCHOOL
JEJU NATIONAL UNIVERSITY

College of Veterinary Medicine

Priyanka Rajan

August 2022

Anti-diabetic and Anti-obesity effects of Flavonoids in Premature citrus extract

Priyanka Rajan

(Supervised by Professor Chang-Hoon Han)

A thesis submitted in partial fulfillment of the requirement for the degree of

Doctor of Philosophy

2022. 08.

This thesis has been examined and approved by

……

Thesis Director, Professor Young Jae Lee
College of Veterinary Medicine, Jeju National University

……

Professor Jae Hoon Kim
College of Applied Life Science, Jeju National University

……..

Professor Se Jae Kim
College of Natural Science, Jeju National University

……..

Professor Chang-Hwan Ahn
College of Veterinary Medicine, Jeju National University

……

Professor Chang-Hoon Han
College of Veterinary Medicine, Jeju National University

College of Veterinary Medicine

GRADUATE SCHOOL

JEJU NATIONAL UNIVERSITY

Table of Contents

List of Tables

List of Figures

List of Abbreviations

2-NBDG	2-[N-(7-Nitrobenz-2-oxa-1,3-diazol-4-yl)amino]-2-deoxy-d-glucose
ACAT	Acyl-coenzyme A:cholesterol acyltransferase
ACC	Acetyl-CoA carboxylase
ADP	Adenosine Diphosphate
AID	Auto inhibitory domain
ALP	Alkaline phosphatase
ALT	Alanine aminotransferase
AMP	Adenosine monophosphate
AMPK	5′-Adenosine monophosphate-activated protein kinase
ANOVA	One-way analysis of variance
ATP	Adenosine triphosphate
AUC	Area under the curve
BSA	Bovine serum albumin
BUN	Blood urea nitrogen
CaMKKβ	Calcium/calmodulin-dependent protein kinase kinase-β
CBM	Carbohydrate binding module
CBS	Cystathionine β-synthase domains
CON	Control
CTD	C-terminal domain
DMEM	Dulbecco’s modified Eagle’s medium
FA	Fatty acid
FASN	Fatty acid synthase
FBS	Fetal bovine serum

GLUT	Glucose transporter
GO	Gene ontology
GS	Glycogen synthase
GSK3β	Glycogen synthase kinase 3 beta
HDL-C	High density lipoprotein cholesterol
HES	Hesperidin
HFD	High-fat diet
HMGCR	3-Hydroxy-3-methyl-glutaryl-coenzyme A reductase
HMGCS	Hydroxymethylglutaryl-CoA synthase
HOMA-IR	Homeostatic model assessment for insulin resistance
IPGTT	Intraperitoneal glucose tolerance test
IPITT	Intraperitoneal insulin tolerance test
IRS	Insulin receptor substrate
LDL-C	Low density lipoprotein cholesterol
LKB1	Liver kinase B1
MET	Metformin
MTT	3-(4,5-Dimethylthiazol-2-yl)-2,5 diphenyl tetrazolium bromide
NAR	Narirutin
NO	Nitric oxide
NOB	Nobiletin
PA	Palmitate
PBS	Phosphate buffered saline
PCE	Premature citrus extract
PDB	Protein Data Bank
PDK1	3-Phosphoinositide-dependent protein kinase-1

PI3K	Phosphatidylinositol 3-kinase
PI3K/Akt	Phosphatidylinositol 3-kinase/protein kinase B
PIP2	Phosphatidylinositol-4,5-bisphosphate
PIP3	Phosphatidylinositol-3,4,5-triphosphate
PPI	Protein-protein interaction
SDS-PAGE	Sodium dodecyl sulphate-polyacrylamide gel electrophoresis
SE	Standard error
SIM	Simvastatin
SIN	Sinensetin
SREBP-2	Sterol regulatory element-binding protein 2
STRING	Search tool for the retrieval of interacting genes/proteins
T2DM	Type 2 diabetes mellitus
TAN	Tangeretin
TC	Total cholesterol
TG	Triglyceride

General Introduction

Obesity and Adipogenesis

Obesity is defined as the accumulation of excessive fat that contributes to the risk of developing insulin resistance, cardiovascular disease, and hyperlipidemia [1]. Adipogenesis is the process of lipid development in various tissues [2]. The liver is a pleiotropic endocrine organ that accesses nutrients and affects metabolism in both local and distal organs [3]. Previous studies have shown that hepatic fat content is the strongest predictor of insulin resistance and precedes the development of obesity [4].

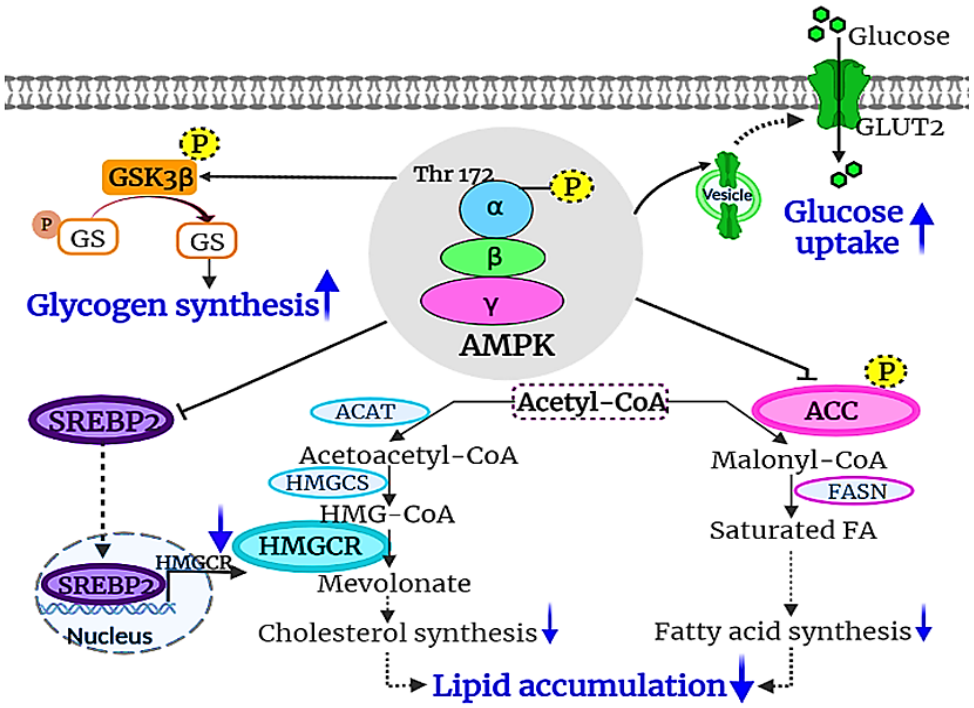

Fig. 1. Role of AMPK in the regulation of lipid and glucose homeostasis

AMPK activation modulates key molecules involved in the biosynthesis of fatty acids and cholesterol, glucose uptake, and glycogen synthesis. ACAT, acyl-coenzyme A:cholesterol acyltransferase; ACC, acetyl-CoA carboxylase; AMPK, 5′-adenosine monophosphate-activated protein kinase; GLUT2, glucose transporter 2; GS, glycogen synthase; GSK3β,

glycogen synthase kinase 3 beta; FA, fatty acid; FASN, fatty acid synthase; HMGCR, 3-hydroxy-3-methyl-glutaryl-coenzyme A reductase; HMGCS, hydroxymethylglutaryl-CoA synthase; PA, palmitate; SREBP-2, sterol regulatory element-binding protein 2.

5′-AMP-activated protein kinase (AMPK) plays a vital role in regulating adipogenesis (Fig. 1) [5]. AMPK activation regulates lipid homeostasis by enhancing the phosphorylation of acetyl-CoA carboxylase (ACC) and inhibiting sterol regulatory element-binding protein 2 (SREBP-2) and 3-hydroxy-3-methylglutaryl-coenzyme A reductase (HMGCR), which are the key proteins in fatty acid and cholesterol biosynthesis [6, 7]. In addition, AMPK activation regulates glucose homeostasis by stimulating glucose uptake and enhancing the phosphorylation of glycogen synthase kinase 3 beta (GSK3β), a key target involved in glycogen synthesis [8, 9].

Diabetes

Diabetes is one of the most common metabolic disorders and is often associated with hyperglycemia [10]. Type 2 diabetes is the most common type of diabetes and arises from an impaired insulin action (insulin resistance) [11]. Insulin resistance occurs when target tissues have reduced sensitivity to the action of insulin, leading to increased plasma glucose levels and decreased glucose utilization [12, 13].

Insulin binding to the insulin receptor promotes its auto phosphorylation, which is required for the amplification of the kinase activity (Fig. 2) [14]. The metabolic effects of insulin are mediated by the phosphorylation of insulin receptor substrate (IRS) proteins and the activation of phosphatidylinositol 3-kinase/protein kinase B (PI3K/Akt) pathways [15]. Akt activation facilitates glucose uptake by translocating glucose transporters [16]. In

addition, Akt is responsible for glycogen synthesis via phosphorylation of GSK3β, which consequently dephosphorylates and activates glycogen synthase [17]. Defects in the Akt pathway or downstream molecules can induce an imbalance in glucose metabolism, generating chronic hyperglycemia [18].

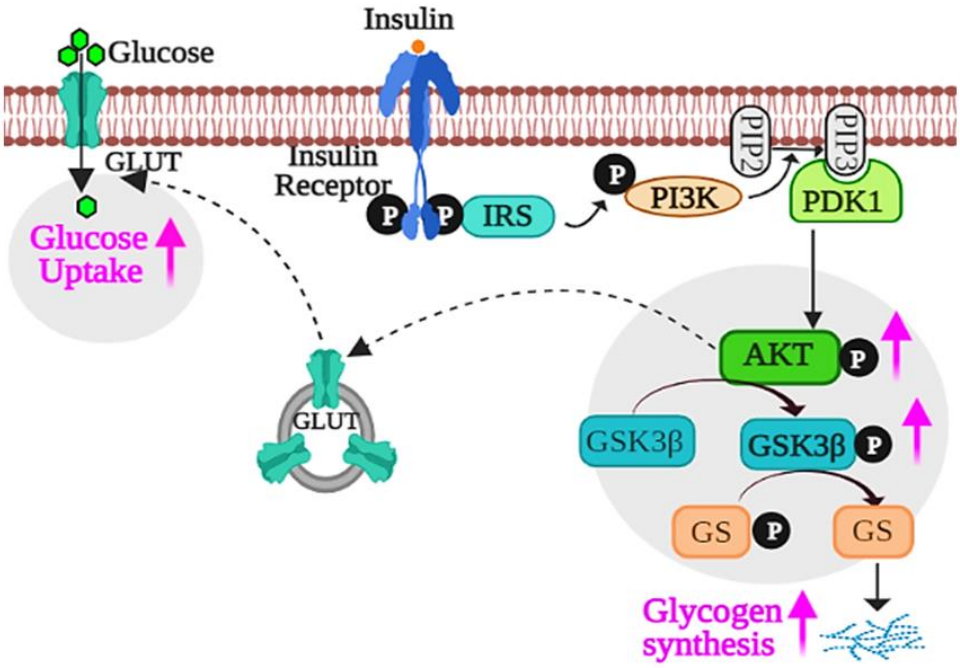

Fig. 2. Insulin signaling pathway

Insulin triggers signaling cascades that facilitate glucose uptake and glycogen synthesis. GLUT, glucose transporter; GS, glycogen synthase; GSK3β, glycogen synthase kinase 3 beta; IRS, insulin receptor substrate; PDK1, 3-phosphoinositide-dependent protein kinase-1; PI3K, phosphatidylinositol 3-kinase; PIP2, phosphatidylinositol-4,5-bisphosphate; PIP3, phosphatidylinositol-3,4,5-triphosphate.

Flavonoids

Flavonoids are a group of natural substances and belong to a class of secondary metabolites having a polyphenolic structure [19]. They are widely found in fruits, vegetables, and beverages [20]. Our previous study observed that premature citrus extract (PCE) is rich in hesperidin, narirutin, nobiletin, sinensetin, and tangeretin (Fig. 3) [21].

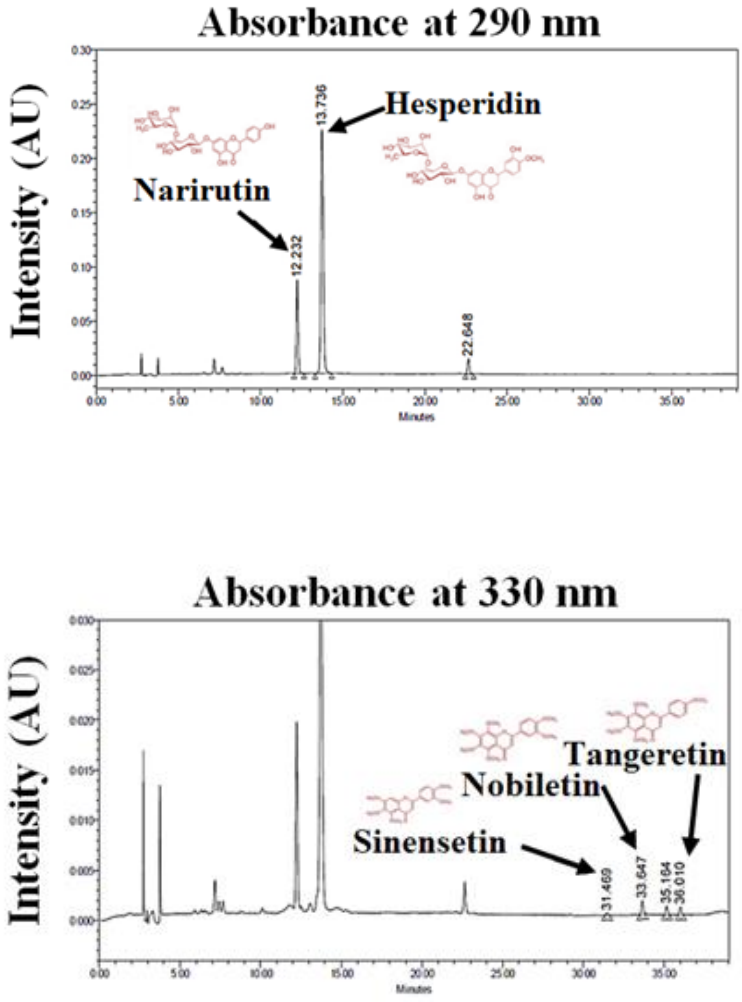

Fig. 3. Chromatogram of premature citrus extract (PCE)

Hesperidin

Hesperidin (HES) is a flavone glycoside, comprising of an aglycone, hesperetin bonded to rutinose (Fig. 4) [22]. It possess various pharmacological properties such as anti-inflammatory, anti-oxidative, anti-diabetic, and anti-obesity [23, 24]. Previous studies demonstrated that HES exhibited anti-diabetic effect by regulating glucose metabolism in diabetic mice and rats [25, 26]. In addition, HES is shown to possess anti-obesity effect by improving fatty acid and lipid metabolism in human and rat [27, 28].

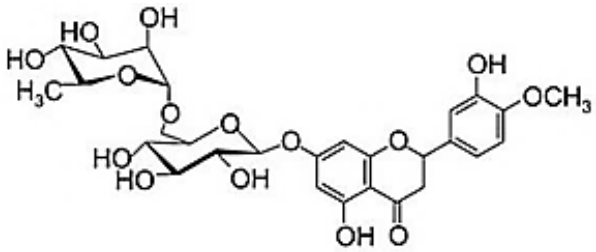

Fig. 4. Chemical structure of hesperidin (HES)

Narirutin

Narirutin (NAR) is a flavanone consisting of the flavanone naringenin bonded with the disaccharide rutinose (Fig. 5) [29]. It is shown to possess wide range of pharmacological activities such as anti-oxidative, anti-diabetic, and anti-obesity activity. An *in vitro* study observed that narirutin showed a potential anti-diabetic activity by inhibiting α-amylase and α-glucosidase [29]. Additionally, NAR showed anti-obesity effect by suppressing triglyceride and total cholesterol in the liver of mice [30].

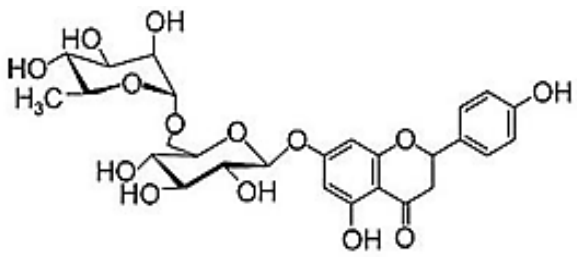

Fig. 5. Chemical structure of narirutin (NAR)

Nobiletin

Nobiletin (NOB) is a polymethoxylated flavone and has been shown to exhibit anti-inflammatory, anti-diabetic and anti-obesity properties (Fig. 6) [31]. A previous study revealed that NOB possess strong anti-diabetic effect by improving glucose tolerance and insulin resistance in high-fat diet-induced obese mice [32]. Furthermore, NOB is shown to have anti-obesity activity by decreasing body weight, fat mass, and total cholesterol in mice [33].

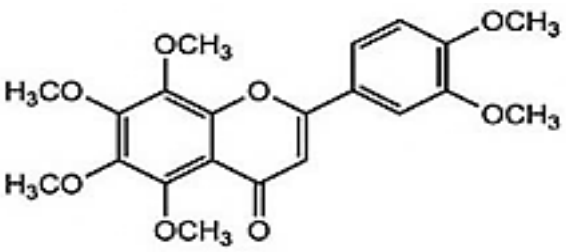

Fig. 6. Chemical structure of nobiletin (NOB)

Sinensetin

Sinensetin (SIN) is a polymethoxylated flavonoid and has been found to possess variety of pharmacological benefits such as anti-inflammatory, anti-obesity and anti-diabetic activity (Fig. 7) [34]. An *invitro* evidence demonstrated that inhibitory effect of SIN on α-amylase and α-glucosidase can be used as an effective strategy for alleviating post-prandial hyperglycemia linked to diabetes [35]. Moreover, SIN showed anti-obesity effect by enhancing lipolysis in adipocytes [36, 37].

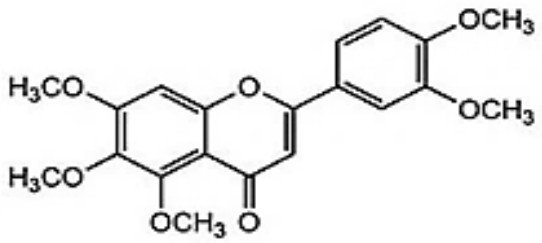

Fig. 7. Chemical structure of sinensetin (SIN)

Tangeretin

Tangeretin (TAN) is a polymethoxylated flavone and has been suggested to have several beneficial effects (Fig. 8) [38]. Previous studies showed that TAN possess anti-diabetic and anti- obesity effect by decreasing blood glucose and total cholesterol in diabetic rats and high-fat diet-induced obese mice, respectively [39]. In addition, TAN is able to enhance glycolytic enzymes, leading to control of glucose metabolism in the diabetic rats [40].

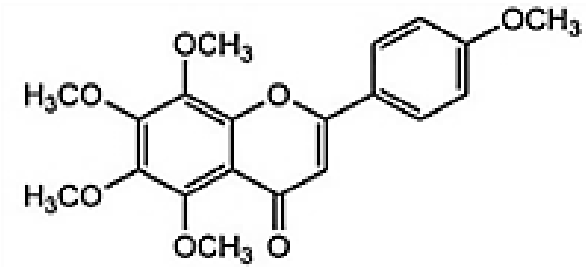

Fig. 8. Chemical structure of tangeretin (TAN)

Molecular docking

Molecular docking is a computational binding analysis that is used to model the interaction between a small molecule and a protein at the atomic level, which helps to characterize the behavior of small molecules in the binding site of target proteins [41]. Docking analysis helps in the prediction of the ligand conformation and assessment of the binding affinity [42]. It has become an increasingly important tool for structure-based drug discovery [43]. In the present study, molecular docking analysis was carried out to examine the binding affinities of the flavonoids to the γ-subunit of AMPK.

Differential gene expression

Differential gene expression analysis is one of the most common applications of RNA-sequencing data [44]. This process allows for the elucidation of the molecular mechanisms underlying biological pathways [45]. In general, diseased group shows a list of genes within a specific tissue that are up- or down-regulated when compared with healthy groups. Whereas, the drug-treated group show differentially expressed genes compared to the untreated group [46]. The main goal of differential gene expression analysis is to examine the connection between gene expression profiles of disease and drug treatment, which is a potentially beneficial drug discovery strategy to aid the treatment of metabolic diseases [46–48]. In the present study, differential gene expression analysis was performed to investigate the effect of flavonoid on expression of genes related to insulin signaling and glucose metabolism in high-fat diet (HFD)-induced obese mice which are yet to be elucidated.

Protein-protein interaction (PPI) networks

PPI networks present gene products that physically interact with each other to achieve particular cellular functions, such as metabolism, cell cycle control, and signal transduction [49]. PPI enable the understanding of pathogenic mechanisms that initiate the onset and progression of diseases and the development of therapeutic approaches. [50]. The genes that have many interactions with other genes are defined as hub genes and these hub genes are more likely to be involved in disease processes [51, 52]. In the present study, PPI network was constructed to elucidate the effect of flavonoid on the expression of hub genes related to insulin signaling and glucose metabolism in HFD-induced obese mice.

Hypothesis

The present study addresses three main research hypotheses:

(1) The five major citrus flavonoids exert anti-adipogenic effects by activating the AMPK pathway.

To test this hypothesis, the effect of flavonoids on lipid accumulation, triglyceride (TG) content, and glucose uptake were evaluated in palmitate (PA)-treated HepG2 cells. To elucidate the underlying molecular mechanisms, AMPK and its downstream substrates involved in lipid metabolism were analyzed. To assess the primary mechanism of action, *in silico* analysis was performed to investigate the AMPK-activating capacity of the flavonoids.

(2) HES exerts anti-diabetic effects by restoring the expression of genes related to insulin signaling and glucose metabolism in the liver.

To test this hypothesis, the effect of flavonoid on glucose uptake and key molecules involved in insulin signaling pathway were evaluated in PA-treated HepG2 cells. Furthermore, the effects of HES on glucose and insulin tolerance were evaluated in high-fat diet (HFD)-induced obese mice. To investigate the underlying molecular mechanisms, the differential gene expression in the liver was analyzed.

(3) The diet containing premature citrus extract possesses anti-obesity and anti-diabetic effects on beagle dogs.

To test this hypothesis, the effects of diet containing premature citrus extract on the levels of TG, cholesterol, and glucose were observed in the serum of beagle dogs. Furthermore, effect of premature citrus extract on functional parameters of liver, kidney, and pancreas were evaluated in the serum of beagle dogs.

Objectives

The present study aimed to investigate the anti-adipogenic and anti-diabetic effects of citrus flavonoids and the underlying molecular mechanisms by evaluating their AMPK-activating capacity and analyzing the differential gene expression related to insulin signaling and glucose metabolism. In addition, the present study investigated the anti-obesity and anti-diabetic effects of premature citrus extract by evaluating the serum parameters in beagle dogs.

The major objectives of this study were:

Objective 1: To investigate the anti-adipogenic effects of flavonoids and their molecular mechanisms on PA-treated HepG2 cells.

Objective 2: To evaluate the anti-diabetic effects of HES and its molecular mechanism of action on PA-treated HepG2 cells and HFD-induced obese mice.

Objective 3: To evaluate the anti-obesity and anti-diabetic effects of diet containing premature citrus extract on beagle dogs.

PART-I

Anti-adipogenic effect of the flavonoids through the activation of AMPK in palmitate (PA)-treated HepG2 cells

1.1. Abstract

Flavonoids are natural polyphenols widely found in citrus fruits and peel and known to possess anti-adipogenic effects. However, the detailed mechanisms for their anti-adipogenic effects remain to be fully elucidated. In the present study, we observed the anti-adipogenic effects of five major citrus flavonoids including hesperidin (HES), narirutin (NAR), nobiletin (NOB), sinensetin (SIN), and tangeretin (TAN) associated with AMPK activation in palmitate (PA)-treated HepG2 cells. Intracellular lipid accumulation and triglyceride (TG) content were quantified using Oil-Red O staining and a TG assay, respectively. Glucose uptake was assessed using a 2-[N-(7-Nitrobenz-2-oxa-1,3-diazol-4-yl)amino]-2-deoxy-d-glucose (2-NBDG) assay. The phosphorylation levels of AMPK, ACC, and GSK3β, as well as the expression levels of SREBP-2 and HMGCR were analyzed using Western blot analysis. The potential interactions between the flavonoids and the γ-subunit of AMPK were investigated using molecular docking. Flavonoid treatment significantly reduced intracellular lipid accumulation and TG content, increased glucose uptake in an insulin-independent manner, increased the phosphorylation levels of AMPK, ACC, and GSK3β, and decreased the expression levels of SREBP-2 and HMGCR in PA-treated HepG2 cells. Molecular docking analysis revealed that the flavonoids bind to CBS domains of the regulatory γ-subunit of AMPK with high binding affinities, and may act as potential AMPK activators. Overall results suggest that the anti-adipogenic effect of flavonoids on PA-treated HepG2 cells results from the activation of AMPK.

Keywords: Anti-adipogenesis, flavonoids, AMPK, molecular docking, HepG2 cells

1.2. Introduction

AMP-activated protein kinase (AMPK) plays a vital role in controlling and regulating adipogenesis, suggesting that its activation may be a promising target for anti-adipogenic therapies [5]. AMPK is a crucial energy sensor that regulates energy homeostasis by decreasing ATP-consuming (fatty acid and cholesterol biosynthesis) and increasing ATP-generating (glucose uptake and fatty acid oxidation) processes [6]. AMPK activation is involved in the regulation of lipid homeostasis by enhancing the phosphorylation of acetyl-CoA carboxylase (ACC) and inhibiting sterol regulatory element-binding protein 2 (SREBP-2) and 3-hydroxy-3-methylglutaryl-coenzyme A reductase (HMGCR), which are key proteins in fatty acid and cholesterol biosynthesis [6, 7]. In addition, AMPK activation regulates glucose homeostasis by stimulating the non-insulin mediated glucose uptake and enhancing the phosphorylation of glycogen synthase kinase 3 beta (GSK3β), a key target involved in glycogen synthesis [8,9]. Therefore, AMPK is a significant target for the treatment of adipogenesis.

AMPK is a serine/threonine protein kinase, which is activated by phosphorylation at Thr172 in the α-subunit [53]. AMP binding to the γ-subunit stimulates Thr172 phosphorylation by upstream kinases including liver kinase B1 (LKB1) and calcium/calmodulin-dependent protein kinase kinase-β (CaMKKβ) [54]. Various *in silico* studies have shown that polyphenols act as positive modulators by interacting with the γ-subunit of AMPK, similarly to AMP [55, 56]. Accordingly, a direct activator of AMPK that mimics the mechanism of action of AMP may be a suitable therapeutic strategy against adipogenesis.

In recent years, more attention has been paid to natural plant flavonoids toward the development of novel anti-adipogenic drugs with high efficacy and few side effects.

Flavonoids are natural polyphenolic compounds present in high concentrations in citrus fruits and peel [57]. A recent study demonstrated that premature citrus extract (PCE) is rich in five flavonoids, including two flavone glycosides (hesperidin (HES) and narirutin (NAR)) and three polymethoxylated flavones (nobiletin (NOB), sinensetin (SIN), and tangeretin (TAN)) [57] (Fig. 12). These flavonoids exhibit a wide range of promising pharmacological properties, including an anti-adipogenic effect [58–60]. However, the detailed underlying mechanisms remain to be fully elucidated. In this context, an adipogenic model was established using palmitate (PA)-treated HepG2 cells [61] to explore the anti-adipogenic effects of the five major citrus flavonoids and their underlying molecular mechanisms.

The present study aimed to investigate the anti-adipogenic effect of citrus flavonoids and the underlying molecular mechanisms. We hypothesized that the five major citrus flavonoids exert an anti-adipogenic effect by activating the AMPK pathway. To test this hypothesis, we assessed the capacity of flavonoids to activate AMPK in PA-treated HepG2 cells. The effect of the flavonoids on lipid accumulation, TG content, and glucose uptake was evaluated. To further elucidate the underlying molecular mechanisms, AMPK and its downstream substrates involved in lipid metabolism were analyzed. To assess the primary mechanism of action, *in silico* analysis was performed to investigate the AMPK-activating capacity of the flavonoids. These results offer valuable molecular insights into the anti-adipogenic effect of flavonoids through AMPK activation (Fig. 9).

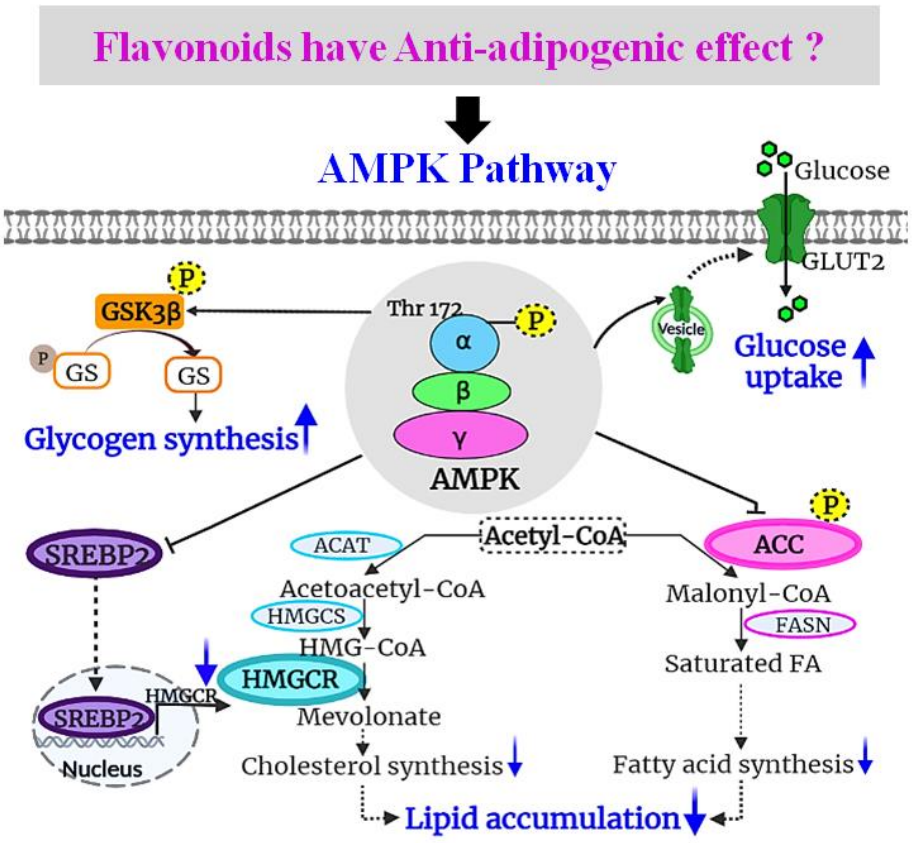

Fig. 9. Hypothetical model for anti-adipogenic effect of the flavonoids

1.3. Materials and Methods

1.3.1. Cell culture and treatment

Human hepatoma HepG2 cells were purchased from Korean Cell Line Bank (KCLB, Korea) and cultured in Dulbecco's modified Eagle's medium (DMEM) supplemented with 10% fetal bovine serum (FBS) and 1% penicillin and streptomycin (Gibco, USA) in a humidified atmosphere at 37 °C under 5% CO_2. HepG2 cells were seeded in 96-well plates. After reaching confluence, cells were serum-starved overnight and exposed to 0.4 mM PA (Sigma-Aldrich, USA) in the presence or absence of 5 μM simvastatin (SIM) (Sigma-Aldrich, USA), 2 mM metformin (MET) (Sigma-Aldrich, USA), and 50 μM HES (LKT Laboratories, USA), NAR (Sigma-Aldrich, USA), NOB (Sigma-Aldrich, USA), SIN (Sigma-Aldrich, USA) or TAN (Sigma-Aldrich, USA) for 24 h. Cells treated with SIM or MET were used as the positive controls (Fig. 10).

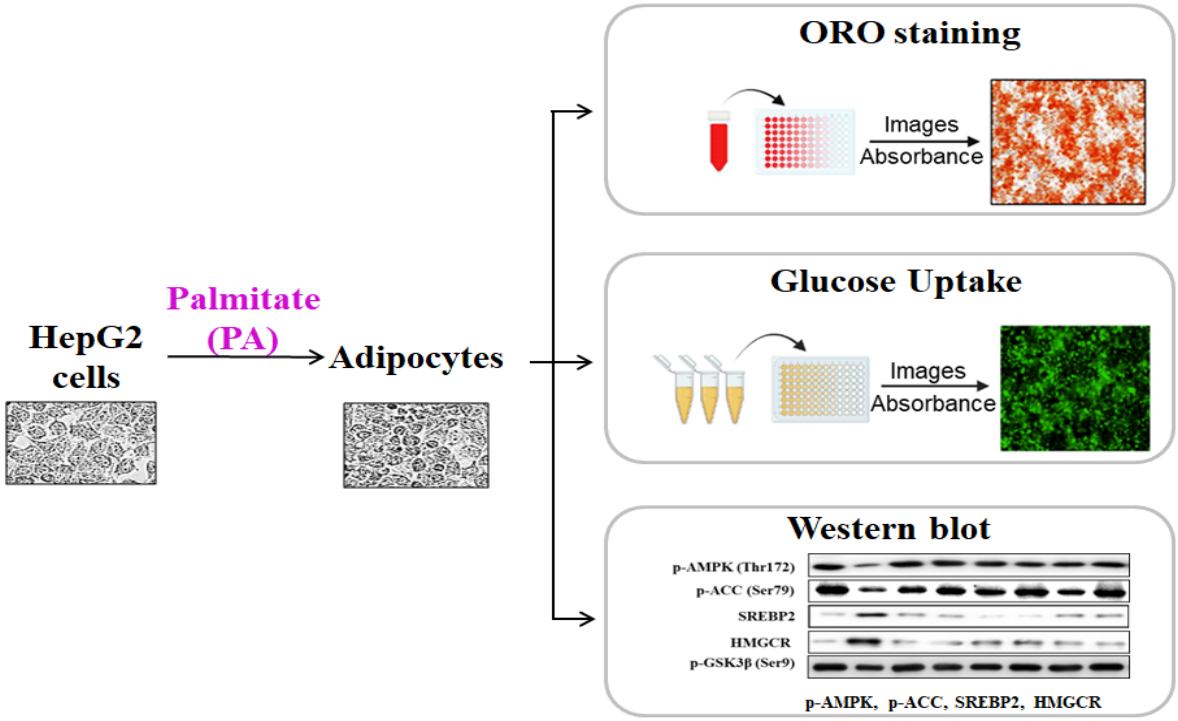

Fig. 10. HepG2 cell culture and treatment

1.3.2. Preparation of PA

A PA-bovine serum albumin (BSA) conjugate was prepared as described previously [62]. Briefly, PA (25 mM) was diluted in NaOH (50 mM) at 70 °C for 30 min and mixed with 10% BSA (Sigma-Aldrich, USA) at 55 °C for 15 min, forming a 5 mM reserving solution. This solution was diluted in serum-free DMEM to obtain the final 0.4 mM PA solution.

1.3.3. Cell Viability Assay

Cell viability was assessed by the 3-(4,5-dimethylthiazol-2-yl)-2,5 diphenyl tetrazolium bromide (MTT) assay using the EZ-cytox assay kit (Dogen Bio, Korea). HepG2 cells were seeded into 96-well plates at a density of 1×10^5 cells/well. Cells were treated with varying concentrations of PA, HES, NAR, NOB, SIN, and TAN for 24 h. After removing the culture media, fresh media containing 10% EZ-cytox in DMEM was added into each well. Cells were maintained at 37 °C and 5% CO2 for 3 h to allow formation of formazan. After incubation, the absorbance at 450 nm was measured using an enzyme-linked immunosorbent assay microplate reader (TECAN, Austria).

1.3.4. Oil Red O staining

To determine intracellular lipid accumulation, Oil Red O staining was performed according to a previously described method with slight modifications [63]. HepG2 cells were plated in 96-well plates at a density of 1×10^5 cells/well. After treatment (as described in section 1.3.1.), HepG2 cells were rinsed with phosphate buffered saline (PBS) and fixed with 10% formaldehyde for 1 h. Cells were rinsed with 60% isopropanol and stained with Oil Red

O (Sigma-Aldrich, USA) for 30 min at room temperature. Cells were rinsed with sterile water four to five times to remove excess staining solution. IncuCyte ZOOM (Essen BioScience, USA) was used to capture and analyze the images at 20× magnification.

1.3.5. TG assay

Cellular triglyceride contents were evaluated using a commercially available triglyceride colorimetric assay kit (BioAssay Systems, USA). After treatment (as described in section 1.3.1.), cells were rinsed with PBS and collected in cell lysis buffer containing 5% Triton X100. Cells were homogenized and centrifuged at 3000 ×*g* for 5 min. The triglyceride content of the supernatant was examined according to the manufacturer's instructions. Protein concentration was quantified using the Bio-Rad DC protein assay (Bio-Rad Laboratories, USA). Triglycerides contents were normalized with the protein concentration determined using BSA as the calibration standard.

1.3.6. 2-NBDG uptake assay

Glucose uptake in HepG2 cells was assessed using a 2-NBDG assay. In short, HepG2 cells were plated in 96-well plates at a density of 1×10^5 cells/well. After treatment (as described in section 1.3.1.), cells were exposed to 40 μM 2-NBDG (Carlsbad, USA) in the presence or absence of 100 nM insulin for 30 min at 37 °C. Cells were rinsed with PBS, and fluorescence images were captured using IncuCyte ZOOM (Essen BioScience, USA) at 20× magnification. Fluorescence analysis was performed using the IncuCyte ZOOM Fluorescent Processing software.

1.3.7. Preparation of cell lysates and Western blot analysis

HepG2 cells were seeded in 24-well plates at a density of 5×10^4 cells/well. After treatment (as described in section 1.3.1.), cells were rinsed with PBS and lysed with ice-cold RIPA buffer (20 mM Tris-HCl pH 7.5, 150 mM NaCl, 1 mM EGTA, 1 mM Na2EDTA, 1% NP-40, 1% sodium deoxycholate, 2.5 mM sodium pyrophosphate, 1 mM NaVO4, 1 μg/mL leupeptin) containing a protease inhibitor. The whole-cell lysate was centrifuged at 12,000 rpm for 10 min, and supernatants were collected and assayed for protein concentration using the Bradford assay kit (Bio-Rad Laboratories, USA). For Western blotting, equal amounts of protein were separated using 10% sodium dodecyl sulphate-polyacrylamide gel electrophoresis (SDS-PAGE) and transferred to a nitrocellulose membrane. Membranes were blocked with 5% non-fat dry milk in Tris-buffered saline containing 0.1% Tween 20. Membranes were incubated with primary antibodies against AMPK (Cell Signaling Technology, USA), p-AMPK (Thr172) (Cell Signaling Technology, USA), ACC (Cell Signaling Technology, USA), p-ACC (Ser79) (Cell Signaling Technology, USA), GSK3β (Cell Signaling Technology, USA), p-GSK3β (Ser9) (Cell Signaling Technology, USA), β-actin (Thermo fisher, USA), SREBP-2 (Thermo fisher, USA), and HMGCR (Thermo fisher, USA), followed by incubation with horseradish peroxidase-conjugated secondary antibodies. Immunoreactive bands were analyzed using a chemi-luminescence bioimaging instrument (NeoScience, Korea).

1.3.8. Molecular docking

The crystal structure of AMPK in complex with AMP (PDB ID 2V8Q) was obtained from the Protein Data Bank (PDB). The Sitemap tool (Schrodinger Software, Germany) was used to identify the four cystathionine β-synthase domains (CBS1, CBS2, CBS3, and CBS4) in the γ-subunit of AMPK. All AMP molecules in the γ-subunit of AMPK were removed for docking of flavonoids. The three-dimensional structure of AMP and flavonoids (HES, NAR, NOB, SIN, and TAN) were obtained from the PubChem database (https://pubchem.ncbi.nlm.nih.gov/) and energetically minimized using the PyRx software (Python Prescription 0.8, The Scripps Research Institute). The grid box used for focused docking was set to 26×44×46 Å to ensure the structure of the γ-subunit of AMPK. Docking experiments were performed using the AutoDock Vina module (Molecular Graphics Lab, The Scripps Research Institute, USA). Based on the binding energy, the best docked pose was selected and 3D images were created using PyMOL (The PyMOL Molecular Graphics System, Ver.2.5.0, Schrodinger, LLC, USA). The docking complex of AMPK was further optimized, validated, and explored using the Discovery Studio visualizer (Ver.21.1.0.20298). Hydrogen bonds and hydrophobic interactions between the receptor and ligand were analyzed using the Ligplot program [64] (Fig. 11).

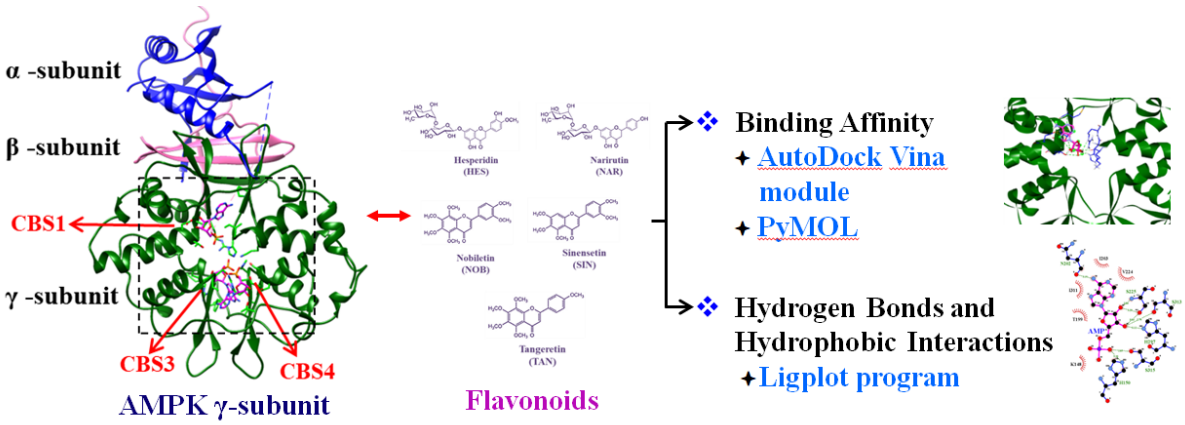

Fig. 11. Molecular docking analysis

1.3.9. Statistical analysis

Data are expressed as the mean ± standard error (SE) of three independent experiments and statistically analyzed using IBM SPSS Statistics (Ver.17.0; USA). Statistical differences among groups were analyzed with one-way analysis of variance (ANOVA) followed by Turkey's test. $p < 0.05$, $p < 0.005$, and $p < 0.0005$ indicate statistically significant differences from the PA-treated control group.

1.4. Results

1.4.1. Cell viability

An MTT assay was performed to evaluate the cytotoxicity of HES, NAR, NOB, SIN, and TAN in HepG2 cells (Fig. 13) and determine the optimal concentrations for subsequent assays. HepG2 cells were treated with increasing concentrations of PA, HES, NAR, NOB, SIN, or TAN for 24 h to examine cell viability. Results demonstrated that PA did not exhibit any cytotoxicity at concentrations up to 500 μM (Fig. 13A). In addition, the flavonoids did not show any cytotoxic effects at concentrations up to 100 μM (Fig. 13B-F). Accordingly, 400 μM PA and 50 μM flavonoids were used in the following experiments.

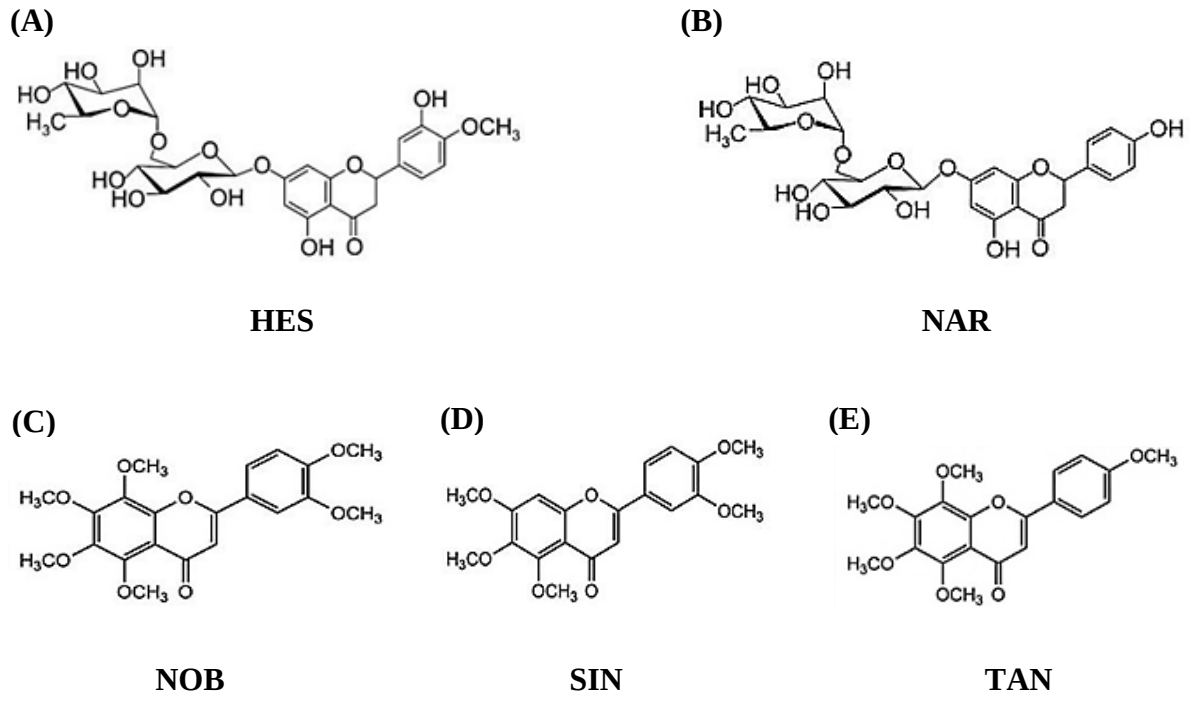

Fig. 12. Chemical structure of (A) HES, (B) NAR, (C) NOB, (D) SIN, and (E) TAN.

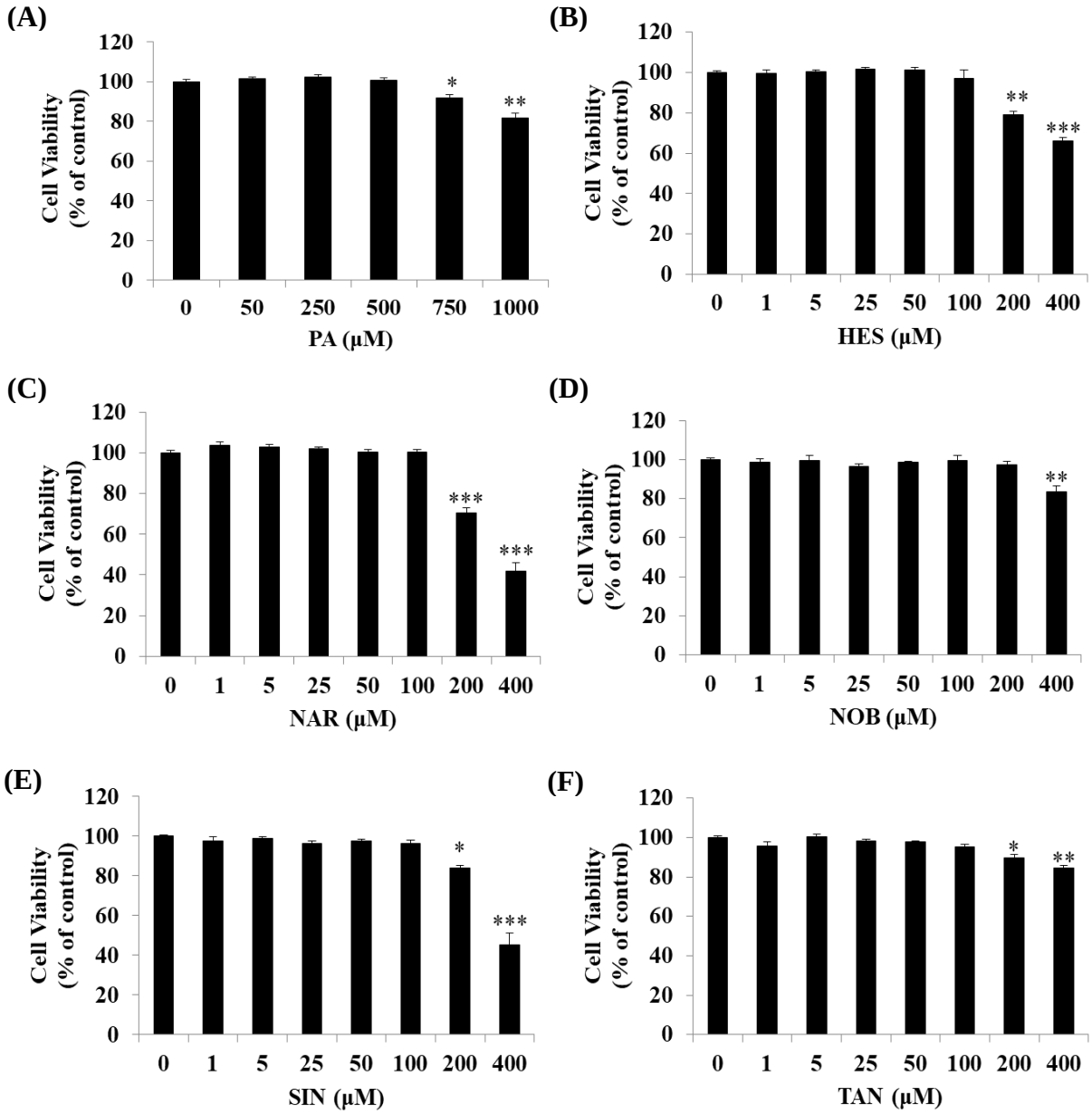

Fig. 13. Effect of the five flavonoids on HepG2 cell viability.

Cells were incubated with increasing concentrations of PA, HES, NAR, NOB, SIN, or TAN for 24 h. An MTT assay was performed to assess cell viability (A-F). Data are represented as the mean ± SE. MTT, 3-(4,5-dimethylthiazol-2-yl)-2,5-diphenyl tetrazolium bromide; PA, palmitate; HES, hesperidin; NAR, narirutin; NOB, nobiletin; SIN, sinensetin; TAN, tangeretin. *$p < 0.05$, **$p < 0.005$, ***$p < 0.0005$ compared to the control.

1.4.2. Intracellular lipid accumulation and TG content

Oil Red O staining and TG assay were performed to assess the effect of HES, NAR, NOB, SIN, and TAN on intracellular lipid accumulation and TG content in HepG2 cells (Fig. 14). HepG2 cells treated with PA significantly increased ($p < 0.0005$) lipid accumulation as well as TG content compared with untreated control cells. Cells treated with SIM (positive control) showed significantly decreased ($p < 0.005$) lipid accumulation and TG content compared with PA-treated control cells. In addition, cells treated with HES, NAR, NOB, SIN, or TAN showed significantly decreased ($p < 0.005$) lipid accumulation and TG content compared with PA-treated control cells (Fig. 14A-C). Overall, these results suggest that HES, NAR, NOB, SIN, and TAN markedly reduced both lipid accumulation and TG content in PA-treated HepG2 cells.

(A)

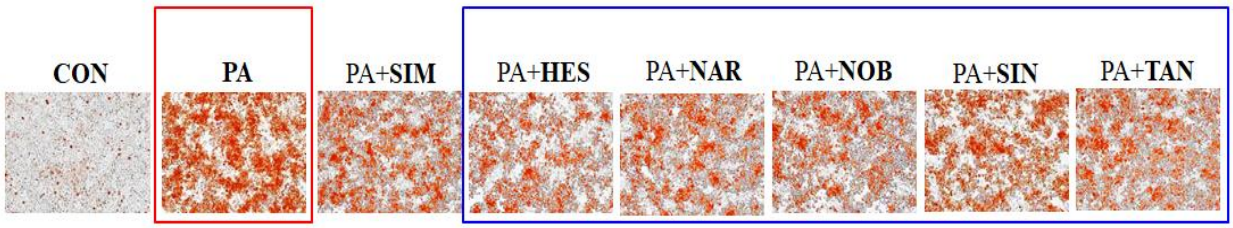

(B)

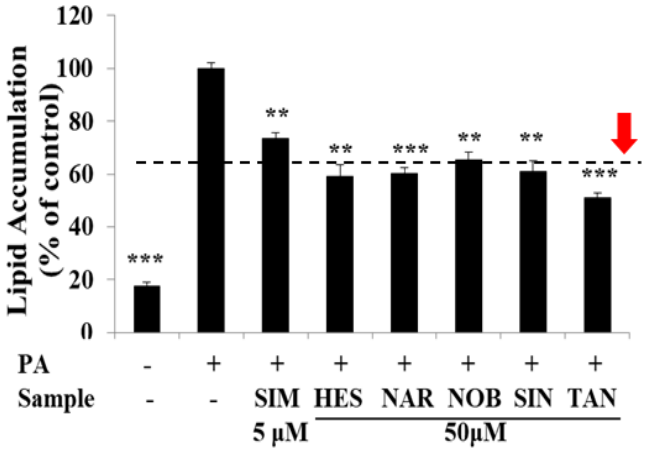

(C)

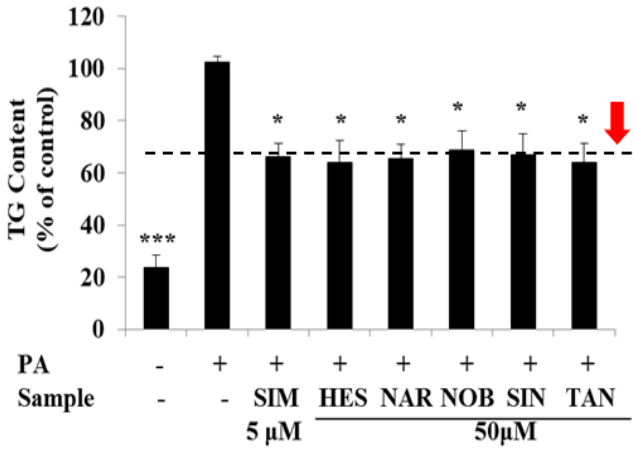

Fig. 14. Effect of the five flavonoids on intracellular lipid accumulation and TG content in PA-treated HepG2 cells.

HepG2 cells were serum starved overnight and incubated in serum-deprived medium containing 400 μM PA with or without 50 μM flavonoids for 24 h. Lipid accumulation was observed using Oil Red O staining and analyzed using IncuCyte ZOOM fluorescence processing software at 20× magnification (A). Quantitative measurement of lipid accumulation using IncuCyte ZOOM fluorescence processing software (B). Relative intracellular TG content was detected using a TG assay kit (C). Data were presented as the mean ± SE. TG, triglyceride; CON, control; PA, palmitate; SIM, simvastatin; HES, hesperidin; NAR, narirutin; NOB, nobiletin; SIN, sinensetin; TAN, tangeretin. *$p < 0.05$, **$p < 0.005$, ***$p < 0.0005$ compared with the PA-treated control.

1.4.3. Glucose uptake

A 2-NBDG assay was performed to investigate the effect of HES, NAR, NOB, SIN, and TAN on glucose uptake in PA-treated HepG2 cells (Fig. 15). The results showed that HepG2 cells treated with PA had decreased glucose uptake compared with untreated control cells. Cells treated with MET (positive control) showed significantly increased ($p < 0.005$) glucose uptake compared with PA-treated control cells. Particularly, cells treated with HES, NAR, NOB, SIN, or TAN showed significantly enhanced ($p < 0.005$) glucose uptake compared to PA-treated control cells regardless of insulin stimulation (Fig. 15A and B). These results suggest that HES, NAR, NOB, SIN, and TAN treatment improved the glucose uptake in an insulin-independent manner in PA-treated HepG2 cells.

(A)

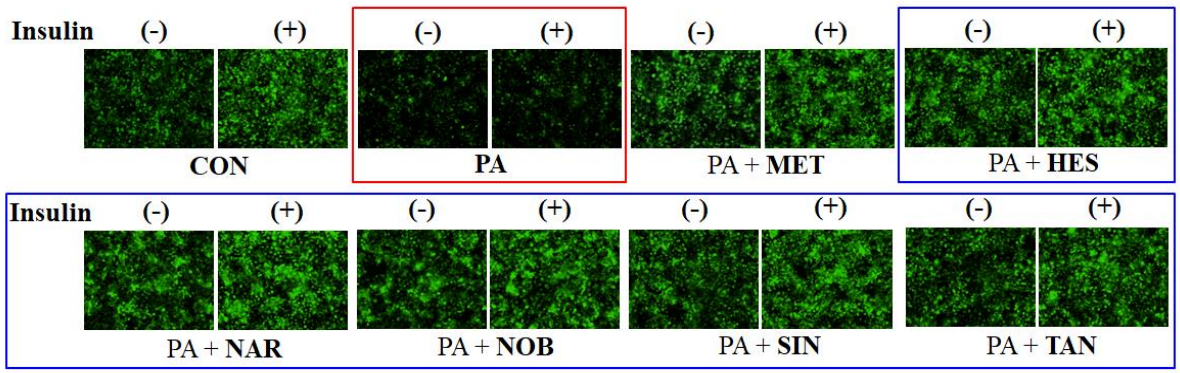

(B)

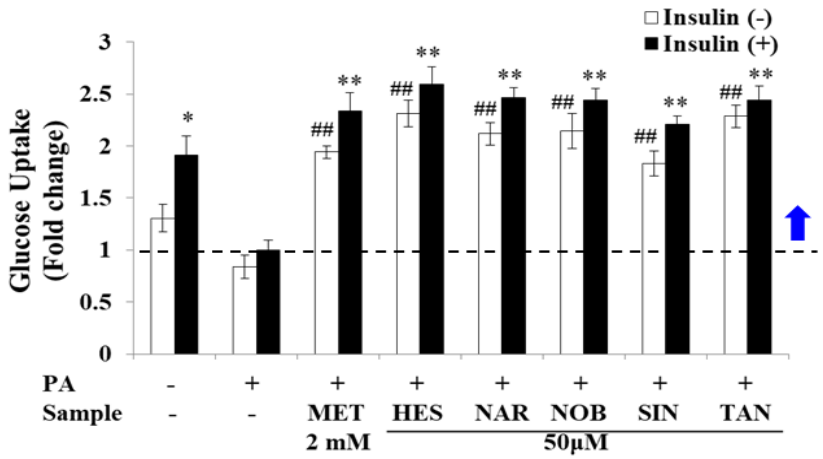

Fig. 15. Effect of the five flavonoids on glucose uptake in PA-treated HepG2 cells.

A glucose uptake assay was performed using the fluorescent D-glucose analogue 2-NBDG. HepG2 cells were serum starved overnight and incubated in serum-deprived medium containing PA with or without 50 μM flavonoids for 24 h, followed by incubation with 40 μM 2-NBDG in the presence or absence of 100 nM insulin for 30 min. Cells were rinsed with PBS. Fluorescence images were captured using IncuCyte ZOOM at 20× magnification (A). Total fluorescence intensities were calculated using IncuCyte ZOOM fluorescence processing software (B). Data are presented as the mean ± SE. 2-NBDG, 2-[N-(7-Nitrobenz-2-oxa-1,3-diazol-4-yl)amino]-2-deoxy-d-glucose; CON, control; PA, palmitate; MET, metformin; HES, hesperidin; NAR, narirutin; NOB, nobiletin; SIN, sinensetin; TAN, tangeretin. *$p < 0.05$, **$p < 0.005$ compared with the insulin-stimulated PA-treated control; $^{\#}p < 0.05$, $^{\#\#}p < 0.005$ compared with the non-insulin-stimulated PA-treated control.

1.4.4. AMPK signaling pathway

The effects of HES, NAR, NOB, SIN, and TAN on the phosphorylation of AMPK (Thr172) and ACC (Ser79), and the expression levels of SREBP-2 and HMGCR in PA-treated HepG2 cells were analyzed by Western blot (Fig. 16). The results demonstrated that treatment with PA significantly decreased ($p < 0.05$) the phosphorylation levels of both AMPK (Thr172) and ACC (Ser79) and increased ($p < 0.005$) the expression levels of SREBP-2 and HMGCR. In contrast, treatment with HES, NAR, NOB, SIN, and TAN significantly increased ($p < 0.05$) the phosphorylation levels of both AMPK (Thr172) and ACC (Ser79) and reduced ($p<0.005$) the expression levels of SREBP-2 and HMGCR in PA-treated HepG2 cells (Fig. 16A-D). These results suggest that the flavonoids activate the AMPK pathway and exhibit an anti-adipogenic effect on PA-treated HepG2 cells.

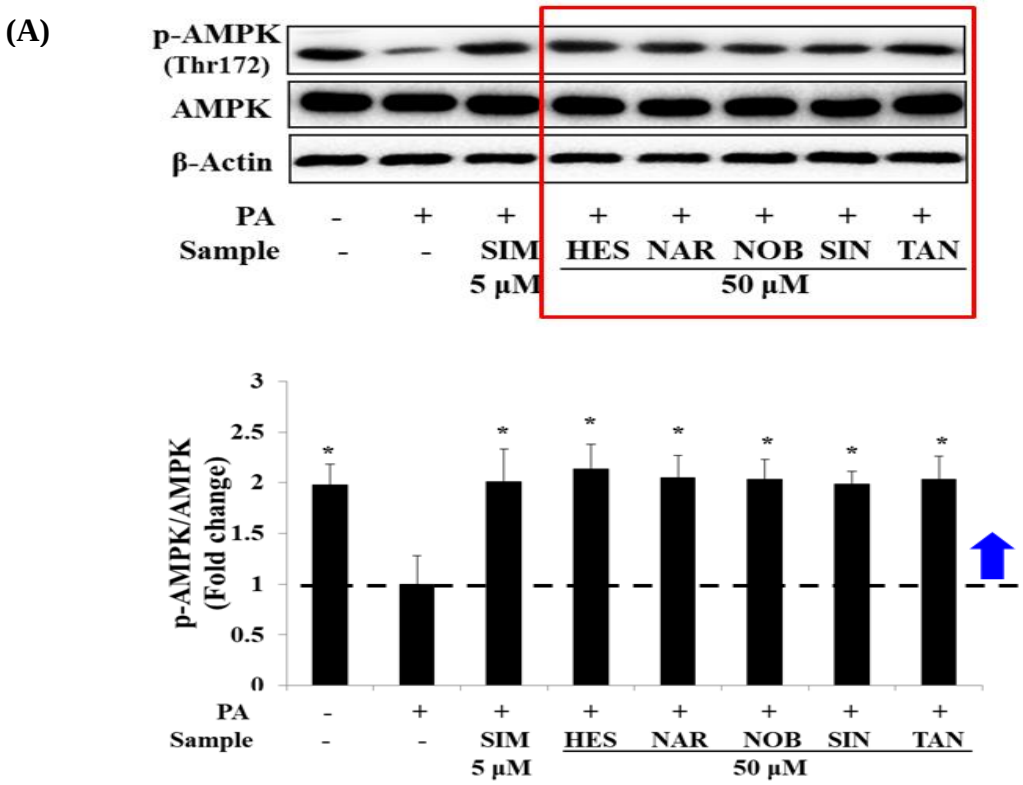

(B)

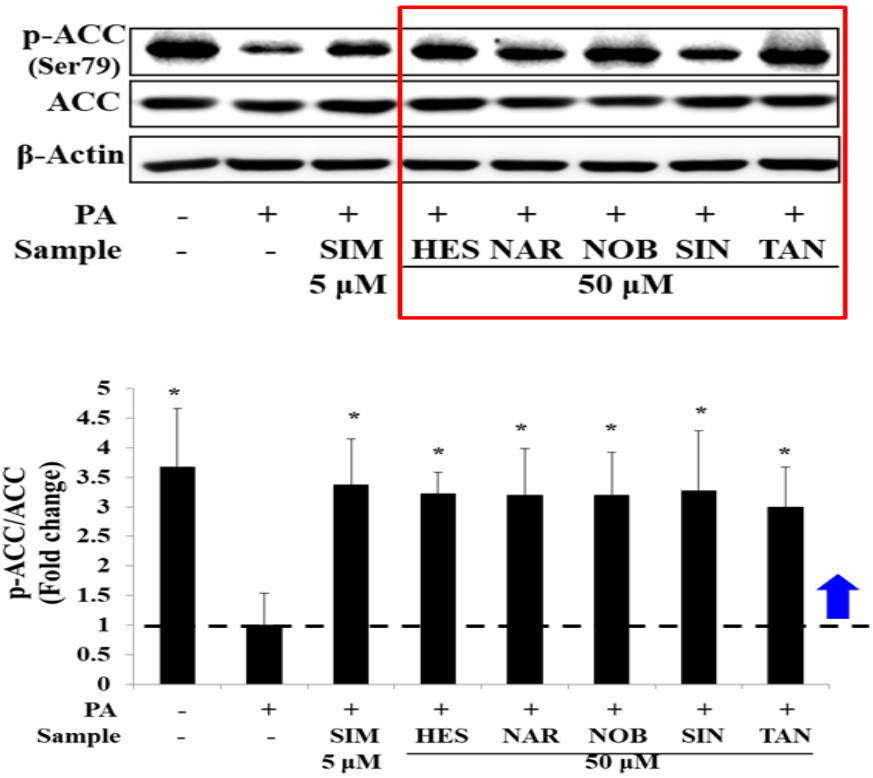

(C)

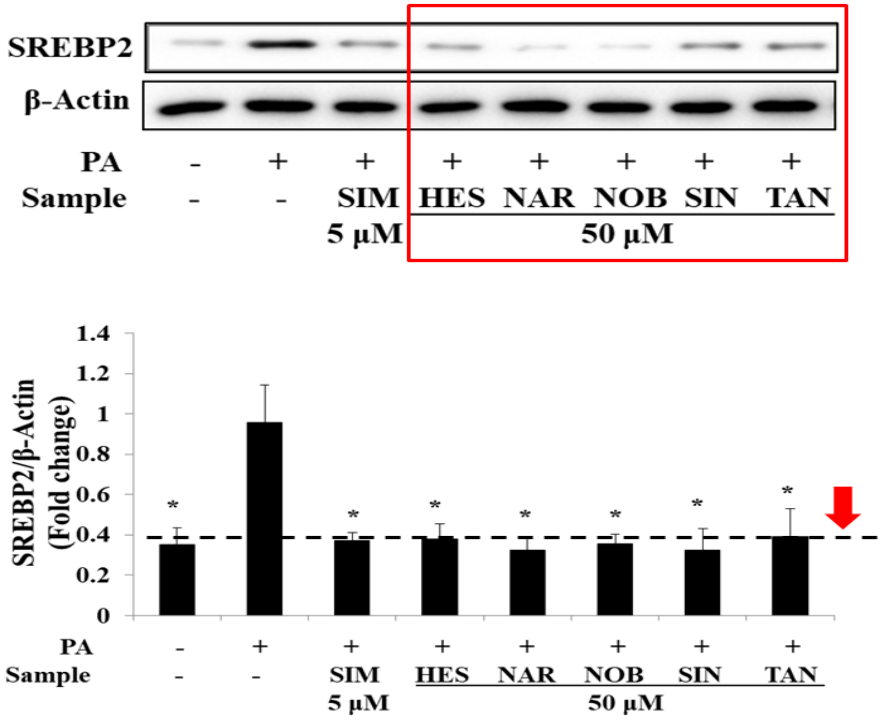

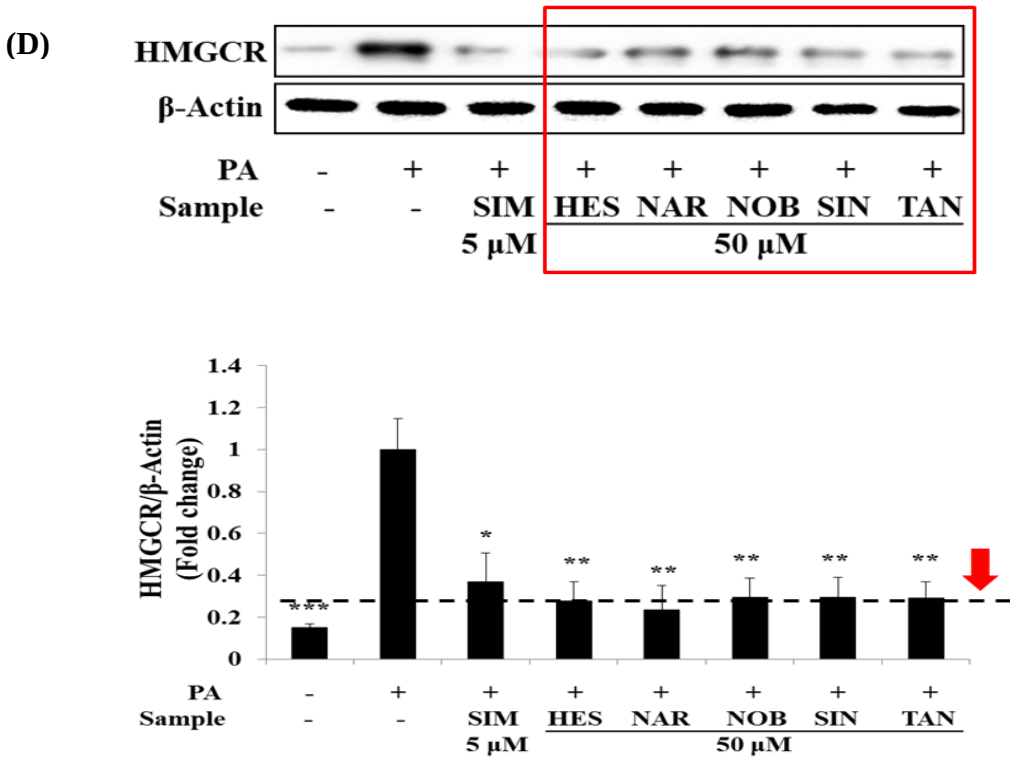

Fig. 16. Effect of the five flavonoids on the phosphorylation levels of AMPK and ACC and the expression levels of SREBP-2 and HMGCR in PA-treated HepG2 cells.

HepG2 cells were serum starved overnight and incubated in serum-deprived medium containing PA with or without flavonoids for 24 h. The levels of p-AMPK, p-ACC, SREBP-2, and HMGCR were determined by Western blotting. Representative immunoblots of p-AMPK (A), p-ACC (B), SREBP-2 (C), and HMGCR (D). Relative protein levels were measured using densitometry analysis. Data are represented as the mean ± SE. AMPK, AMP-activated protein kinase; ACC, acetyl-CoA carboxylase; SREBP-2, sterol regulatory element-binding protein 2; HMGCR, 3-hydroxy-3-methylglutaryl-coenzyme A reductase; PA, palmitate; SIM, simvastatin; HES, hesperidin; NAR, narirutin; NOB, nobiletin; SIN, sinensetin; TAN, tangeretin. *$p < 0.05$, **$p < 0.005$, ***$p < 0.0005$ compared to PA-treated control.

1.4.5. Phosphorylation of GSK3β

The effects of HES, NAR, NOB, SIN, and TAN on the phosphorylation of GSK3β in PA-treated HepG2 cells were observed via Western blot analysis (Fig. 17). Densitometry analysis revealed that HepG2 cells treated with PA have significantly reduced ($p < 0.05$) the phosphorylation level of GSK3β compared with those of untreated control cells. However, MET treatment significantly increased ($p < 0.05$) the phosphorylation level of GSK3β compared with PA-treated control cells. Treatment with HES, NAR, NOB, SIN, or TAN significantly increased ($p < 0.05$) the phosphorylation level of GSK3β compared with PA-treated control cells (Fig. 17). These results show that the flavonoids increase the phosphorylation level of GSK3β in PA-treated HepG2 cells.

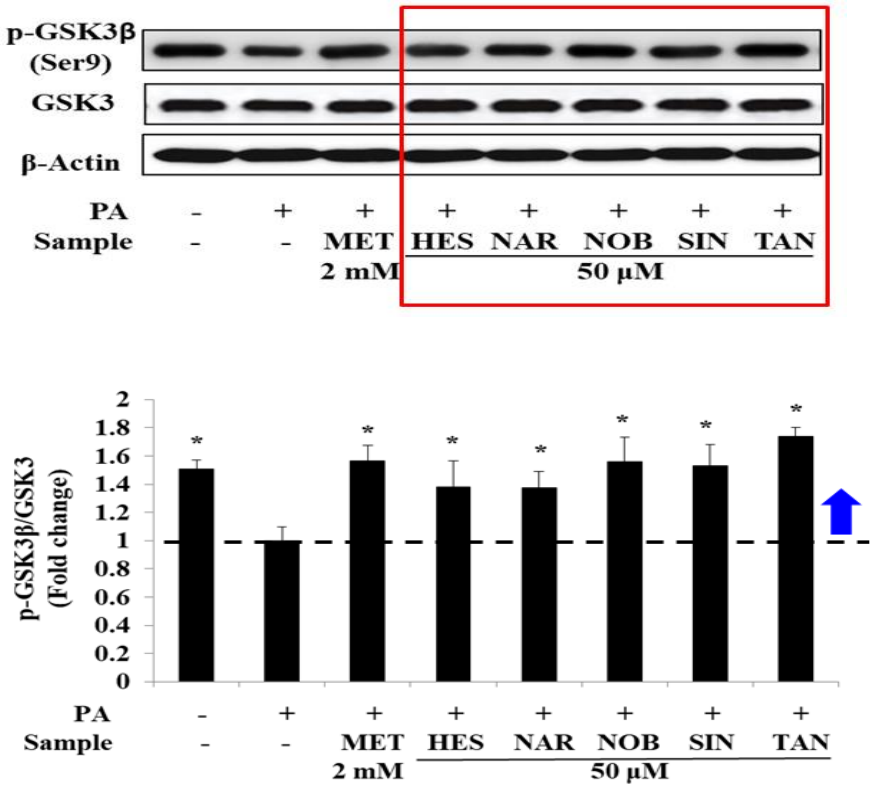

Fig.17. Effect of the five flavonoids on the phosphorylation level of GSK3β in PA-treated HepG2 cells.

HepG2 cells were serum starved overnight and incubated in serum-deprived medium containing PA with or without 50 μM flavonoids for 24 h. The p-GSK3β was determined by Western blotting. Data are represented as the mean ± standard error. GSK3β, glycogen synthase kinase 3 beta; PA, palmitate; MET, metformin; HES, hesperidin; NAR, narirutin; NOB, nobiletin; SIN, sinensetin; TAN, tangeretin. *$p < 0.05$ compared to PA-treated control.

1.4.6. Molecular docking analysis

Molecular docking was performed to determine potential interactions between the flavonoids (HES and NAR) and the γ-subunit of AMPK (Fig. 18). Fig. 18A and B represent the crystallographic structure and domain structure of the α, β, and γ subunits of AMPK. The γ-subunit contains four tandem repeats of CBS domains. Among these four domains, only three (CBS1, CBS3, and CBS4) bind to their true modulators, adenine nucleotides including AMP, ADP, and ATP. As shown in Table 1, the flavonoids (HES, NAR, NOB, SIN, and TAN) bind to the binding sites (CBS1, 3, and 4) with high binding affinity, close to that of AMP. In particular, HES and NAR showed a higher binding affinity than that of AMP in all three CBS domains. These two flavonoids also formed more hydrogen bonds or hydrophobic interactions than AMP (Table 1). Overall, these results show that the flavonoids bind to the regulatory γ-subunit of AMPK with high binding affinities and suggest that the flavonoids may serve as positive modulators of AMPK activation.

(A)

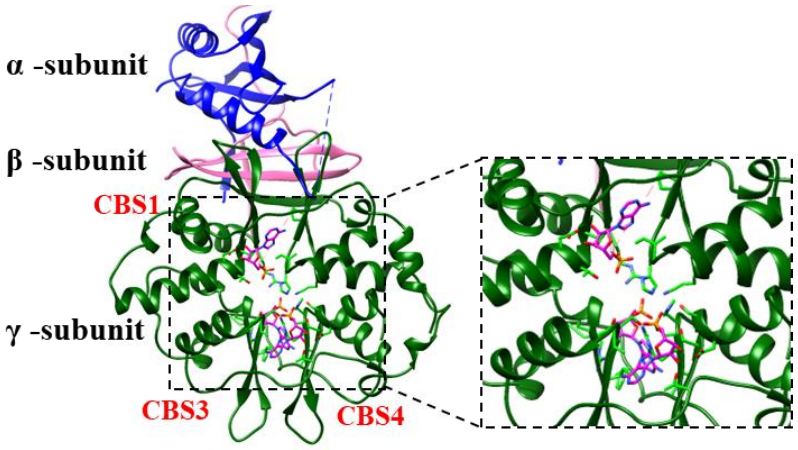

(B)

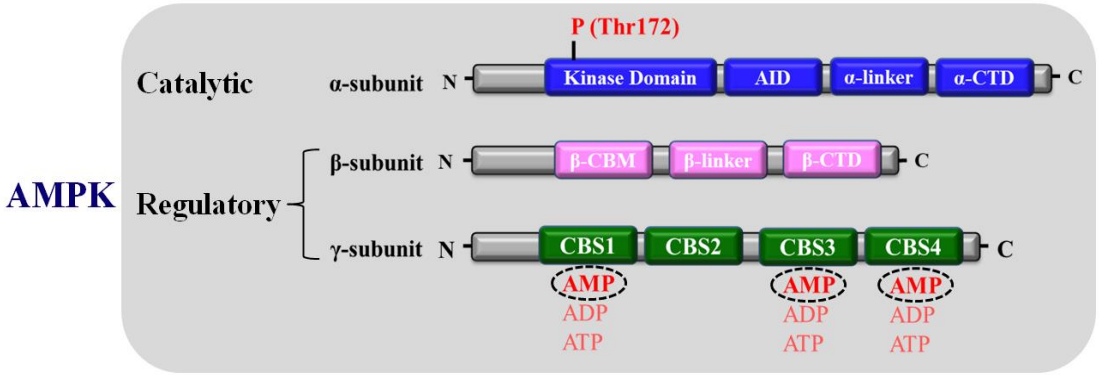

(C)

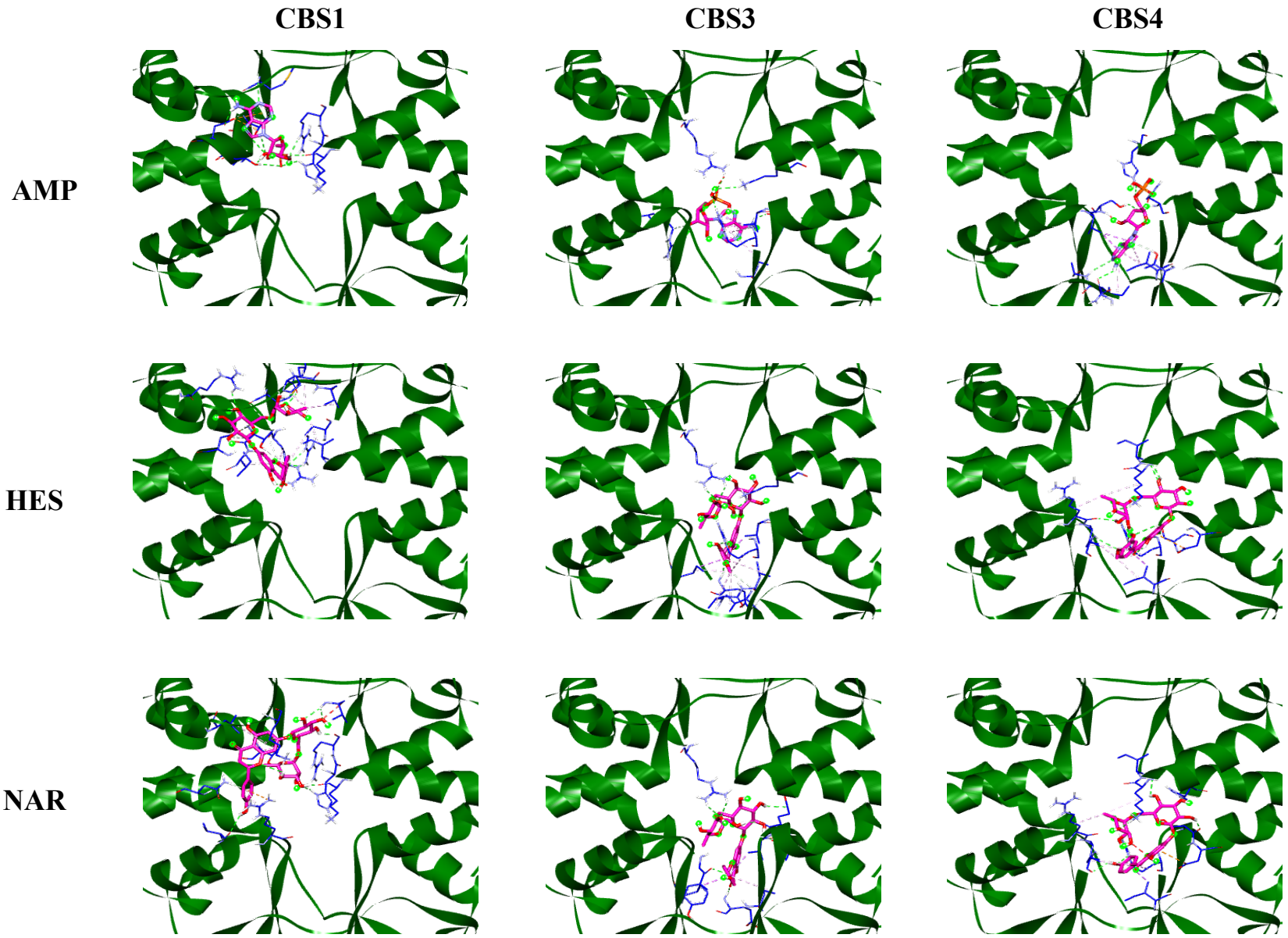

(D)

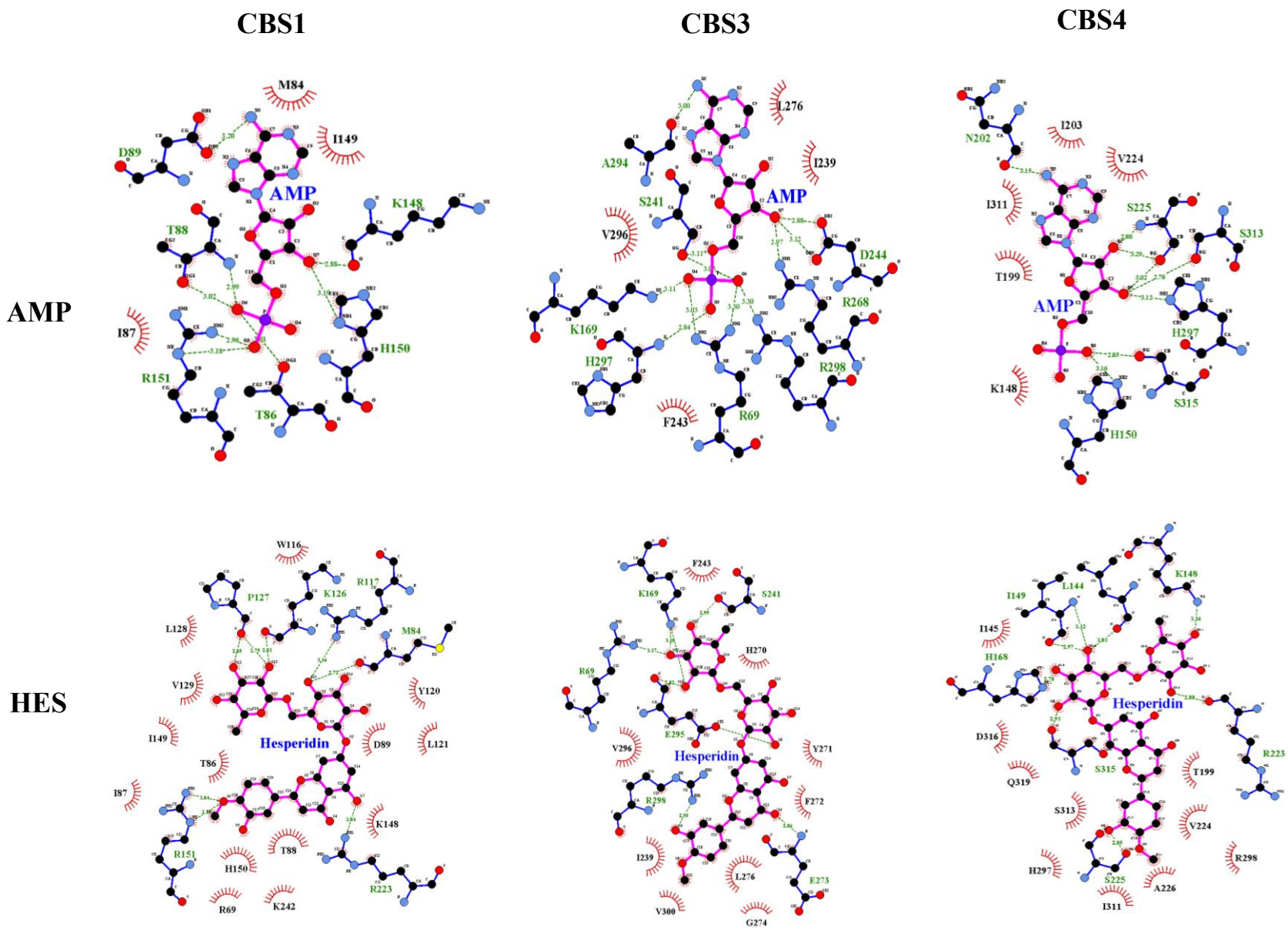

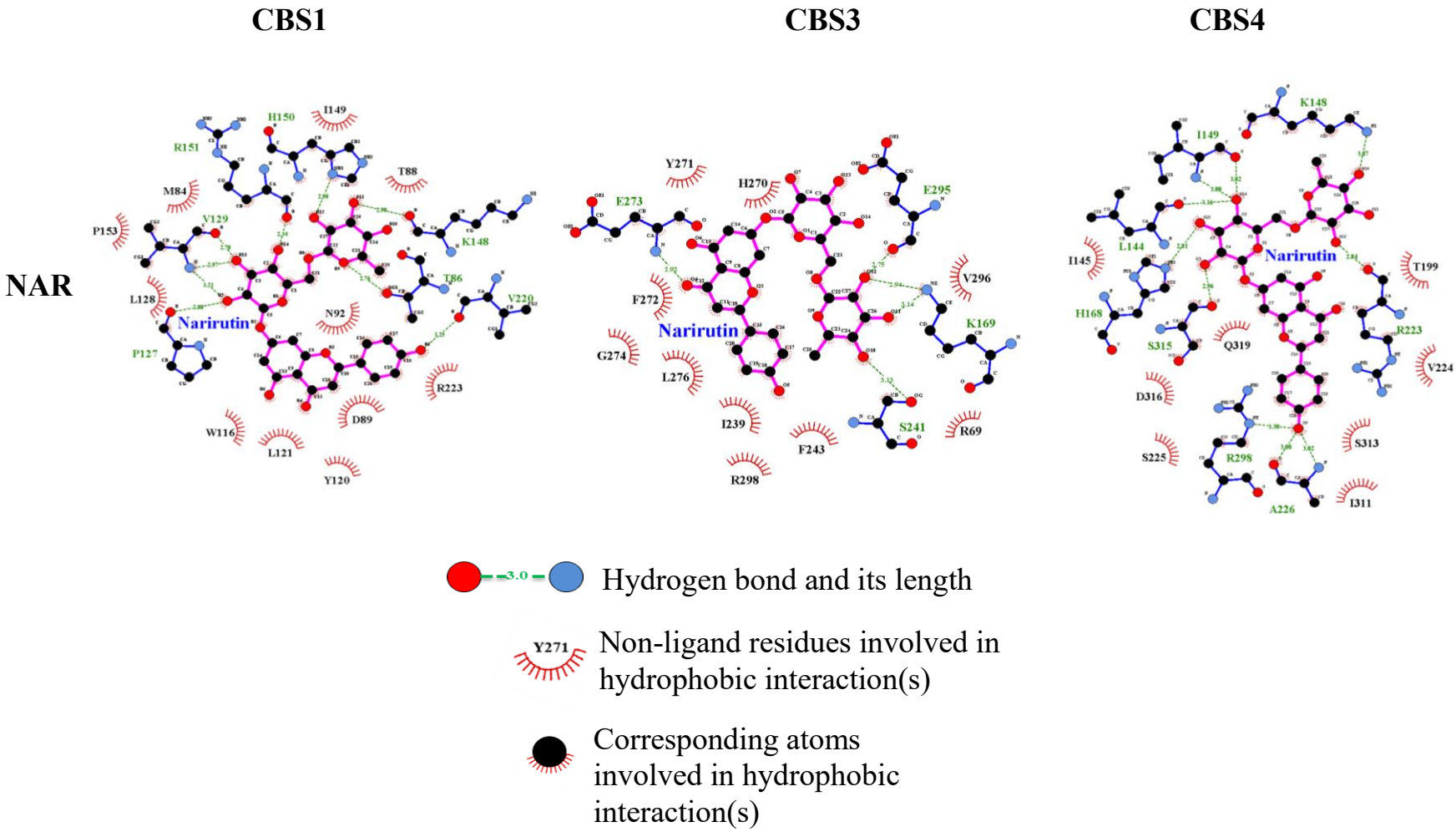

Fig. 18. Molecular docking and binding interaction of the five flavonoids to the CBS domains of the γ-subunit of AMPK.

Crystallographic structure of mammalian AMPK, representing the α (blue), β (pink), and γ (green) subunits. Three AMP molecules (represented are sticks) are bound at the nucleotide-binding sites in domains CBS1, CBS3, and CBS4 (A). Schematic representation of the domain arrangement of the α, β, and γ subunits of AMPK. The phosphorylation and nucleotide-binding sites in the α and γ subunits, respectively, are indicated in red (B). Interactions of AMP or flavonoids (HES and NAR) with the CBS1, CBS3, and CBS4 domains of the γ-subunit of AMPK (C). Hydrogen bonds and hydrophobic interactions between the flavonoids (HES and NAR) and the γ-subunit of AMPK, as determined using the Ligplot program (D). AMPK, AMP-activated protein kinase; AID, auto inhibitory domain; CBM, carbohydrate binding module; CTD, C-terminal domain; CBS, cystathionine beta-synthase domain; HES, hesperidin; NAR, narirutin.

Table 1. Binding energy of AMP and flavonoids at the three CBS domains of the γ-subunit of AMPK

Molecule	Description	Binding site of γ-subunit of AMPK		
		CBS1	**CBS3**	**CBS4**
AMP	**Binding energy (kcal/mol)**	-7.8	-7.4	-8.1
	Hydrogen bonds	D89, T88, K148, R151, H150, T86	A294, S241, D244, R268, R298, K169, H297, R69	N202, S225, S313, H297, S315, H150
	Hydrophobic interactions	M84, I149, I87	L276, I239, V296, F243	I203, V224, I311, T199, K148
HES	**Binding energy (kcal/mol)**	-9.1	-9	-8.8
	Hydrogen bonds	P127, K126, R117, M84, R151, R223	K169, S241, R69, E295, R298, E273	L144, K148, I149, H168, S315, R223, S225
	Hydrophobic interactions	W116, L128, V129, I149, T86, I87, D89, T120, L121, K148, T88, H150, K242, R69	F243, H270, V296, Y271, F272, I239, L276, V300, G274	I145, D316, Q319, S313, T199, V224, R298, H297, A226, I311
NAR	**Binding energy (kcal/mol)**	-8.3	-9	-9.3
	Hydrogen bonds	H150, R151, V129, K148, T86, V220, P127	E273, E295, K169, S241	K148, I149, L144, H168, S315, R223, R298, A226
	Hydrophobic interactions	I149, T88, M84, P153, L128, N92, R223, D89, W116, L121, Y120	Y271, H270, F272, V296, G274, L276, I239, F243, R69, R298	I145, T199, Q319, D316, V224, S313, S225, I311
NOB	**Binding energy (kcal/mol)**	-7.5	-7	-7.7
	Hydrogen bonds	M84, H150, K242	R298	T199, S225
	Hydrophobic interactions	R117, V182, K126, D89, W116, L121, L128, G83, T88, T86, I149, R223	L276, I239, V296, F272, S241, H270, R69, F243	A204, A226, I203, V224, I311, R298, N202, S315, K148, H150, I145, I149
SIN	**Binding energy (kcal/mol)**	-7.6	-6.9	-7.8
	Hydrogen bonds	M84, H150	R298	S225
	Hydrophobic interactions	V82, G83, K126, L121, L128, R117, I149, W116, D89, T86, T88, K242, R223	L276, I239, F272, V296, H270, S241, F243, R69	A204, R298, A226, I311, I203, V224, N202, T199, S313, Q319, D316, K148, S315, I145
TAN	**Binding energy (kcal/mol)**	-6.9	-7.1	-7.3
	Hydrogen bonds	M84	R298	S225, T199
	Hydrophobic interactions	V82, R117, G83, W116, K126, L128, L121, T86, D89, I149, T88, H150, R223	I239, F272, L276, S241, H270, V296, R69, F243	I311, V224, A226, R298, S315, K148, I145

1.5. Discussion

The present study evaluated the anti-adipogenic effect of citrus flavonoids associated with AMPK activation in PA-treated HepG2 cells. This study observed that the flavonoids significantly reduced both intracellular lipid accumulation and TG content, and enhanced the glucose uptake with insulin-independent manner in PA-treated HepG2 cells. In addition, the flavonoid-mediated AMPK activation increased phosphorylation level of ACC, and decreased the expression levels of SREBP-2 and HMGCR which are crucial for lipogenesis and cholesterol biosynthesis. Furthermore, the flavonoids increased phosphorylation levels of GSK3β which is a key enzyme in glycogen synthesis. Molecular docking analysis revealed that the flavonoids bind to CBS domain in the regulatory γ-subunit with high binding affinities suggesting that the flavonoids could be possible positive modulator for the activation of AMPK (Fig. 19).

The present study demonstrated that the five flavonoids suppress the PA-induced intracellular lipid accumulation and high TG content in HepG2 cells. A previous study has shown that a mixture of citrus peel flavonoids reduced the intracellular TG accumulation induced by oleic acid in HepG2 cells [65]. In addition, tangeretin is known to reduce the lipid accumulation and TG content in the liver of high-fat diet-induced obese mice [66]. Therefore, the present study confirms that flavonoids may play an essential role in the reduction of intracellular lipid accumulation and TG content in PA-treated HepG2 cells.

In the present study, flavonoid treatment increased the phosphorylation levels of AMPK and ACC and decreased the expression levels of SREBP-2 and HMGCR in PA-treated HepG2 cells. The activation of AMPK is involved in the regulation of liver lipogenesis, lipid oxidation, and cholesterol synthesis via protein phosphorylation or differential gene expression [67, 68]. AMPK activation enhances the phosphorylation of ACC, which is a key rate-limiting enzyme involved in fatty acid biosynthesis [69]. ACC

phosphorylation leads to its inactivation and, consequently, to the inhibition of malonyl-CoA formation, thereby inhibiting *de novo* lipogenesis and stimulating fatty acid oxidation [70]. Nobiletin has been shown to phosphorylate AMPK and inhibit lipogenesis through phosphorylation of ACC in high glucose-treated HepG2 cells [71]. Furthermore, AMPK activation inhibits the transcriptional activity of SREBP-2, which functions as a major transcriptional regulator of cholesterol biosynthesis [72]. HMGCR, a rate-limiting enzyme of cholesterol biosynthesis, is a target of SREBP-2 [73]. Apigenin, a plant flavonoid, suppresses total cholesterol and TG content and decreases SREBP-2 and HMGCR expression in palmitic acid-treated HepG2 cells [74]. The present study confirms that flavonoids effectively inhibit lipid accumulation via the AMPK signaling pathway in PA-treated HepG2 cells.

In the present study, citrus flavonoids increased the phosphorylation of GSK3β in PA-treated HepG2 cells. AMPK phosphorylates and inhibits its downstream substrates, including GSK3β, which promotes glucose utilization for glycogenesis [75]. Nobiletin is known to control glucose homeostasis by eliciting the AMPK-mediated phosphorylation of GSK3β in PA-treated HepG2 cells [58]. The present study also revealed that AMPK activation by flavonoids enhances glucose uptake in an insulin-independent manner. The phosphorylation of AMPK is known to promote membrane translocation of the glucose transporter GLUT2 and enhance the glucose uptake in an insulin-independent manner in liver [76]. Overall, our results indicate that flavonoids regulate hepatic glucose metabolism by enhancing glucose uptake and glycogenesis via the AMPK signaling pathway.

In the present study, *in silico* molecular docking showed that the citrus flavonoids bind to all the three CBS domains in the γ-subunit of AMPK. AMPK is a heterotrimer consisting of a catalytic α- and two regulatory β- and γ-subunits [54]. The γ-subunit contains four tandem repeats of CBS domains [77]. Among these, three (CBS1, CBS3, and CBS4) are involved in the binding of adenine nucleotides, including AMP, ADP, and ATP [78]. AMP

binding to CBS domains releases the auto inhibitory domain from the catalytic domain in the α-subunit [53]. This active conformation allows Thr172 to be phosphorylated by upstream kinases, including LKB1 and CaMKKβ [54]. In addition, the active form of AMPK prevents phosphatases from accessing Thr172 at the catalytic subunit [79]. A previous study using *in silico* analyses has proposed that kaemferide is a promising AMPK activator [55]. A previous study has shown that naringenin, a flavonoid found in fruits, has anti-adipogenic properties by binding to the AMP-binding sites at the γ-subunit of AMPK and acting as an agonist [56]. In the present study, molecular docking analysis revealed that flavonoids directly activate AMPK as positive modulators by interacting with the R groups of the CBS domains in the γ-subunit.

In summary, the present study indicates that flavonoids reduce the lipid accumulation and TG content in PA-treated HepG2 cells by increasing the phosphorylation levels of both AMPK and ACC, while reducing the expression levels of SREBP-2 and HMGCR (Fig. 20). In addition, the flavonoid-mediated AMPK activation increases glucose uptake and phosphorylation of GSK3β, thereby enhancing glycogen synthesis. Overall, these results suggest that citrus flavonoids have anti-adipogenic effects on PA-treated HepG2 cells via the AMPK signaling pathway. These findings offer valuable insights into the anti-adipogenic mechanism of flavonoids, particularly relevant for future studies aiming at treating obesity.

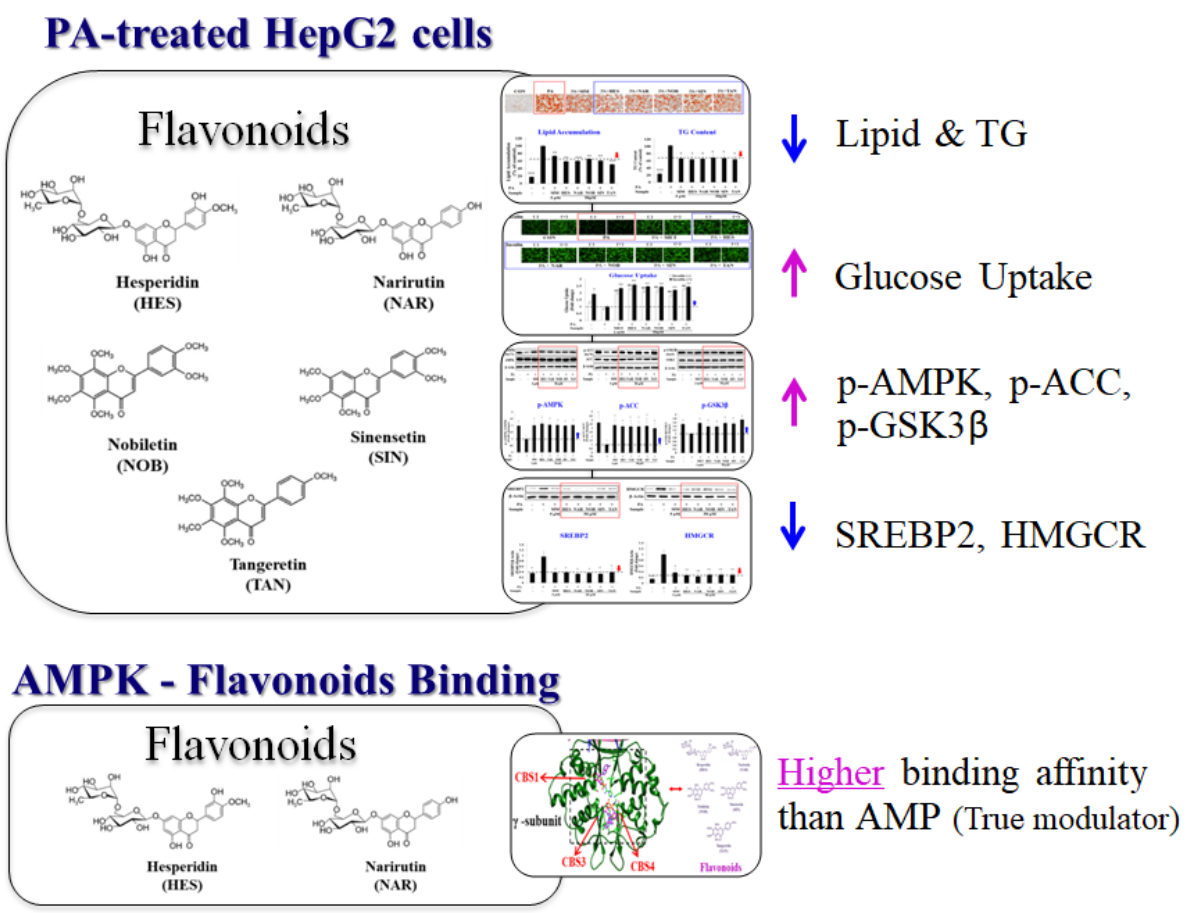

Fig. 19. Summary of anti-adipogenic effect of flavonoids

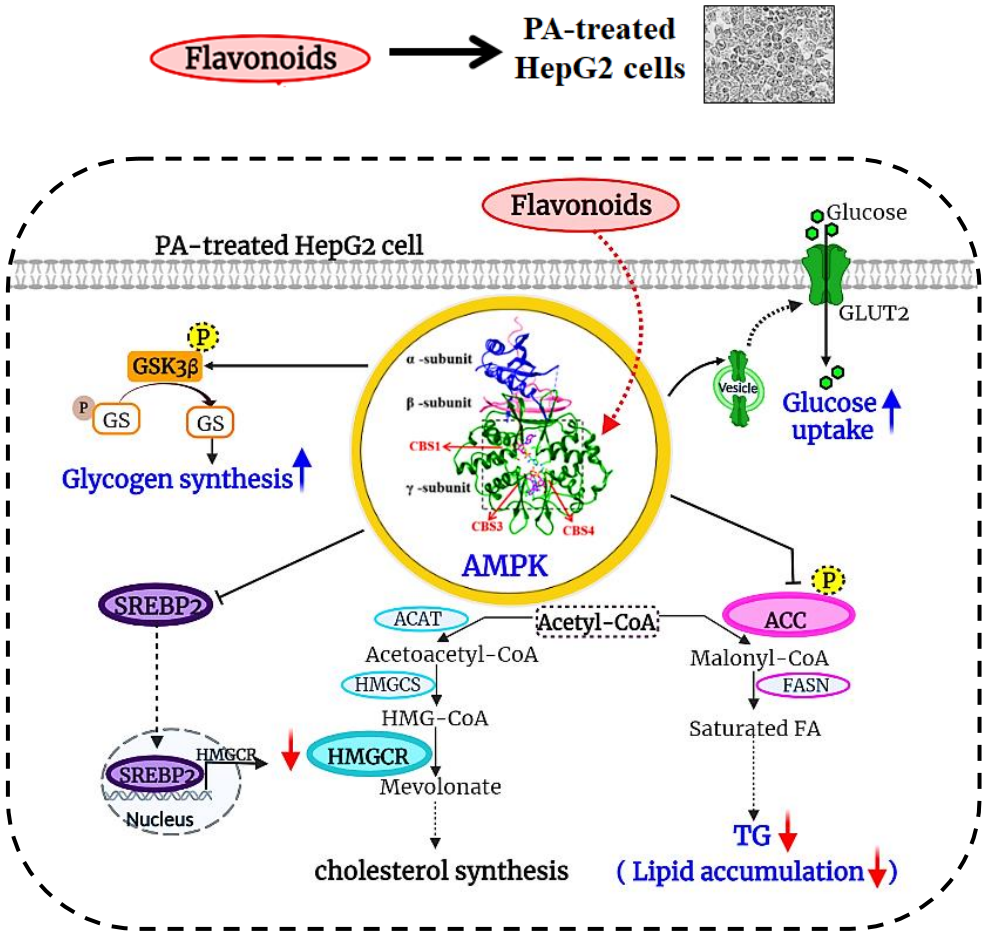

Fig. 20. Proposed mechanism for the anti-adipogenic effect of flavonoids associated with AMPK activation in PA-treated HepG2 cells.

AMPK, AMP-activated protein kinase; ACC, acetyl-CoA carboxylase; FASN, fatty acid synthase; SREBP-2, sterol regulatory element-binding protein 2; ACAT, acyl-coenzyme A:cholesterol acyltransferase; HMGCS, hydroxymethylglutaryl-CoA synthase; HMGCR, 3-hydroxy-3-methyl-glutaryl-coenzyme A reductase; GLUT2, glucose transporter 2; GSK3β, glycogen synthase kinase 3 beta; GS, glycogen synthase.

PART-II

Anti-diabetic effect of hesperidin on palmitate-treated HepG2 cells and high fat diet-induced obese mice

2.1. Abstract

The present study examined the relationship between the anti-diabetic effect of hesperidin (HES) and differential gene expression in HES treated high fat diet (HFD)-induced obese mice. Based on a 2-[N-(7-Nitrobenz-2-oxa-1,3-diazol-4-yl)amino]-2-deoxy-d-glucose (2-NBDG) uptake assay, treatment with HES restored glucose uptake to control levels in an insulin-independent manner in palmitate (PA)-treated HepG2 cells. Western blot analysis confirmed that HES increased the insulin-stimulated phosphorylation of Akt and GSK3β in insulin-resistant PA-treated HepG2 cells. High fat diet (HFD)-induced obese mice treated with HES showed reduced serum insulin, blood glucose, and homeostatic model assessment for insulin resistance (HOMA-IR) values. In addition, both glucose tolerance and insulin tolerance were significantly improved to normal level by HES in HFD-induced obese mice. RNA sequencing disclosed that the expression levels of twelve up-regulated and six down-regulated genes related to insulin signaling and glucose metabolism were restored to normal level by HES in the liver of HFD-induced obese mice. A protein-protein interaction (PPI) network was constructed via search tool for the retrieval of interacting genes/proteins (STRING) analysis, and *Eno1*, *Pik3cd*, *Hk2*, *Trib3*, *Myc*, *Nos3*, *Ppargc1a*, and *Igf2* were located in the functional hubs of the PPI network of glucose metabolism. Furthermore, Western blot analysis confirmed that HES improved insulin sensitivity and glucose homeostasis by normalizing the expression levels of hexokinase-II, enolase-1, and PI3 kinase p110δ to normal level. Overall, these results suggest that HES exerts a potential anti-diabetic effect by normalizing the expression levels of genes related to the insulin signaling and glucose metabolism, which were perturbed in the liver of HFD-induced obese mice.

Keywords: Hesperidin, insulin resistance, HepG2 cells, obese mice, RNA sequencing

2.2. Introduction

Insulin signaling plays an important role in regulating whole-body glucose homeostasis by promoting glycolysis and inhibiting gluconeogenesis [80]. Protein kinase B (Akt) is the major downstream target and the key molecule mediating the metabolic effects of insulin signaling [81]. Insulin-mediated activation of Akt facilitates glucose uptake by translocating glucose transporters [82]. In addition, Akt is responsible for glycogen synthesis via phosphorylation of glycogen synthase kinase 3 beta (GSK3β), which subsequently dephosphorylates and activates glycogen synthase [83]. Defects in the Akt pathway or downstream molecules can induce an imbalance in glucose metabolism, generating chronic hyperglycemia [84, 85].

Obesity impairs the ability of insulin to regulate glucose homeostasis, which leads to hyperglycemia and eventually results in type 2 diabetes mellitus (T2DM) [86, 87]. It also accelerates the dysregulation of several intrinsic pathways that elicit insulin resistance [86]. Obesity-associated diabetes is evidenced by increased blood glucose levels as a result of insulin resistance [88]. Therefore, restoration of the dysregulated pathways that lead to insulin resistance and hyperglycemia in obesity may provide a therapeutic strategy for the treatment of obesity-induced diabetes. In the present study, palmitate (PA)-treated HepG2 cells and high fat diet (HFD)-induced obese mice were used as an appropriate hepatic insulin resistance and obesity animal models, respectively, which exhibit severe insulin resistance and hyperglycemia [89, 90].

Hesperidin (HES) is a flavonoid glycoside abundantly present in citrus peel and Its chemical structure contains an aglycon bonded to rutinose, a disaccharide [91]. HES exhibits a wide range of promising pharmaceutical effects, including anti-diabetic properties [92]. HES is known to prevent hyperglycemia by improving insulin sensitivity in diabetic rats [93,

94]. However, the detailed mechanism of its anti-diabetic effect and its relation with specific genes associated with diabetes has not yet been thoroughly established.

The present study aimed to investigate the anti-diabetic effect of HES and the underlying molecular mechanism of action. We hypothesized that HES exerts its anti-diabetic effects by restoring the expression of genes related to insulin signaling and glucose metabolism to normal level in the liver of HFD-induced obese mice. To test this hypothesis, we evaluated the effects of HES on glucose uptake and the modulation of the insulin signaling pathway in PA-treated HepG2 cells and on glucose and insulin tolerance in HFD-induced obese mice. In particular, to investigate the molecular mechanism underlying anti-diabetic effects, differential gene expression in the liver of HFD-induced obese mice was analyzed (Fig. 21).

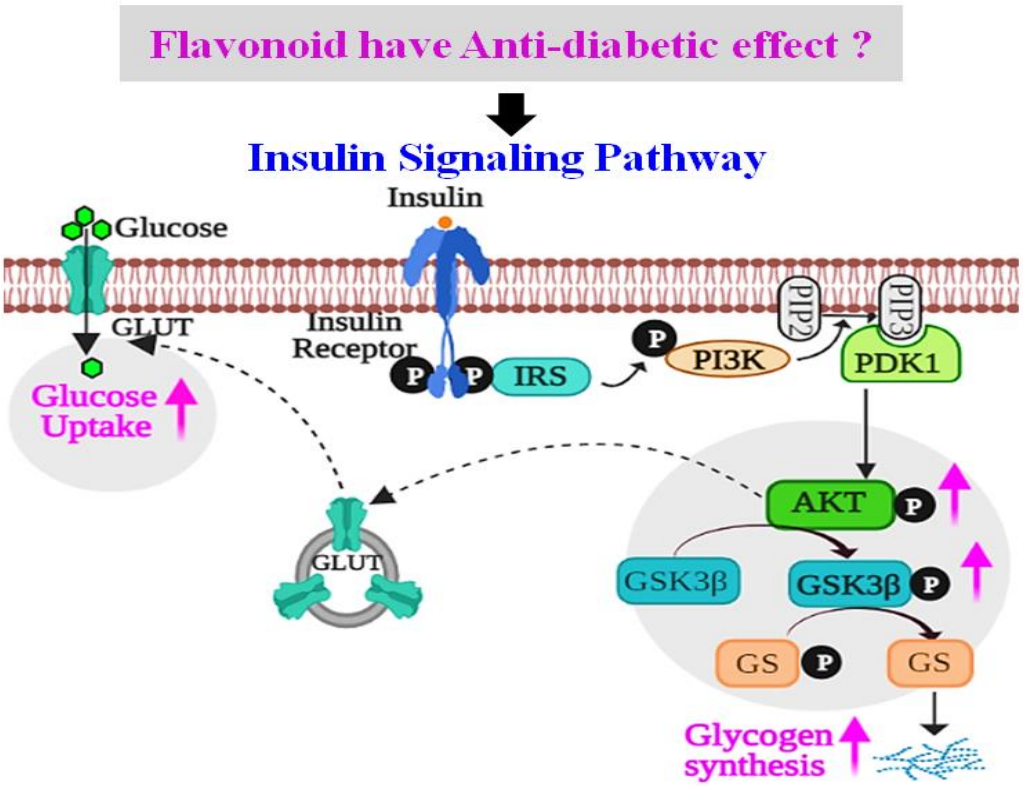

Fig. 21. Hypothetical model for anti-diabetic effect of HES

2.3. Materials and Methods

2.3.1. Materials and chemicals

Human hepatoma HepG2 cell line was obtained from the Korean Cell Line Bank (KCLB, South Korea). Dulbecco's Modified Eagle's Medium (DMEM) and fetal bovine serum (FBS) were obtained from Gibco (USA). HES was obtained from LKT laboratories (USA). PA, metformin (MET), human insulin, and bovine serum albumin (BSA) were purchased from Sigma Aldrich (USA). 2-[N-(7-Nitrobenz-2-oxa-1,3-diazol-4-yl)amino]-2-deoxy-d-glucose (2-NBDG) was purchased from Invitrogen (CA, USA). Antibodies against p-Akt, Akt, p-GSK3β, GSK3, hexokinase-II, enolase-1, and PI3 Kinase p110 δ were purchased from Cell Signaling Technology (USA). EZ-Western Lumi Pico was purchased from DoGenBio (South Korea). All other reagents were purchased from commercial sources and were of analytical grade or higher.

2.3.2. Cell culture and treatment

Human hepatoma HepG2 cells were cultured in DMEM supplemented with 10% FBS and 1% penicillin and streptomycin in a humidified atmosphere at 37 °C under 5% CO_2. HepG2 cells were seeded in 96-well plates. After reaching confluence, cells were serum-deprived overnight and exposed to 0.4 mM PA in the presence or absence of MET (2 mM) and HES (10 or 50 μM) for 24 h. Cells treated with MET were used as the positive control (Fig. 22).

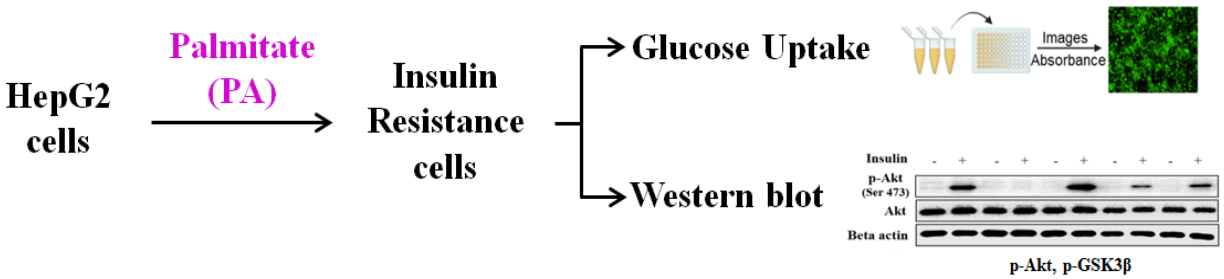

Fig. 22. HepG2 cell culture and treatment

2.3.3. Preparation of PA

A PA-BSA conjugate was prepared as described previously [95]. Briefly, a PA stock (25 mM) was diluted in NaOH (50 mM) at 70 °C for 30 min and mixed with 10% BSA at 55 °C for 15 min, forming a 5 mM reserving solution. This solution was mixed in serum-free DMEM to obtain the final 0.4 mM PA solution.

2.3.4. 2-NBDG uptake assay

Glucose uptake in HepG2 cells was monitored using a 2-NBDG assay, as previously described [96]. After treatment (as described in section 2.3.2.), cells were exposed to 40 μM 2-NBDG in the presence or absence of insulin (100 nM) for 30 min at 37 °C. Cells were rinsed with phosphate buffer saline (PBS), and fluorescence images were captured using IncuCyte ZOOM (Essen BioScience, USA) at 20× magnification. Fluorescence analysis was performed using the IncuCyte ZOOM Fluorescent Processing software.

2.3.5. Preparation of cell lysates and Western blot analysis

After treatment (as described in section 2.3.2.), cells were stimulated with or without 100 nM insulin for 30 min before harvesting. Cells were rinsed with PBS and lysed with ice-cold RIPA buffer (20 mM Tris-HCl pH 7.5, 150 mM NaCl, 1 mM EGTA, 1 mM Na_2EDTA, 1% NP-40, 1% sodium deoxycholate, 2.5 mM sodium pyrophosphate, 1 mM $NaVO_4$, 1μg/mL leupeptin) containing a protease inhibitor. The whole-cell lysate was centrifuged at 12,000 rpm for 10 min, and supernatants were collected and assayed for protein concentration using the Bradford assay kit (Bio-Rad Laboratories, USA). For western blotting, equal amounts of protein were separated using 10% sodium dodecyl sulphate-polyacrylamide gel electrophoresis (SDS-PAGE) and transferred to a nitrocellulose membrane. Membranes were blocked with 5% non-fat dry milk in Tris-buffered saline containing 0.1% Tween 20. Membranes were incubated with the respective primary antibodies followed by incubation with horseradish peroxidase-conjugated secondary antibodies. Immunoreactive bands were analyzed using a chemiluminescence bioimaging instrument (NeoScience, Korea). Densitometric analysis was performed using ImageJ analysis software.

2.3.6. Animals

Five-week-old male mice (C57BL/6) weighing 18–23 g were obtained from Orient Bio (Korea). The mice were maintained in cages at regular temperature (21 °C) and humidity (45% ± 10%) and subjected to cycles of 12-hour light and dark for one week before initiation of experiments. All experiments were performed in accordance with the experimental animal guidelines of the Jeju National University Animal Center and were approved by the Animal Care and Use Committee (IACUC) of Jeju National University, Jeju, Korea (approval number: 2020-0047).

2.3.7. Sample treatment

C57BL/6 mice were randomly divided into four groups (n=5) and fed the respective experimental diets for 10 weeks. The normal group received normal chow diet (4.8% (w/w) fat); the HFD group received high fat diet (60% (w/w) fat); the MET group received high fat diet supplemented with metformin (100 mg/kg body weight); and the HES group received high fat diet supplemented with hesperidin (100 mg/kg body weight). The samples were administered orally and mice were given *ad libitum* access to food and water. Sample treatment was continued for 10 weeks. At the end of the experiment, the mice were fasted overnight and sacrificed. Blood was collected and stored at −80 °C for further analysis (Fig. 23).

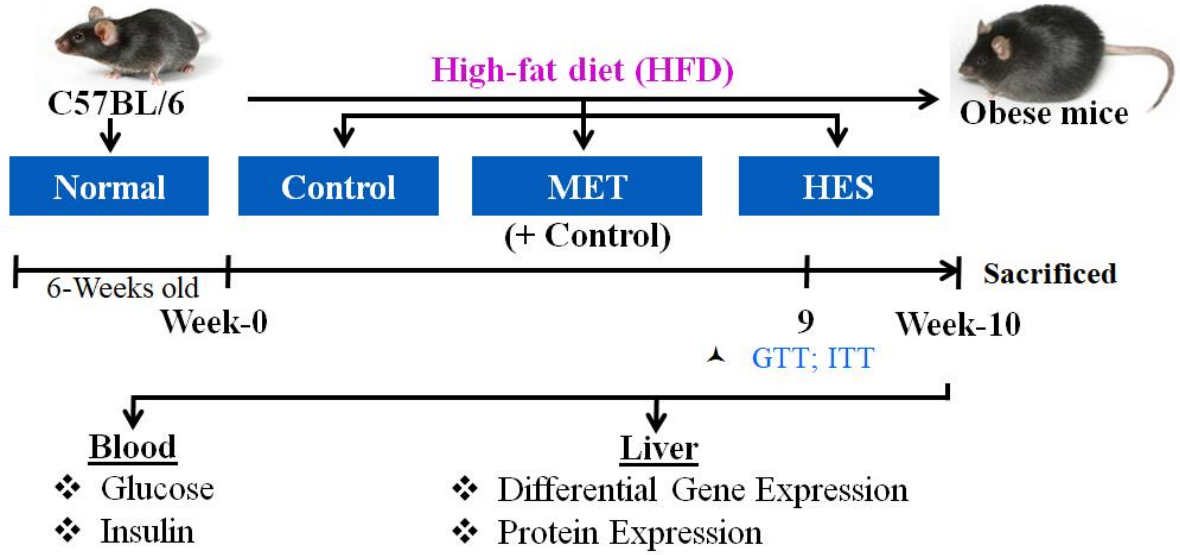

Fig. 23. Experimental design of the animal study

2.3.8. Intraperitoneal glucose tolerance test (IPGTT)

After 8 weeks of treatment, mice were fasted for 14 h before administration of glucose. Mice were intraperitoneally injected with glucose (1g/kg body weight). Blood glucose levels were measured using a blood glucose monitor (Lipidpro, OSANG healthcare, Korea) and blood samples from the tail vein at 0, 30, 60, 90, and 120 min after the injection.

2.3.9. Intraperitoneal insulin tolerance test (IPITT)

After 8 weeks of treatment, mice were fasted for 6 h before administration of insulin. Human insulin (1 IU/kg body weight) was injected intraperitoneally. Blood glucose levels were measured at different time points (0, 30, 60, 90, and 120 min) after the injection.

2.3.10. Blood glucose, serum insulin, and HOMA-IR

Blood glucose levels were measured at the end of treatments using blood collected from the tail of mice fasted for 14 h. The concentrations of blood glucose were determined using a blood glucose monitor (Lipidpro, OSANG healthcare, Korea). Fasting serum insulin levels were determined using an ELISA kit (Crystal Chem, USA) according to the manufacturer's instructions. The homeostatic model assessment for insulin resistance (HOMA-IR) was calculated using fasting insulin and glucose values as follows: [glucose (mg/dL) × insulin (μU/mL)]/405.

2.3.11. RNA isolation, library preparation, sequencing, and data analysis

RNA sequencing analysis was performed as previously described [97–99]. Total RNA was isolated from liver tissues using an Easy-blue RNA extraction kit (iNtRON Biotechnology, Korea). The RNA quality was assessed using an Agilent 2100 bioanalyzer and an RNA 6000 Nano Chip (Agilent Technologies, Netherlands). Based on the manufacturer's instructions, libraries for RNAs were constructed using a Quantseq 3′ mRNA-Seq Library Prep Kit (Lexogen, Austria). High-throughput sequencing was performed as single-end 75 sequencing using NextSeq 500 (Illumina, USA). QuantSeq 3′ mRNA-Seq reads were aligned using Bowtie2 version 2.1.0 [100]. Differentially expressed genes were determined based on counts from unique and multiple alignments using EdgeR within R version 3.2.2 and Bioconductor version 3.0 [101]. The read count data were processed based on the quantile normalization method using Genowiz™ version 4.0.5.6 (Ocimum Biosolutions, India). Gene classification was achieved using the Medline database (National Centre for Biotechnology Information, USA) (Fig. 24).

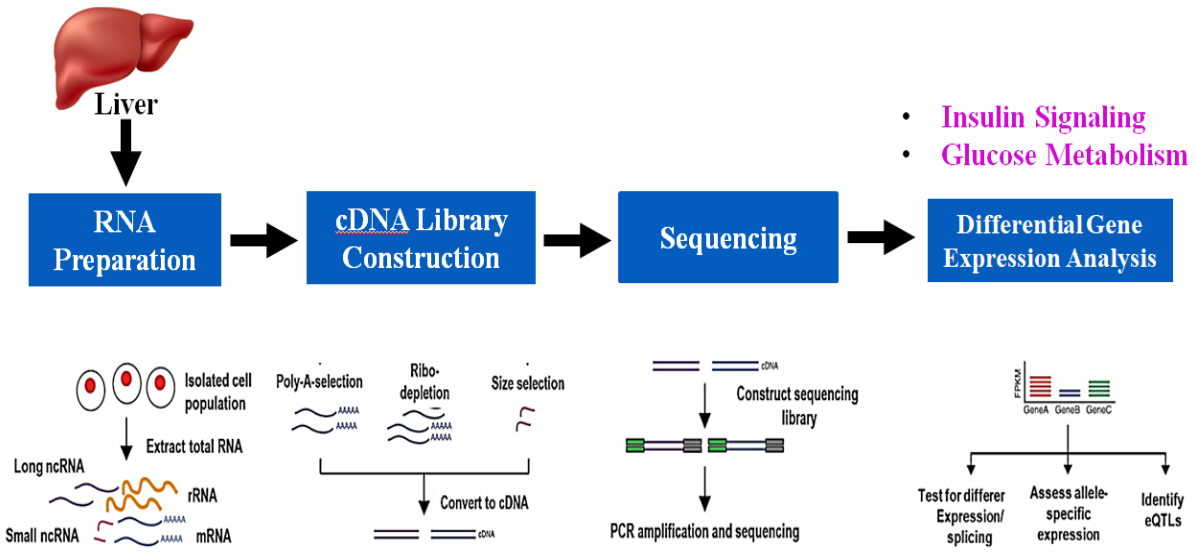

Fig. 24. Process of RNA sequencing analysis

2.3.12. Statistical analysis

Data are expressed as the mean ± standard error (SE) and were statistically analyzed using IBM SPSS Statistics (Ver.17.0; USA). Statistical differences among groups were analyzed with one-way analysis of variance (ANOVA) followed by Tukey's test. Differences were considered statistically significant at $p < 0.05$.

2.4. Results

2.4.1. Glucose uptake

The effects of HES on glucose uptake in PA-treated HepG2 cells were analyzed using a 2-NBDG assay (Fig. 25). Glucose uptake was reduced in PA-treated HepG2 cells compared with the control (Fig. 25A and B). In contrast, the treatment with MET (positive control) significantly increased ($p < 0.005$) the glucose uptake compared with PA-treated control cells. Particularly, treatment with HES significantly enhanced ($p < 0.005$) glucose uptake compared to PA-treated control cells regardless of insulin stimulation. These results suggest that HES improves glucose uptake in an insulin-independent manner in PA-treated HepG2 cells.

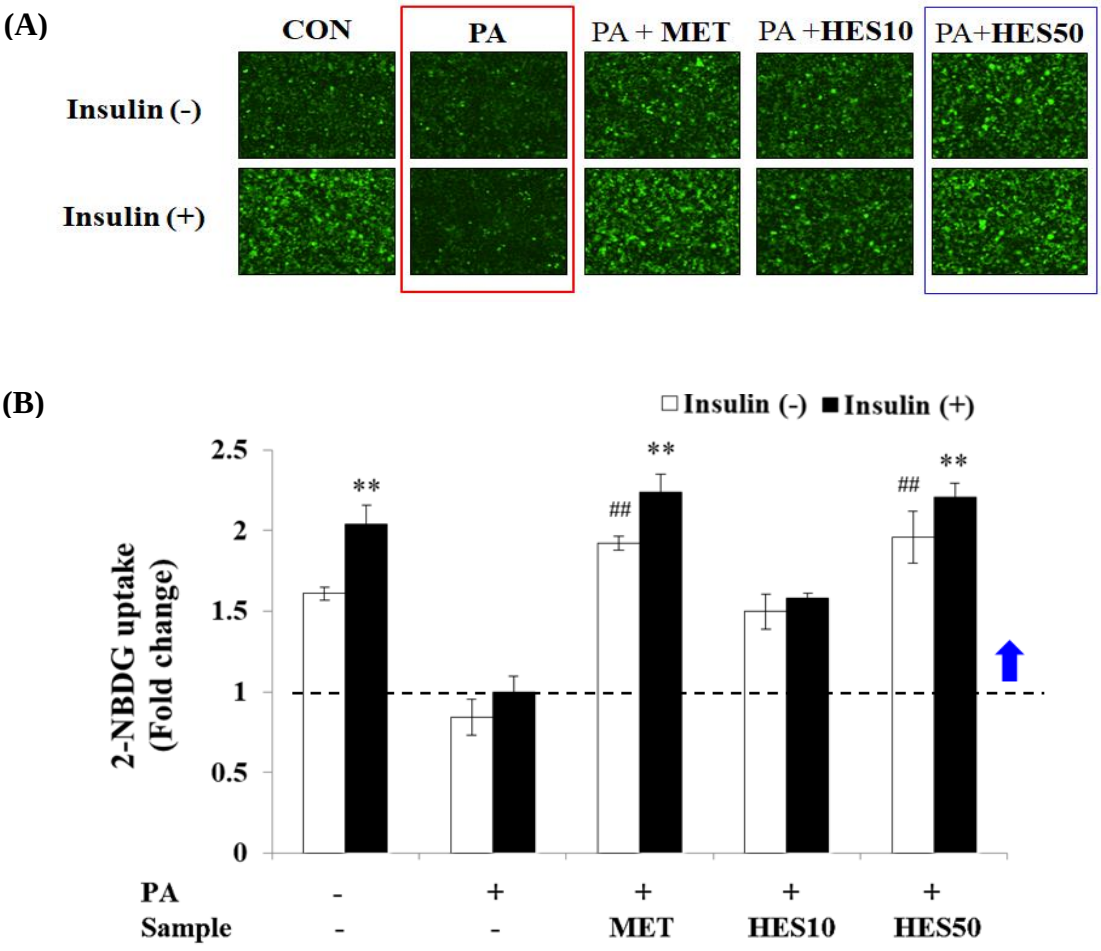

Fig. 25. Effects of HES on glucose uptake in PA-treated HepG2 cells.

The glucose uptake assay was performed using the fluorescent D-glucose analogue 2-NBDG. Serum starved HepG2 cells were treated with different samples for 24 h, followed by incubation with 2-NBDG in the presence or absence of insulin for 30 min. Cells were rinsed with PBS, and the fluorescence images were captured using IncuCyte ZOOM at 20× magnification (A). Total fluorescence intensities were calculated using the IncuCyte ZOOM fluorescence processing software (B). Data are presented as the mean ± SE. $^{**}p < 0.005$ compared with the insulin-stimulated PA-treated control; $^{\#\#}p < 0.005$ compared with the non-insulin-stimulated PA-treated control group.

2.4.2. Insulin signaling pathway

Western blot analysis was performed to observe the effect of HES on the phosphorylation levels of key enzymes involved in the insulin signaling pathway (Fig. 26). Based on densitometry analysis, PA-treated HepG2 cells did not show insulin-stimulated phosphorylation of Akt and GSK3β (Fig. 26A and B). In contrast, cells treated with MET showed a significant increase in ($p < 0.0005$) the insulin-stimulated phosphorylation of Akt and GSK3β compared with PA-treated control cells. Similarly, HES remarkably increased ($p < 0.0005$) the insulin-stimulated phosphorylation of Akt and GSK3β compared to PA-treated control cells. These results suggest that HES restores insulin sensitivity by increasing insulin-mediated phosphorylation of Akt and GSK3β in PA-treated HepG2 cells.

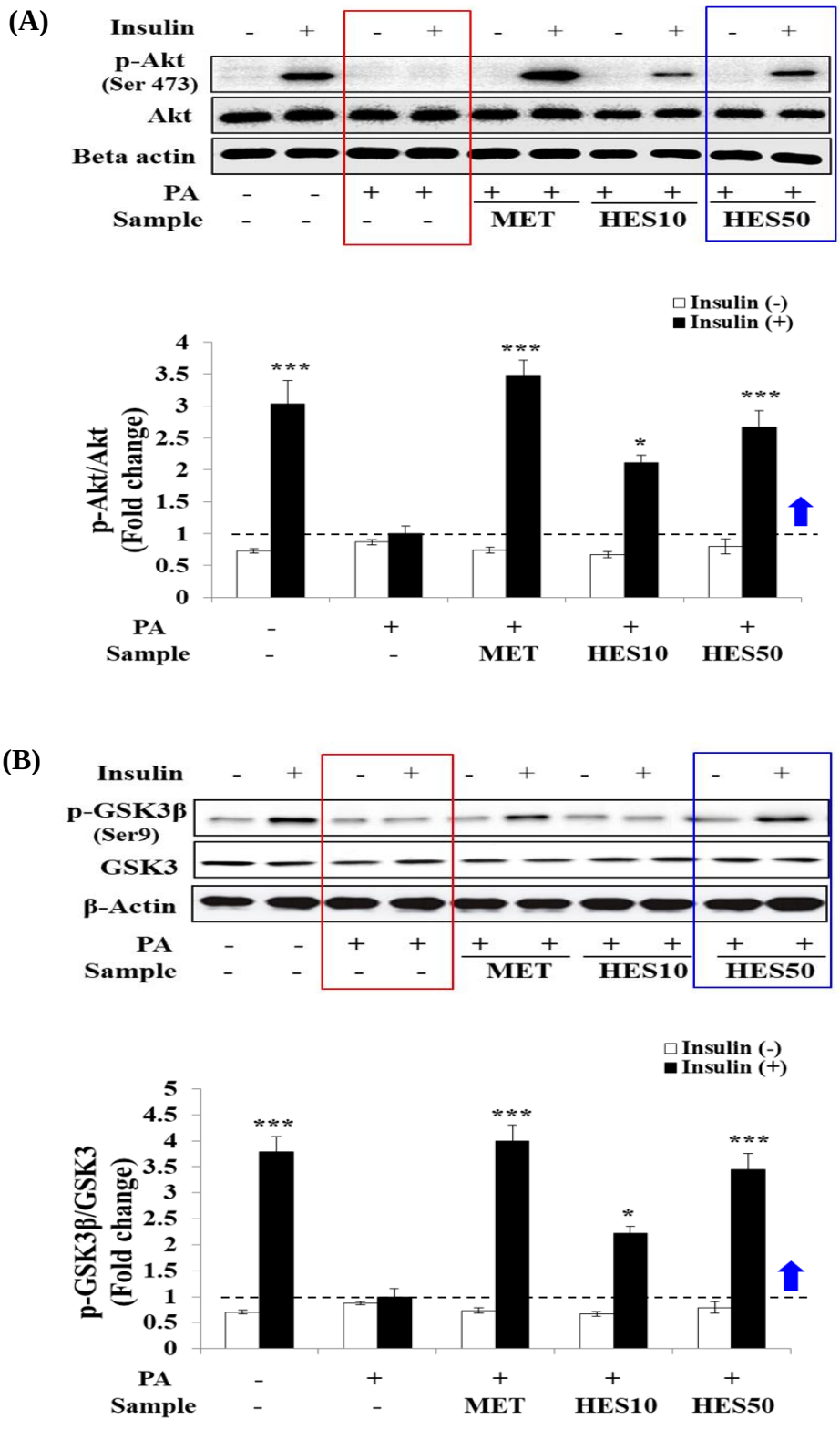

Fig. 26. Effects of HES on the phosphorylation levels of Akt and GSK3β in PA-treated HepG2 cells.

Serum starved HepG2 cells were treated with different samples for 24 h, followed by incubation with or without insulin for 30 min. Western blot analysis of p-Akt (A) and p-GSK3β (B). Data are presented as the mean ± SE. *$p < 0.05$, ***$p < 0.0005$ compared with the PA-treated control group.

2.4.3. Glucose tolerance

To evaluate the effect of HES on glucose tolerance, an IPGTT was performed in HFD-induced obese mice eight weeks after treatment with HES (Fig. 27). After the injection of glucose, the normal mice restored normal blood glucose levels 60 min after glucose injection, whereas HFD-induced obese control mice did not restore normal levels up to 120 min after injection (Fig. 27A and B). However, treatment of HFD-induced obese mice with MET showed significantly reduced ($p < 0.05$) blood glucose levels and area under the curve (AUC) values compared with HFD-induced obese control mice. Moreover, HES treated HFD-induced obese mice showed significantly decreased ($p < 0.05$) blood glucose levels and AUC values at the end of the tests compared to HFD-induced obese control mice. These results demonstrated that HES improves glucose tolerance in HFD-induced obese mice.

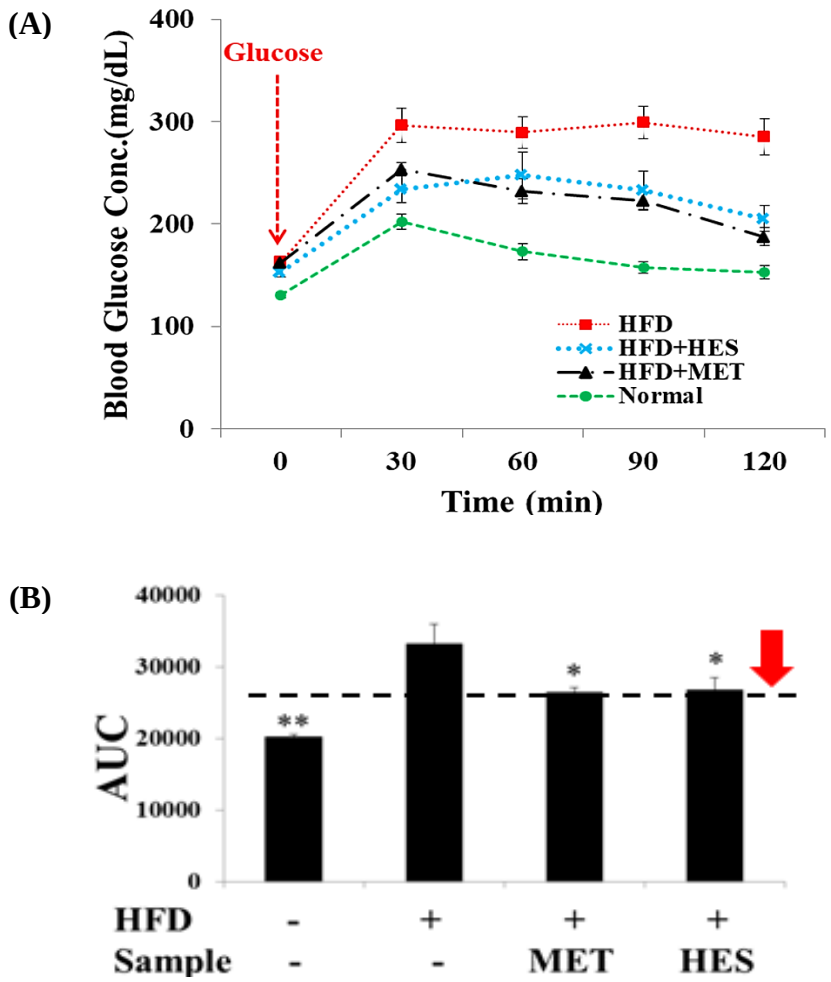

Fig. 27. Effect of HES on glucose tolerance in HFD-induced obese mice.

IPGTT was performed eight weeks after administration of samples to HFD-induced obese mice. Mice were fasted for 14 h and blood glucose levels were measured at 0, 30, 60, 90, and 120 min after intraperitoneal injection of glucose (1g/kg body weight). Blood glucose profile during IPGTT (A) and AUCs (B). Data are represented as the mean ± SE. *$p < 0.05$, **$p < 0.005$ compared with the HFD-induced obese control group.

2.4.4. Insulin sensitivity

To evaluate the effect of HES on insulin sensitivity in HFD-induced obese mice, an IPITT was performed eight weeks after treatment with HES (Fig. 28). Normal mice maintained normal blood glucose levels after insulin injection, whereas HFD-induced obese control mice showed elevated blood glucose levels 60 min after insulin injection (Fig. 28A and B). However, MET treated mice showed higher rates of blood glucose disappearance and exhibited significantly reduced ($p < 0.0005$) AUC values. Particularly, treating HFD-induced obese mice with HES showed significantly reduced ($p < 0.005$) blood glucose levels and AUC values compared to HFD-induced obese control mice. These results indicate that HES significantly improves insulin sensitivity in HFD-induced obese mice.

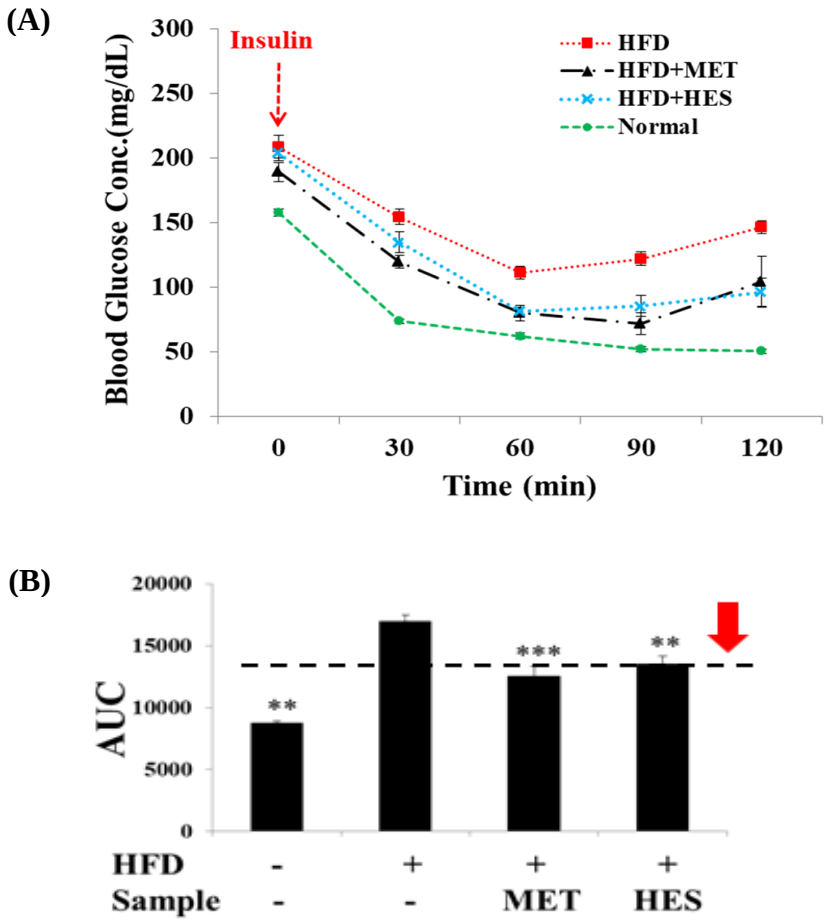

Fig. 28. Effect of HES on the insulin tolerance in HFD-induced obese mice.

An IPITT was performed eight weeks after administration of samples to HFD-induced obese mice. Mice fasted for 6 h and blood glucose levels were measured at 0, 30, 60, 90, and 120 min after insulin injection. Blood glucose profile during IPITT (A) and AUCs (B). Data are represented as the mean ± SE. $^{**}p < 0.005$, $^{***}p < 0.0005$ compared with the HFD-induced obese control group.

2.4.5. Serum parameters

To observe the effect of HES on insulin resistance, both fasting blood glucose and insulin levels were measured and the HOMA-IR index was calculated (Fig. 29). The results demonstrated that HFD-induced obese control mice showed significantly higher fasting blood glucose levels ($p < 0.005$) and serum insulin levels ($p < 0.0005$) than those of normal mice (Fig. 29A-C). However, the treatment of HFD-induced obese mice with MET showed significantly decreased values of blood glucose ($p < 0.05$), serum insulin ($p < 0.0005$), and HOMA-IR index ($p < 0.0005$) compared to HFD-induced obese control mice. Similarly, HES treatment significantly decreased the blood glucose ($p < 0.05$), serum insulin ($p < 0.0005$), and HOMA-IR values ($p < 0.0005$) in HFD-induced obese mice. These results indicate that treatment with HES for ten weeks improves insulin sensitivity in HFD-induced obese mice.

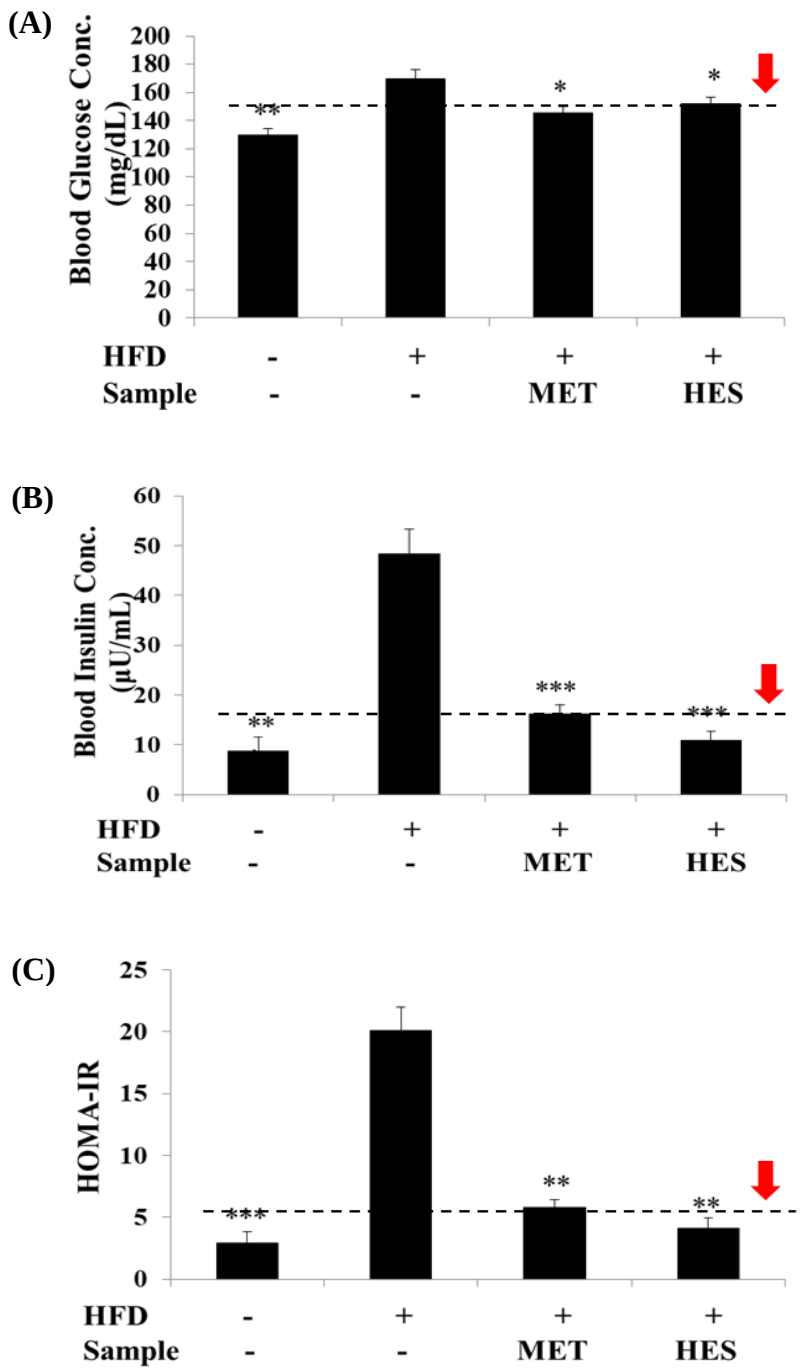

Fig. 29. Effect of HES on insulin resistance in HFD-induced obese mice.

Fasting blood glucose (A), and serum insulin (B) were evaluated 10 weeks after administration of samples to HFD-induced obese mice. HOMA-IR (C) was calculated as follows: [fasting glucose (mg/dL) × fasting insulin (μU/mL)]/405. Data are represented as the mean ± SE. *$p < 0.05$, **$p < 0.005$, ***$p < 0.0005$ compared with the HFD-induced obese control group.

2.4.6. Differential gene expression

RNA sequencing analysis was performed to determine the effect of HES on the expression levels of genes related to insulin signaling and glucose metabolism in the liver of HFD-induced obese mice liver (Fig. 30). The functional annotation of genes was performed through gene ontology (GO) analysis. As shown in Fig. 30A and B, a large proportion of the genes in insulin signaling and glucose metabolism was altered in HES-treated and control HFD-induced obese control mice as compared with normal mice. The expression levels of the twelve up-regulated (> 2-fold) genes (including *Eno1*, *Pik3cd*, *Hk2*, and *Trib3*) and six down-regulated (< 0.6-fold) genes (including *Myc*, *Nos3*, *Ppargc1a*, and *Igf2*) were normalized to normal level by HES treatment (Table 2 and 3). To understand the relationship between these genes, a protein-protein interaction (PPI) network was established using STRING analysis and visualized as nodes and edges (Fig. 30C). The normalized up-regulated genes including *Eno1*, *Pik3cd*, *Hk2*, and *Trib3* were closely located and interacted directly with each other within the PPI network. In addition, normalized down-regulated genes including *Myc*, *Nos3*, *Ppargc1a*, and *Igf2* were closely located and formed a functional hub in the PPI network. Overall, these results suggest that HES improves insulin sensitivity and glucose tolerance by normalizing the expression of genes related to insulin signaling pathway and glucose metabolism in the liver of HFD-induced obese mice.

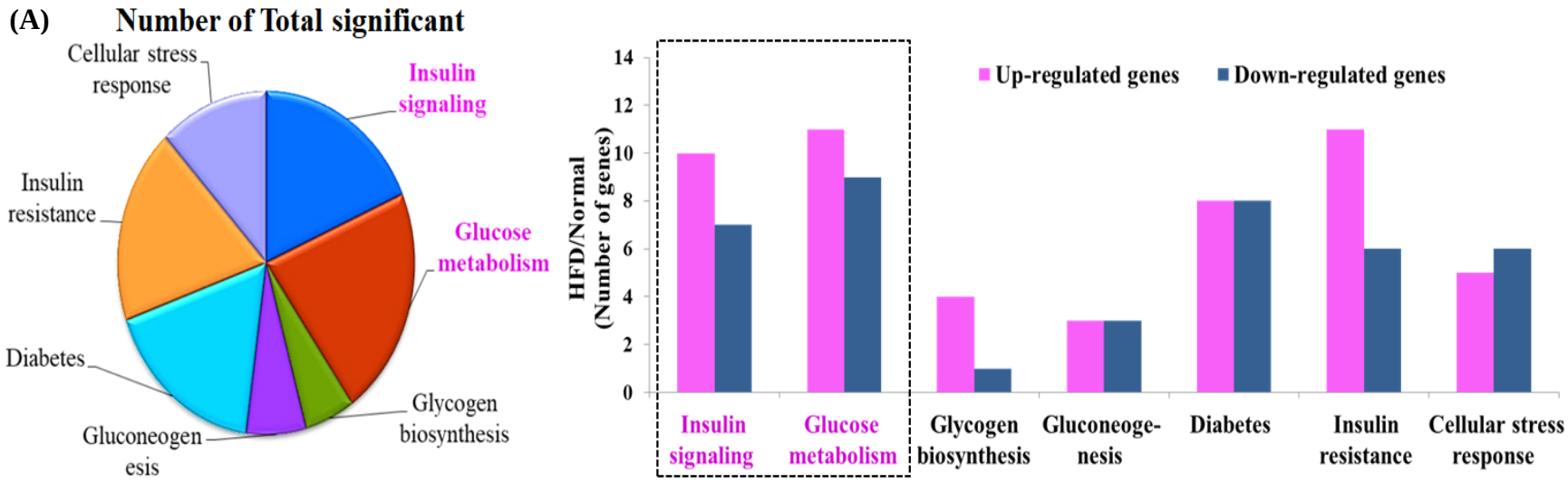

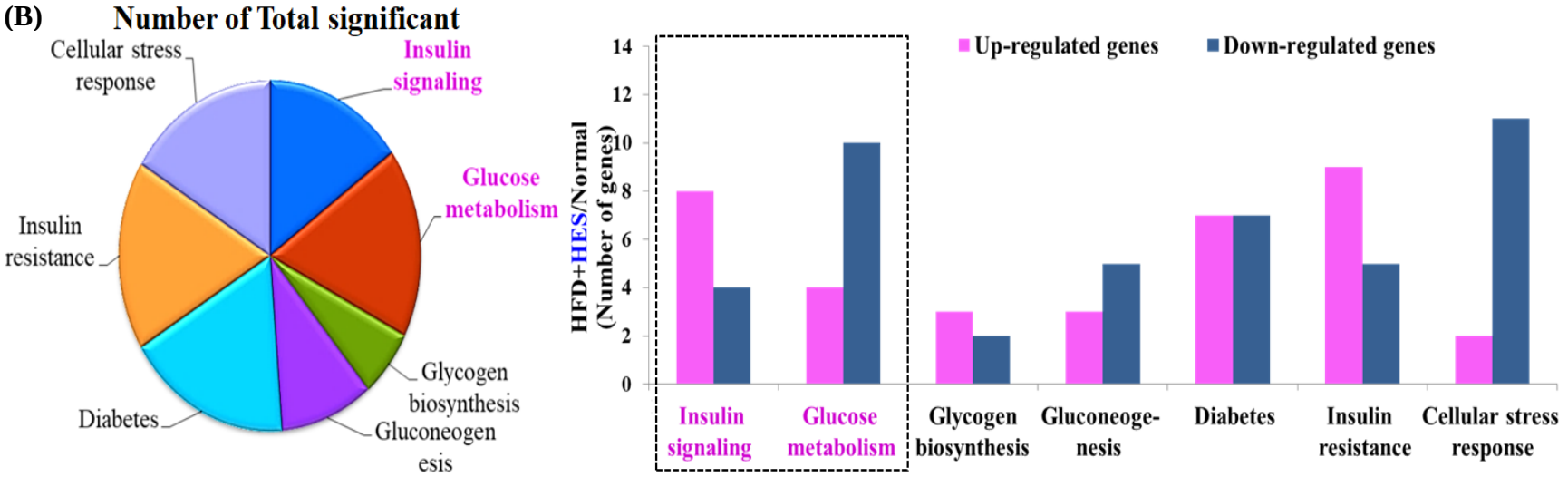

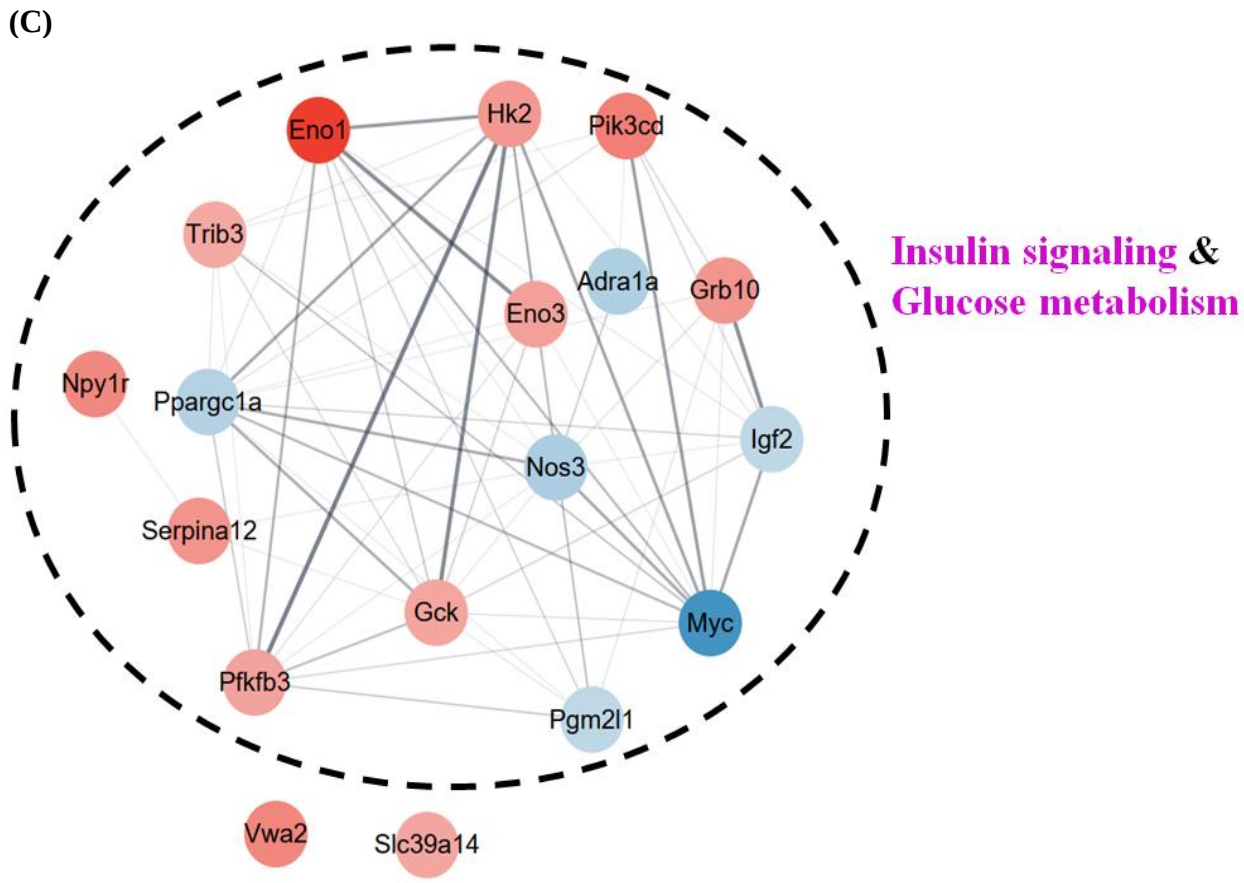

Fig. 30. Effect of HES on the differential expression of genes in the liver of HFD-induced obese mice.

GO analysis of HFD-induced obese control mice compared with normal mice (A) and HES-treated HFD-induced obese mice compared with normal mice (B). The pie chart indicates functional categorization of the differentially expressed genes in HFD-induced obese mice liver. The bar graph represents the number of genes up- or down-regulated. PPI network of normalized genes related to glucose metabolism and insulin signaling in HES-treated HFD-induced obese mice (C). Red circles represent up-regulated genes and blue circles represent down-regulated genes in HFD-induced obese control mice that were restored to normal level after HES treatment.

Table 2. Up-regulated genes related to insulin signaling and glucose metabolism in HFD-induced obese mice liver that were normalized by HES

Gene symbol	HFD/ Normal	HFD+MET/ Normal	HFD+HES/ Normal	Gene name
Eno1	5.644	0.999	**0.982**	Enolase 1
Pik3cd	3.053	0.768	**1.352**	Phosphatidylinositol 3-kinase
Vwa2	2.850	0.999	**0.989**	Von Willebrand factor A 2
Npy1r	2.794	2.056	**0.980**	Neuropeptide Y receptor Y1
Serpina12	2.499	1.959	**1.332**	Serine (or cysteine) peptidase inhibitor
Grb10	2.468	1.511	**1.236**	Growth factor receptor bound protein
Hk2	2.401	0.962	**0.791**	Hexokinase 2
Eno3	2.240	1.433	**1.223**	Enolase 3
Pfkfb3	2.186	2.774	**1.322**	6-Phosphofructo-2-kinase
Gck	2.133	1.405	**1.215**	Glucokinase
Slc39a14	2.111	1.941	**1.441**	Solute carrier family 39
Trib3	2.081	1.035	**1.297**	Tribbles pseudokinase 3
Slc2a2	1.963	2.477	**2.423**	Solute carrier family 2

The values shown are normalized relative to those of the normal group. HFD, high fat diet; MET, metformin; HES, hesperidin.

Table 3. Down-regulated genes related to insulin signaling and glucose metabolism in HFD-induced obese mice liver that were normalized by HES

Gene symbol	HFD/ Normal	HFD+MET/ Normal	HFD+HES/ Normal	Gene name
Myc	0.171	0.222	**0.925**	Myelocytomatosis oncogene
Nos3	0.486	0.646	**0.791**	Nitric oxide synthase 3
Adra1a	0.493	1.448	**1.245**	Adrenergic receptor
Ppargc1a	0.521	0.902	**0.903**	peroxisome proliferative activated receptor
Igf2	0.576	0.391	**1.000**	Insulin-like growth factor 2
Pgm2l1	0.577	0.985	**0.999**	Phosphoglucomutase 2-like 1

The values shown are normalized relative to those of the normal group. HFD, high fat diet; MET, metformin; HES, hesperidin.

2.4.7. Protein expressions

Western blot analysis was performed to evaluate the effect of HES on the expression levels of hexokinase-II, enolase-1, and PI3 kinase p110δ in the liver of HFD-induced obese mice (Fig. 31). The expression of these proteins was significantly ($p < 0.0005$) increased in HFD-induced obese mice compared with normal mice (Fig. 31A-C). Treatment of HFD-induced obese mice with HES normalized ($p < 0.005$) the expression levels to normal level. These results further confirm that HES improves insulin sensitivity and glucose tolerance by normalizing the expression levels of proteins involved in insulin signaling pathway and glucose metabolism in the liver of HFD-induced obese mice.

(A)

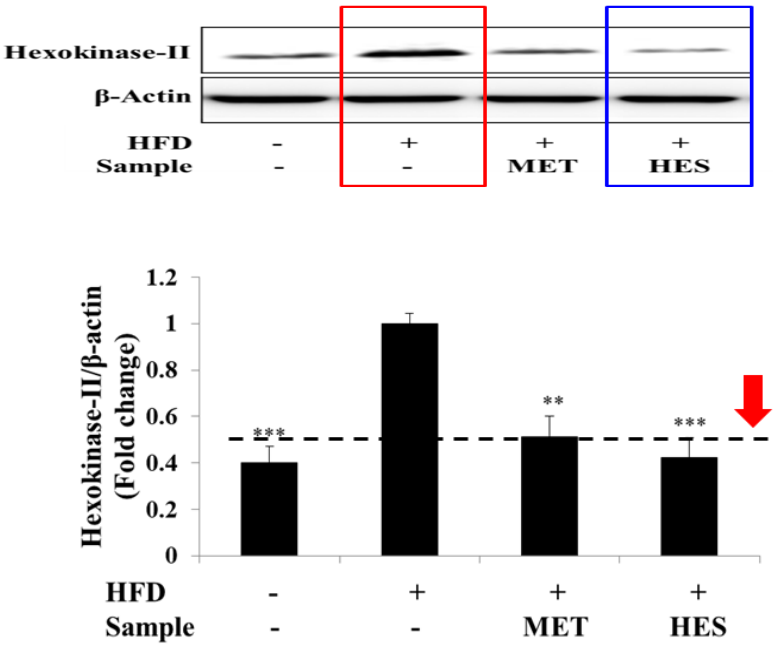

(B)

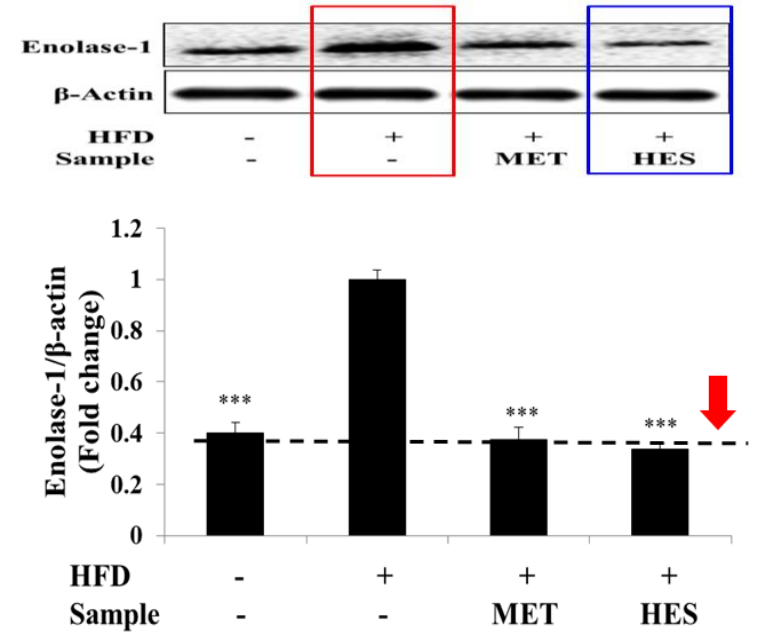

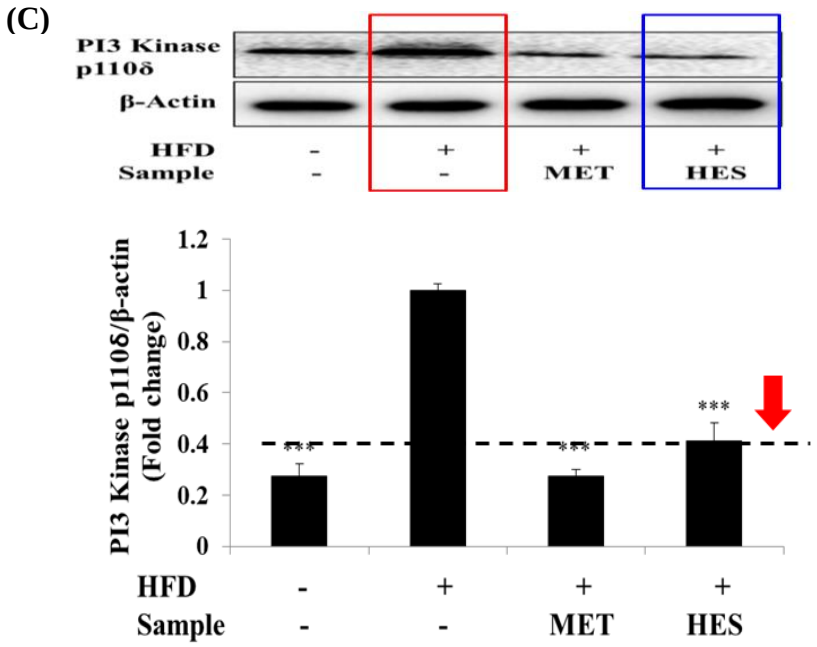

Fig. 31. Effects of HES on the expression levels of hexokinase-II, enolase-1, and PI3 kinase p110δ in the liver of HFD-induced obese mice.

Western blot analysis of hexokinase-II (A), enolase-1 (B), and PI3 kinase p110δ (C) expressions in the liver of HFD-induced obese mice. Data are presented as the mean ± SE. $^{**}p < 0.005$, $^{***}p < 0.0005$ compared with the HFD-induced obese control group.

2.5. Discussion

The present study investigated the molecular mechanism underlying the anti-diabetic effect of HES on insulin-resistant PA-treated HepG2 cells and HFD-induced obese mice. The results demonstrated that HES treatment enhanced the 2-NBDG uptake in an insulin-independent manner and increased the phosphorylation levels of Akt and GSK3β in insulin-resistant PA-treated HepG2 cells. The supplementation of HES to HFD-induced obese mice reduced serum insulin, blood glucose, and HOMA-IR values, and improved both glucose tolerance and insulin sensitivity. In addition, RNA sequencing analysis disclosed that HES normalized the expression levels of genes related to insulin signaling and glucose metabolism including *Eno1*, *Pik3cd, Hk2*, *Trib3*, *Myc*, *Nos3*, *Ppargc1a*, and *Igf2* in the liver of HFD-induced obese mice. Furthermore, HFD-induced obese mice treated with HES normalized the expression levels of proteins including hexokinase-II, enolase-1, and PI3 kinase p110δ, which are involved in the insulin signaling and glucose metabolism (Fig. 32).

The current study revealed that HES stimulates glucose uptake regardless of insulin stimulation in PA-treated HepG2 cells. Hepatic glucose uptake is catalyzed by a family of glucose transport proteins and is mostly an insulin-independent process [102]. The glucose transporter GLUT-2 is highly expressed in the liver and is responsible for glucose transport regardless of insulin stimulation [103]. A previous study has reported that HES enhances glucose uptake by increasing the expression of GLUT-2 in lipopolysaccharide-induced insulin-resistant HepG2 cells [104]. Therefore, the enhanced glucose uptake mediated by HES, independent of insulin stimulation, observed in this study may result from increased GLUT-2 expression in PA-

treated HepG2 cells. Indeed, we also observed that the expression of *slc2a2*, which encodes GLUT-2, was enhanced by HES in the liver of HFD-induced obese mice (Table 2).

In the present work, HES increased the insulin-stimulated phosphorylation of Akt and GSK3β in insulin-resistant PA-treated HepG2 cells. Akt is an important mediator of insulin signaling and its phosphorylation in response to insulin is crucial for glycogen synthesis via phosphorylation of GSK3β [105, 106]. A previous study has reported that nobiletin, a polymethoxylated flavone, alleviates insulin resistance by increasing the insulin-stimulated phosphorylation of Akt and GSK3β in insulin-resistant PA-treated HepG2 cells [107]. Therefore, the present finding suggests that HES improves insulin resistance via increasing the phosphorylation of Akt and GSKβ in PA-treated HepG2 cells.

The present study observed that treatment with HES reduced serum insulin, blood glucose, and HOMA-IR values and improved glucose tolerance and insulin sensitivity in HFD-induced obese mice. A previous study has reported that HES improves insulin resistance in goto-kakizaki rats with T2DM [93]. In addition, HES prevents hyperglycemia by improving insulin sensitivity in HFD-induced insulin-resistant rat [94]. Consistent with these previous studies, the present study results suggest that HES prevents hyperglycemia by improving insulin sensitivity in HFD-induced obese mice.

In the current investigation, RNA sequencing analysis revealed that HES normalizes the expression levels of genes related to insulin signaling and glucose metabolism in the liver of HFD-induced obese mice. The results showed that HES normalized genes that were up-regulated in HFD-induced obese mice, including *Eno1*, *Pik3cd*, *Hk2*, and *Trib3*. *Eno1* converts 2-phosphoglycerate to phosphoenolpyruvate and its upregulation leads to hyperglycemia in

diabetic mice [(108,109)29, 30]. *Pik3cd* plays a major role in B-cell activation and its overexpression induces B-cell mediated autoimmune inflammation, which leads to insulin resistance in obese mice and humans [110, 111]. *Hk2* is the first rate-limiting enzyme in glycolysis [112] and its overexpression leads to metabolic dysfunction and the development of insulin resistance in diabetic human [112, 113]. In addition, *Trib3* inhibits the insulin-mediated activation of Akt and its up-regulation contributes to hyperglycemia and insulin resistance in db/db diabetic mice [114]. Therefore, the results of the present study suggest that HES restores insulin sensitivity and glucose clearance by normalizing the expression of these genes in HFD-induced obese mice.

The present study showed that HES also normalizes the expression levels of genes involved in insulin signaling and glucose metabolism that were downregulated in the liver of HFD-induced obese mice, including *Myc*, *Nos3*, *Ppargc1a*, and *Igf2*. *Myc* plays a crucial role in enhancing glucose uptake by increasing the expression of GLUT-2; its downregulation leads to hyperglycemia in the liver of HFD-induced obese mice [115, 116]. *Nos3* is involved in regulation of nitric oxide (NO) metabolism; decreased NO bioavailability leads to diabetes in humans and mice [117–119]. *Ppargc1a* is a key protein in the insulin-mediated suppression of hepatic glucose production; its dysregulation is associated with insulin resistance in patients with diabetes [120, 121]. *Igf2* is involved in the regulation of the PI3K/Akt signaling pathway; its dysregulation is associated with insulin resistance [122]. Therefore, the obtained results suggest that HES restores insulin sensitivity and glucose tolerance by normalizing the expression of *Myc*, *Nos3*, *Ppargc1a*, and *Igf2* in HFD-induced obese mice.

The present study further confirmed that HES normalizes the expression levels of proteins including hexokinase-II, enolase-1, and PI3 kinase p110δ, which are involved in the

insulin signaling and glucose metabolism in the liver of HFD-induced obese mice. In a previous study, normalization of hexokinase-II protein levels by hesperetin restored glucose metabolism in high glucose-treated endothelial cells [123]. In other studies, inhibition of enolase-1 by enolase binding molecule alleviated hyperglycemia in db/db diabetic mice [109] and inhibition of PI3 kinase p110δ by its inhibitor stopped the progression of autoimmune diabetes in diabetic mice [110]. In this regard, the present finding provides additional evidence to prove that the beneficial effect of HES on insulin sensitivity and glucose clearance results from the normalization of protein expression in HFD-induced obese mice.

In conclusion, the present study suggests that HES improves glucose uptake in an insulin-independent manner and exerts an insulin-sensitizing effect by increasing insulin-mediated phosphorylation of Akt and GSK3β in PA-treated HepG2 cells. Furthermore, HES improves insulin sensitivity and glucose tolerance in HFD-induced obese mice. This effect results from the normalization of the expression of genes (including *Eno1*, *Pik3cd*, *Hk2*, *Trib3*, *Myc*, *Nos3*, *Ppargc1a*, and *Igf2*) and proteins (including hexokinase-II, enolase-1, and PI3 kinase p110δ) which are altered in HFD-induced obese mice (Fig. 33). Hence, the overall results evidenced that HES possess a promising therapeutic solution for diabetes.

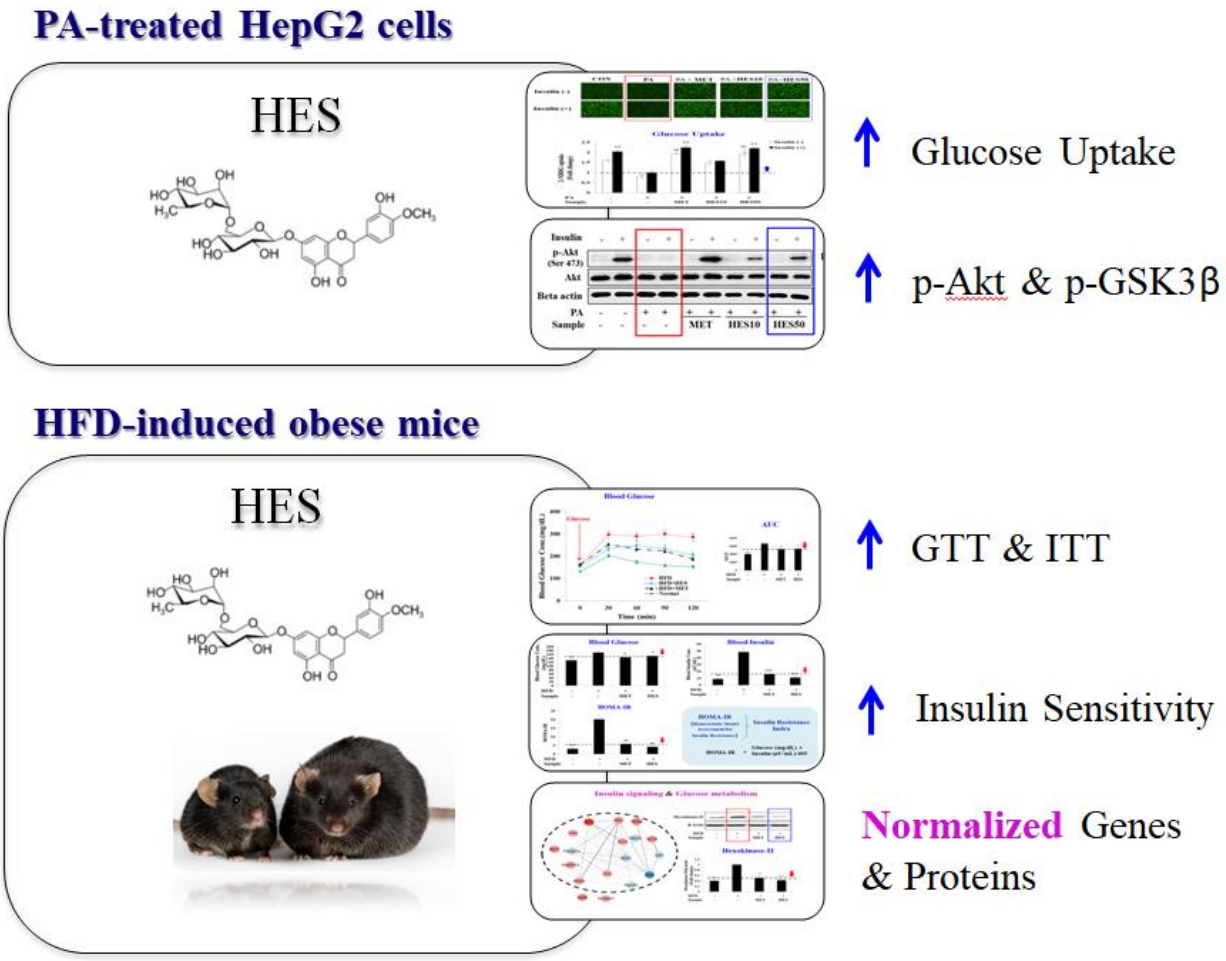

Fig. 32. Summary of anti-diabetic effect of HES

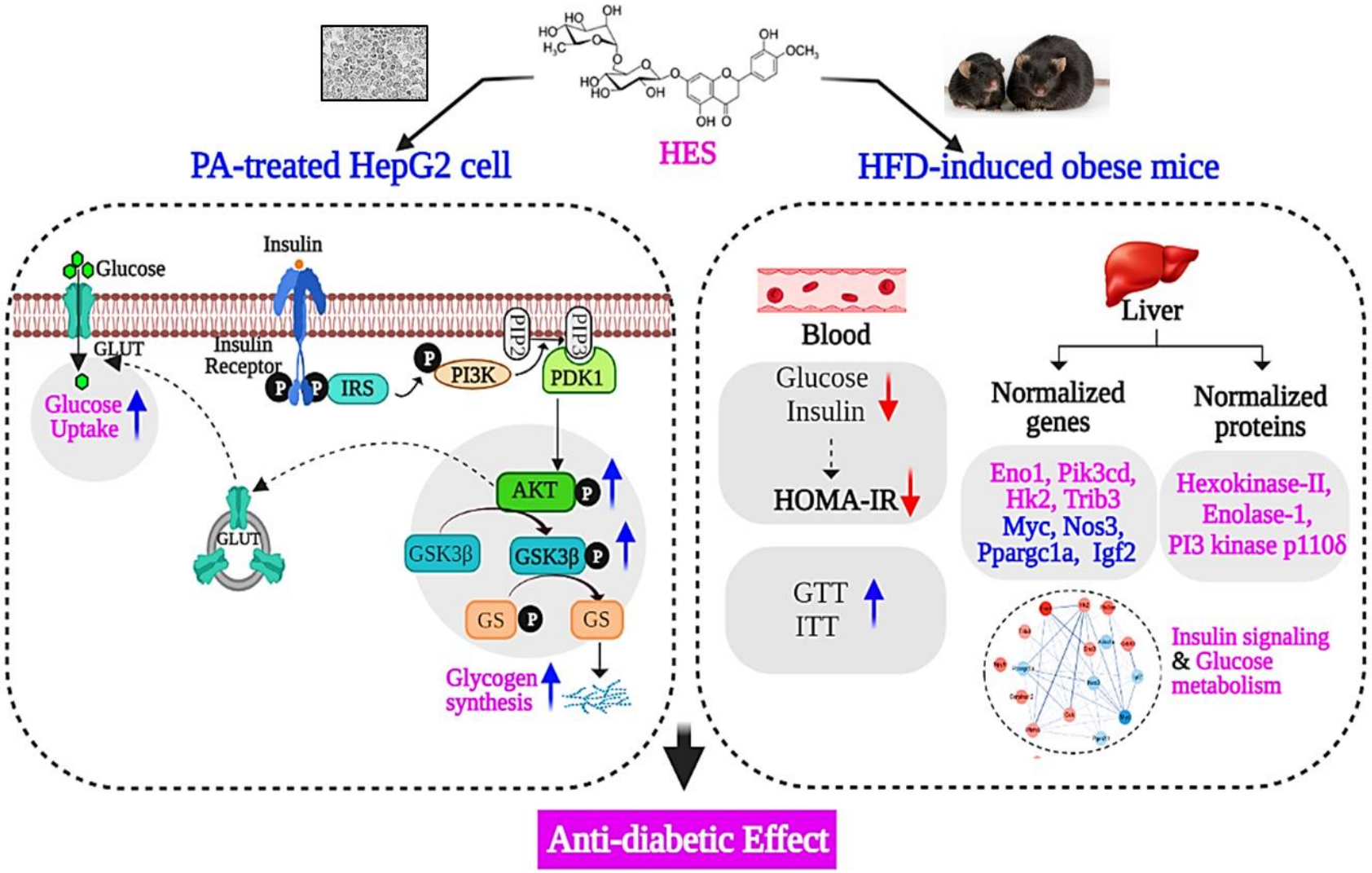

Fig. 33. Proposed mechanism for the anti-diabetic effect of HES in PA-treated HepG2 cells and HFD-induced obese mice

PART-III

Effects of premature citrus extract on serum parameters in beagle dogs

3.1. Abstract

The present study was conducted to examine the effect of premature citrus extract (PCE) on the serum parameters of beagle dogs. The body weight did not significantly differ between the groups supplemented with PCE and control group throughout the experiment. The groups supplemented with PCE showed significantly decreased serum triglyceride levels compared with the control group at week 12. Serum cholesterol analysis confirmed that the PCE-supplemented group had significantly decreased serum levels of low-density lipoprotein-cholesterol and increased serum levels of the beneficial high-density lipoprotein-cholesterol compared to those in the control group at week 12. In addition, the group supplemented with PCE for 12 weeks showed significantly decreased serum glucose levels compared with those in the control group at week 0. Furthermore, serological tests revealed that PCE did not alter functional parameters of liver, kidney, and pancreas in the serum of beagle dogs over 12 weeks. These results suggest that supplementation of PCE in the diet decreased triglyceride, low-density lipoprotein-cholesterol, and glucose levels and increased the high-density lipoprotein-cholesterol level without affecting the functional parameters of liver, kidney, and pancreas in the serum of beagle dogs.

Keywords: Premature citrus extract; serum parameter; triglyceride; cholesterol; beagle dog

3.2. Introduction

High cholesterol and triglyceride (TG) concentrations in dogs are associated with a wide range of diseases including dyslipidemia and diabetes mellitus [124]. Cholesterol is synthesized via a cascade of enzymatic reactions known as the mevalonate pathway, and TG is synthesized by esterification of fatty acids with glycerol [125, 126]. Previous studies showed that an increased body weight leads to higher rates of cholesterol and TG synthesis [127]. Therefore, several efforts have been made to normalize the serum levels of cholesterol and TG [128].

Citrus fruit has been widely studied as a source of polyphenols and bioactive compounds, mainly flavonoids [128, 129]. Premature citrus fruits have attracted attention from both the pharmaceutical and food industries because they contain higher concentrations of flavonoids compared to mature fruit [130, 131]. Previous studies revealed that citrus fruits have various health benefits, such as anti-diabetic and anti-obesity activity in mice [132–134]. However, whether premature citrus extract (PCE) influences anti-diabetic and anti-obesity activity in beagle dogs remains unclear. Therefore, the effects of a diet containing PCE on the serum parameters of beagle dogs were examined.

The present study hypothesized that a diet containing PCE would have anti-obesity and anti-diabetic effects on beagle dogs, as observed in mice. To test this hypothesis, the effects of a diet containing PCE on the levels of TG, cholesterol, and glucose were evaluated in the serum of beagle dogs (Fig. 34).

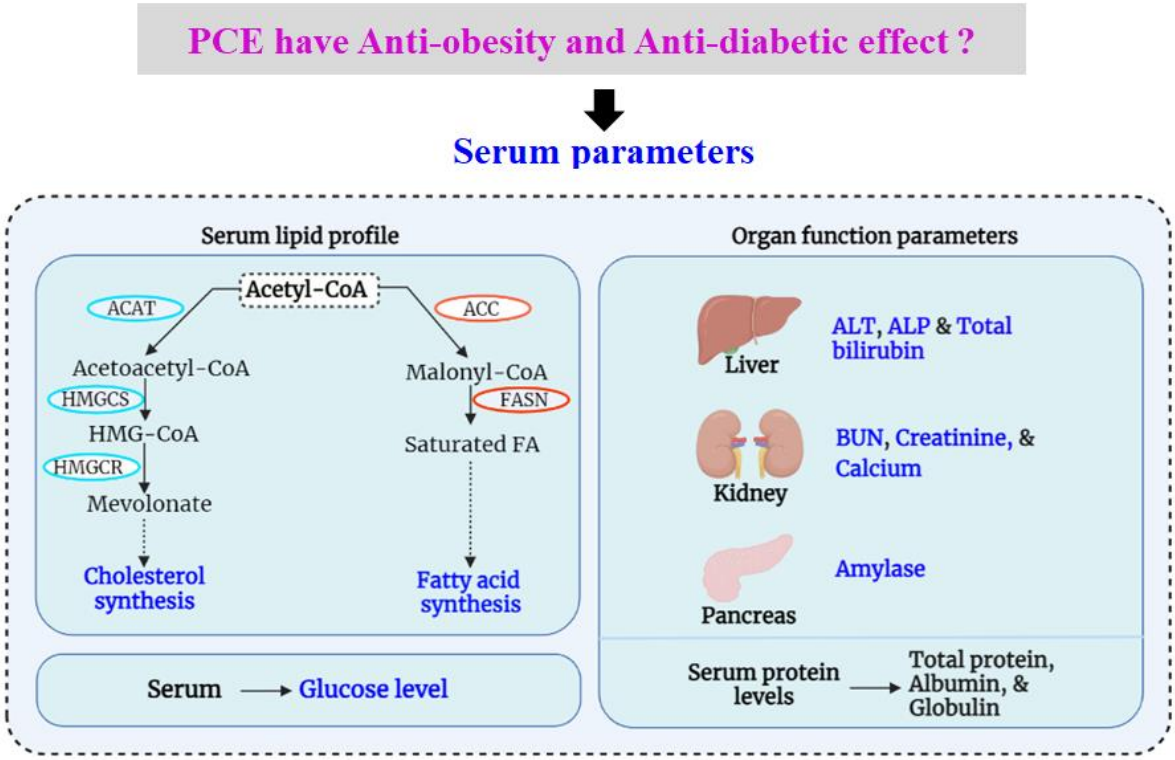

Fig. 34. Hypothetical model for anti-adipogenic effect of flavonoids

3.3. Materials and Methods

3.3.1. Preparation of diet containing PCE

PCE was prepared by BK-bio (Gyeonggi-do, Korea). A diet with or without PCE was manufactured and supplied by i-Tech (Korea) (Fig. 35).

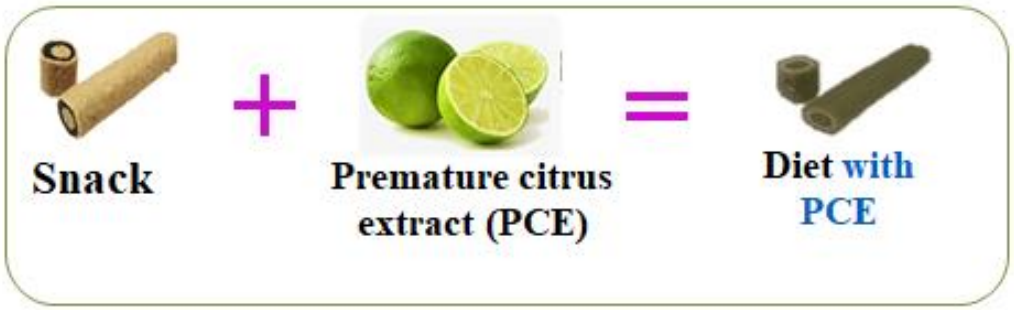

Fig. 35. Preparation of diet with premature citrus extract

3.3.2. Animals

Five-month-old beagle dogs (6 male; 6 female) weighing 8.1–9.4 kg were purchased from Kipron Bio (Korea). Each dog was housed in a separate cage at a relative humidity of 30–70% and temperature of 23–28 °C. The study protocol was reviewed and approved by the Animal Experimental Ethics Committee of Jeju National University (IACUC No. 2021-0025).

3.3.3. Animal experiment

The dogs were randomly allocated into two groups, with each group comprised of three male and three female beagles; the control group was fed a diet without PCE (spiru 300 g + diet without PCE 100 g) and the sample group was fed a diet containing PCE (spiru 300 g + diet with PCE 100 g). Each dog was fed approximately 400 g of spiru and diet with or without PCE twice per day for 12 weeks. The body weight and serum parameters were assessed once every 2 weeks to evaluate the effects of PCE in both the control and sample groups. Serum was separated from the collected blood following centrifugation at 3500 ×*g* for 15 min at 4 °C and stored at -20 °C for further analysis (Fig. 36).

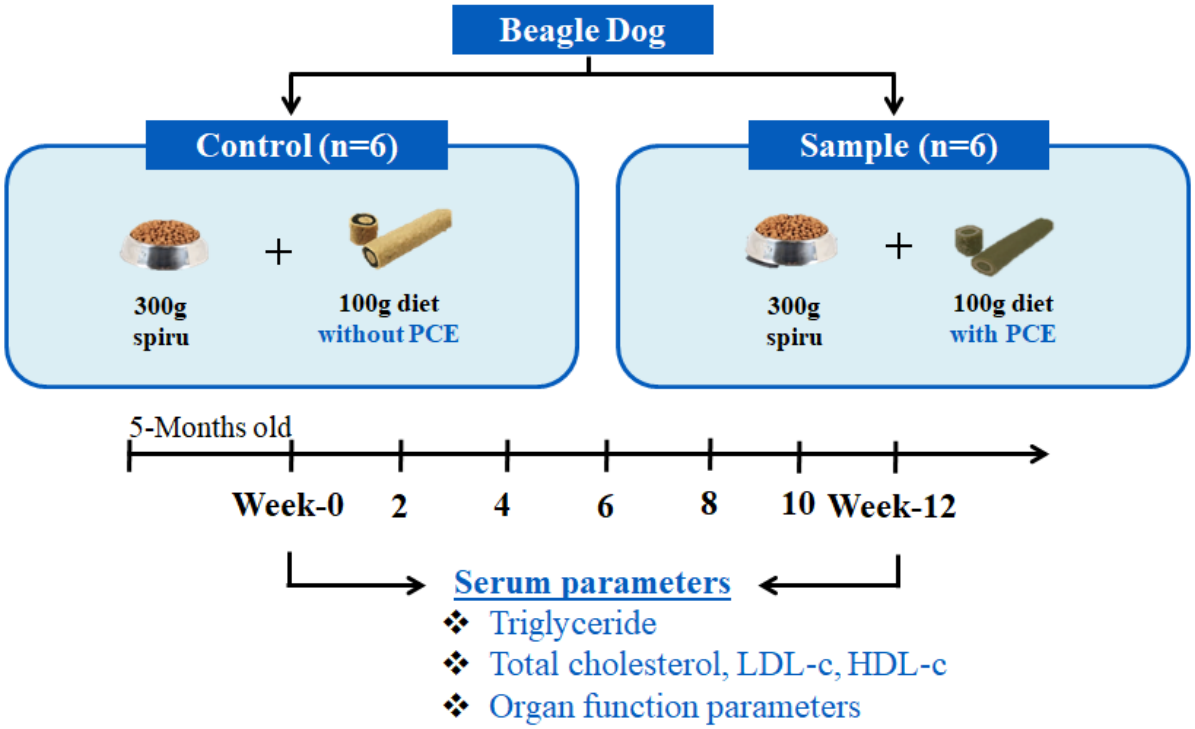

Fig. 36. Experimental design of the animal study

3.3.4. Serum TG level

Serum TG levels were quantified using a commercially available colorimetric EnzyChrom™ TG assay kit (BioAssay Systems, USA). After every 2 weeks of sample treatment, the TG level was measured in the serum of both the control and experimental groups. Briefly, 20 μL of each serum sample was diluted by 10-fold with sterile distilled water. Working solution (100 μL assay buffer, 100 μL of enzyme mix, 5 μL lipase, 1 μL ATP, and 1 μL dye) was added to the diluted serum, and the mixture was incubated at room temperature for 30 min. Absorbance was measured with an enzyme-linked immunosorbent assay microplate reader (Sunrise TW, BIOTECH Co., Austria) at 570 nm. A TG standard was prepared according to the manufacturer's instructions.

3.3.5. Serum total cholesterol, low density lipoprotein cholesterol and high density lipoprotein cholesterol level

Colorimetric quantification of total cholesterol (TC), low-density lipoprotein-cholesterol (LDL-C), and high-density lipoprotein-cholesterol (HDL-C) in the serum was performed using an EnzyChrom™ AF HDL and LDL/VLDL assay kit (BioAssay Systems) according to the manufacturer's instructions. After every 2 weeks of sample treatment, the levels of TC, LDL-C, and HDL-C were measured in the serum of both the control and sample-treated groups. Briefly, 20 μL of precipitation solution was added to 20 μL of each serum sample. After mixing well, centrifugation was performed at 9,500 ×g for 5 min. Working solution was prepared as follows. For the HDL assay, 24 μL of the supernatant was diluted in 96 μL of assay buffer. For the LDL assay, 40 μL of PBS was added to the pellet and mixed by pipetting. Next, 24 μL of this mixture was diluted in 96 μL of assay buffer. For the TC assay, 12 μL of serum was diluted in 108 μL of assay buffer. For the assays, 50 μL of

each of TC, HDL, and LDL working solution was transferred into the wells of a clear flat-bottom 96-well plate. To each well, 50 μL of the reaction mixture (55 μL assay buffer, 1 μL enzyme mix, and 1 μL dye) was added and incubated at room temperature for 30 min. The absorbance was measured with an enzyme-linked immunosorbent assay microplate reader (Sunrise TW, BIOTECH Co., Austria) at 570 nm. A cholesterol standard was prepared according to the manufacturer's instructions.

3.3.6. Other serum parameters

Serum parameters were analyzed and quantified with a Comprehensive Diagnostic Profile Rotor and Abaxis VetScan VS2 Chemistry Analyzer (Abaxis Inc., USA) according to the manufacturer's instructions. After every 2 weeks of sample treatment, functional parameters of liver, kidney, and pancreas were measured in the serum of both the control and sample-treated groups. Briefly, 100 μL of serum was dispensed into the rotor through sample port. The rotor was loaded into the analyzer's rotor drawer, and the serum was processed by the analyzer to measure glucose, alanine aminotransferase (ALT), alkaline phosphatase (ALP), total bilirubin, blood urea nitrogen (BUN), creatinine, calcium, amylase, total protein, albumin, and globulin levels, which are markers of organ functions including liver, kidney, and pancreas.

3.3.7. Statistical analysis

All data obtained in this experiment were expressed as the mean ± standard error (SE), and one-way analysis of variance (ANOVA) was performed, followed by Turkey's test (SPSS 17.0, USA) to determine the significance of differences between groups. A $p < 0.05$ was considered to indicate statistically significant differences compared to the control group.

3.4. Results

3.4.1. Body weight change

The effect of PCE extract on the body weight changes of beagle dogs was evaluated for 12 weeks (Fig. 37). The group supplemented with PCE showed no significant difference in body weight compared with that of the control group throughout the experiment (Fig. 37A and B). The result manifest that the diet containing PCE did not affect the body weight of beagle dogs compared with the control group.

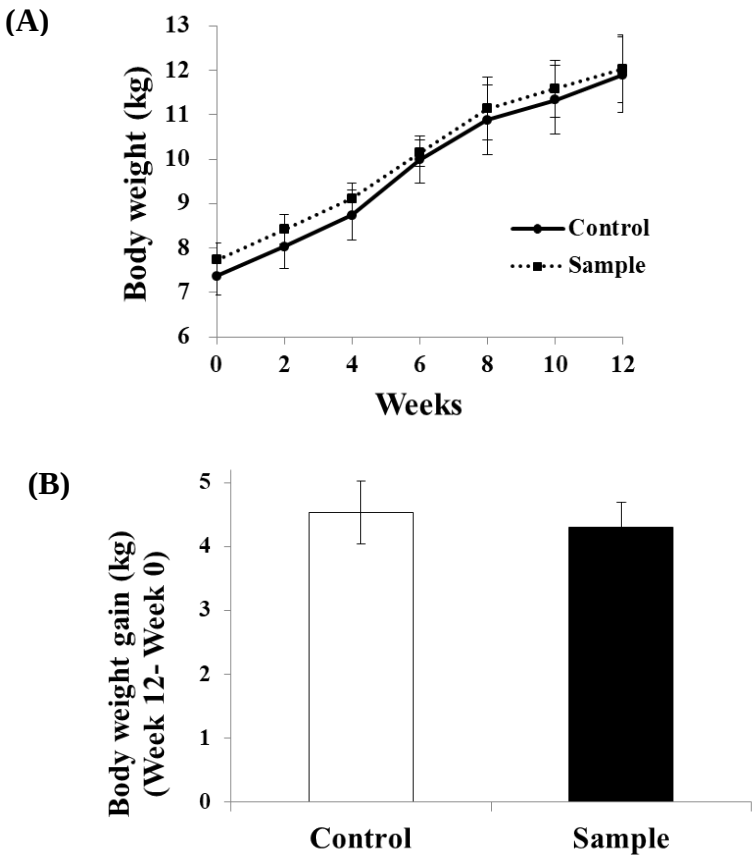

Fig. 37. Effects of diet containing PCE on body weight changes in beagle dogs.

After every 2 weeks of sample treatment, body weight (A) and body weight gain (B) were compared between the control and sample groups. Data are presented as the mean ± SE.

3.4.2. Serum TG level

The effect of PCE on TG levels in the serum of beagle dogs was monitored for 12 weeks (Fig. 38). In the sample-treated group, serum TG levels tended to decrease from weeks 0 to 12. Moreover, at the end of the treatment (week 12), the sample-treated group showed significantly decreased ($p < 0.0005$) serum TG levels compared to the levels at week 0. Particularly, at week 12, the sample-treated group exhibited significantly decreased ($p < 0.05$) serum TG levels compared to those in the control group. This result indicates that PCE-supplemented diet feeding for 12 weeks significantly decreased TG levels in the serum of beagle dogs.

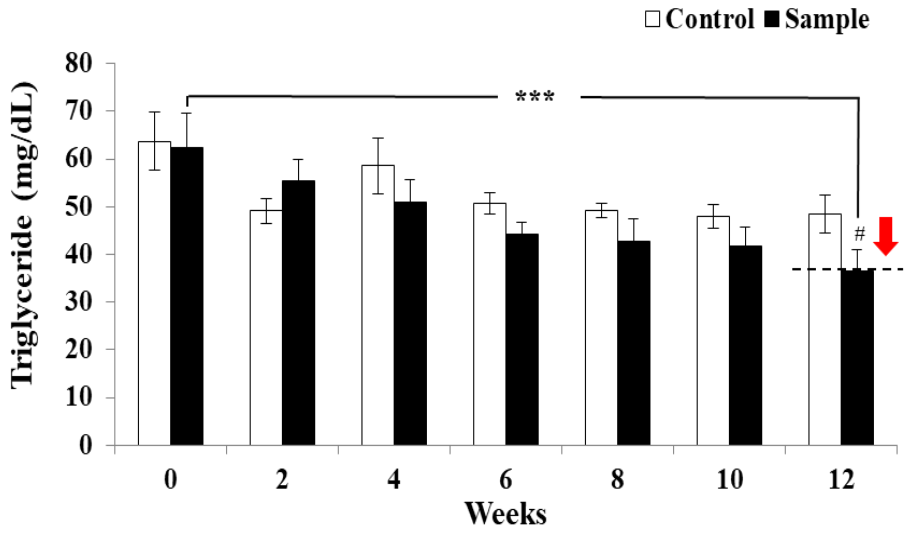

Fig. 38. Effects of diet containing PCE on serum TG level in beagle dogs.

After every 2 weeks of sample treatment, blood was collected from both the control and sample groups, and serum was separated by centrifugation. The serum level of TG was determined in both groups. Data are presented as the mean ± SE. $^{\#}p < 0.05$ compared to the control group. ***$p < 0.0005$ compared to the group at week 0.

3.4.3. Serum cholesterol levels

The effects of PCE on TC, LDL-C, and HDL-C levels were monitored in beagle dogs for 12 weeks (Fig. 39). The results revealed that in the sample-treated group, serum TC levels tended to decrease from week 8 (Fig. 39A). Moreover, at the end of treatment (week 12), the sample-treated group significantly decreased ($p < 0.05$) serum TC levels compared to those at week 0. Additionally, at week 12, the sample-treated group showed decreased serum TC levels compared with those in the control group; however, the difference was not significant.

The sample-treated group revealed that serum LDL-C levels tended to decrease from week 8 (Fig. 39B). At the end of treatment (week 12), the sample-treated group showed a significant decrease ($p < 0.0005$) in serum LDL-C levels compared to those at week 0. Additionally, at week 12, the sample-treated group exhibited a significant decrease ($p < 0.05$) in serum LDL-C levels compared with those in the control group.

The sample-treated group showed that serum HDL-C levels tended to increase from weeks 0 to 12 (Fig. 39C). Moreover, at the end of treatment (week 12), the sample-treated group showed significantly increased ($p < 0.0005$) serum HDL-C levels compared with those at week 0. Additionally, at week 12, the sample-treated group exhibited significantly increased ($p < 0.05$) serum HDL-C levels compared with those in the control group. These results indicate that PCE-supplemented diet feeding for 12 weeks significantly decreased LDL-C levels and increased HDL-C levels in the serum of beagle dogs.

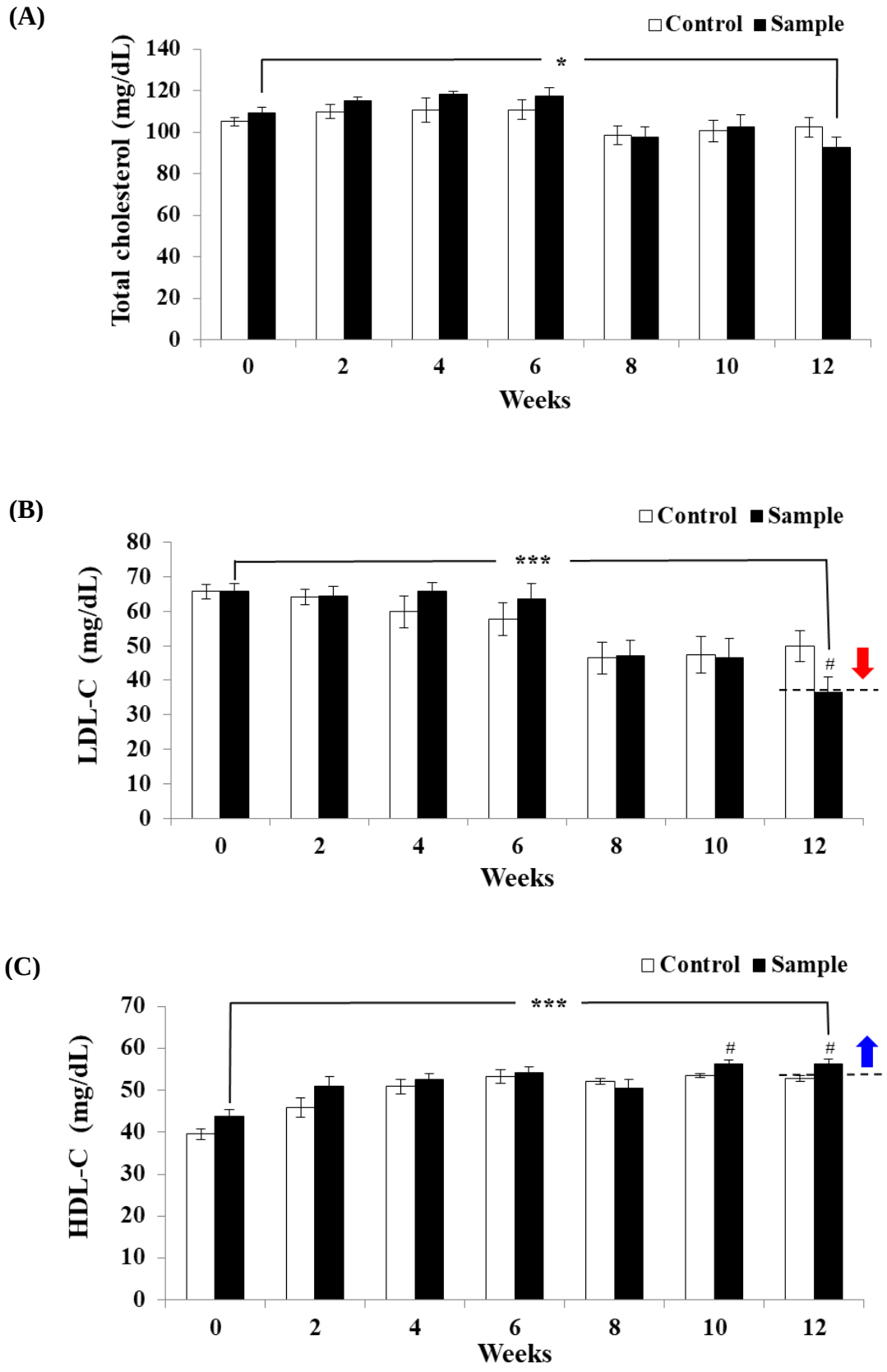

Fig. 39. Effects of diet containing PCE on serum cholesterol levels in beagle dogs.

After every 2 weeks of sample treatment, blood was collected from both the control and sample groups, and serum was separated by centrifugation. The serum levels of TC (A), LDL-C (B), and HDL-C (C) were measured in both groups. Data are presented as the mean ± SE. $^{\#}p < 0.05$ compared with control group. *p < 0.05, ***p < 0.0005 compared to sample group at week 0.

3.4.4. Serum glucose level

The effect of PCE on blood glucose level was evaluated in beagle dogs for 12 weeks (Fig. 40). In the sample-treated group, serum glucose levels tended to decrease after week 2. Additionally, at week 12, the sample-treated group showed significantly decreased ($p < 0.05$) serum glucose levels compared to those at week 0. These results reveal that PCE-supplemented diet feeding for 12 weeks reduced serum glucose levels in beagle dogs.

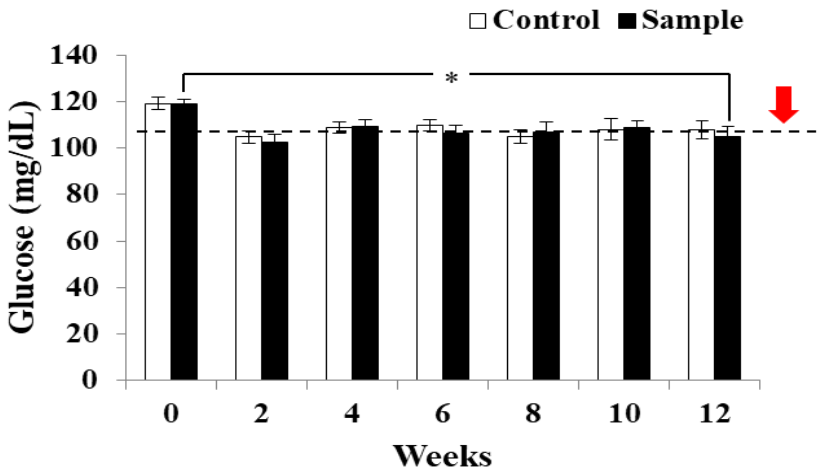

Fig. 40. Effect of diet containing PCE on serum glucose level in beagle dogs.

After every 2 weeks of sample treatment, the serum glucose level was measured in both the control and sample groups. Data are presented as the mean ± SE. *p < 0.05 compared to that at week 0.

3.4.5. Liver function

The effect of PCE on liver function was evaluated by analyzing ALT, ALP, and total bilirubin levels in the serum of beagle dogs for 12 weeks (Fig. 41). The sample-treated group showed significantly increased ($p < 0.05$) serum ALT levels compared with those in the control group at week 2, 6, and 10 (Fig. 41A). However, the sample-treated group did not show significant alterations in the serum ALP and total bilirubin levels compared with those in the control group (Fig. 41B and C). Additionally, at week 12, neither the control nor sample-treated group showed significantly different serum ALT, ALP, and total bilirubin levels compared with those at week 0. This result suggests that PCE-supplemented diet feeding for 12 weeks did not alter serum ALT, ALP, and total bilirubin levels in beagle dogs.

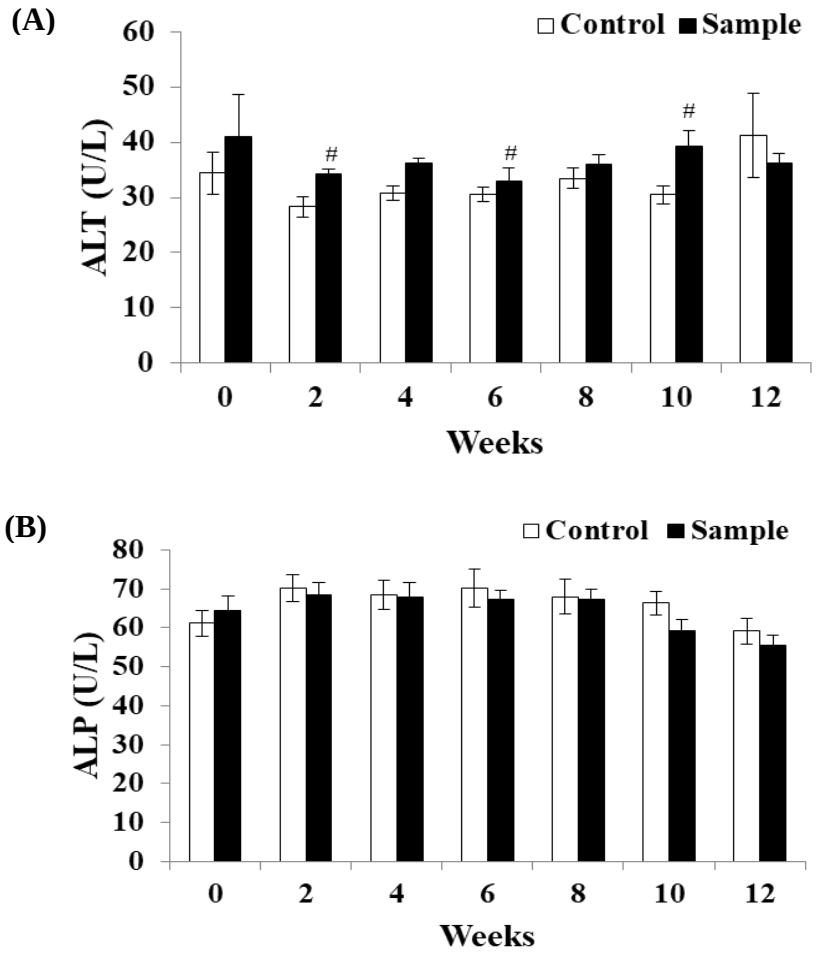

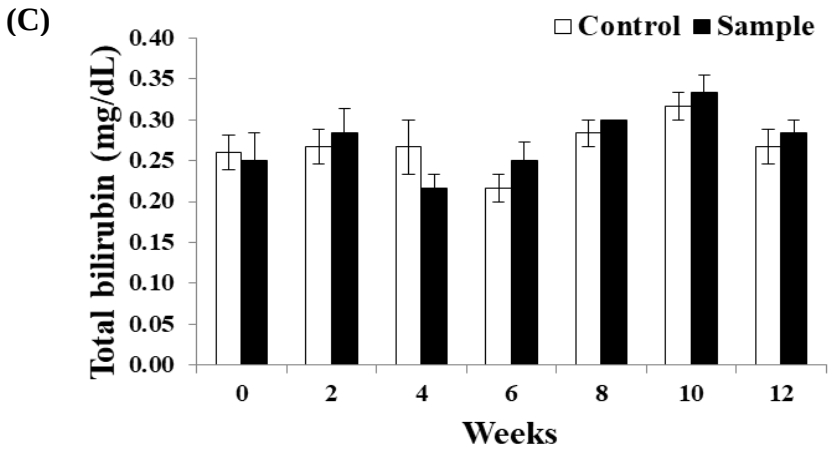

Fig. 41. Effect of diet containing PCE on liver function in beagle dogs.

After every 2 weeks of sample treatment, functional parameters of liver including ALT (A), ALP (B), and total bilirubin (C) levels were evaluated in the serum of both the control and sample groups. Data are presented as the mean ± SE. $^{\#}p < 0.05$ compared to control group.

3.4.6. Kidney function

The effect of PCE on kidney function was evaluated by analyzing serum BUN, creatinine, and calcium levels in beagle dogs for 12 weeks (Fig. 42). The results showed that in the sample-treated groups, serum BUN levels were significantly decreased ($p < 0.005$) at week 12 compared to those at week 0 (Fig. 42A). However, in the sample-treated group, the serum creatinine and calcium levels were not significantly altered compared with those in the control group at week 12 of treatment (Fig. 42B and C). These results confirm that PCE-supplemented diet feeding did not alter the serum levels of creatinine and calcium but decreased BUN levels in the serum of beagle dogs.

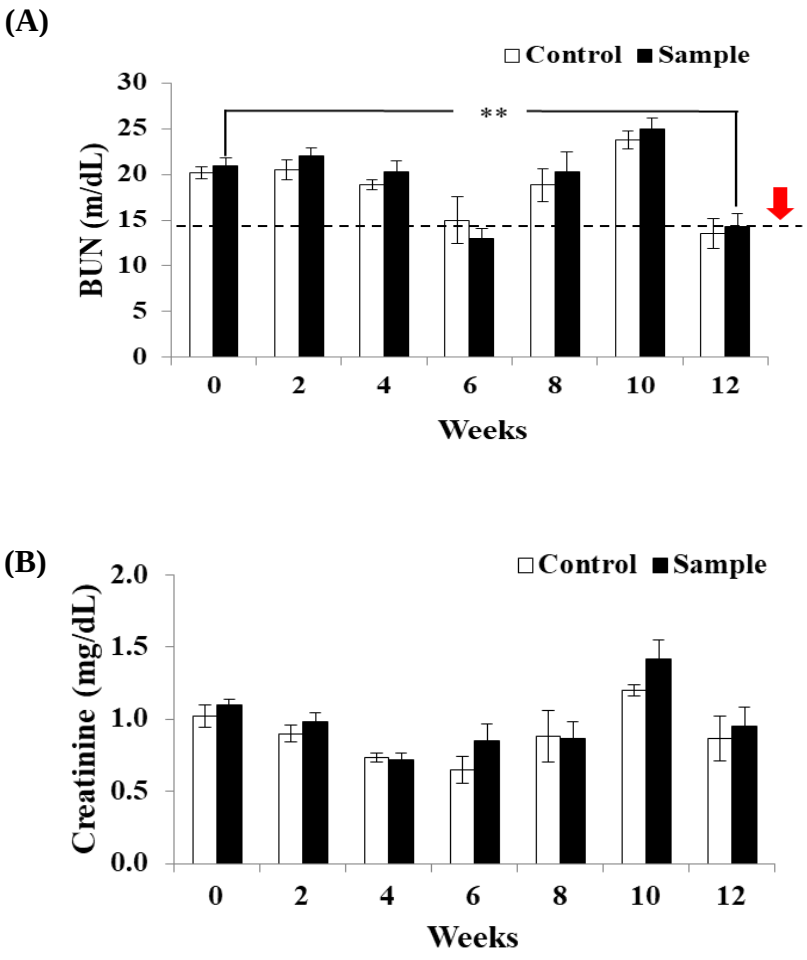

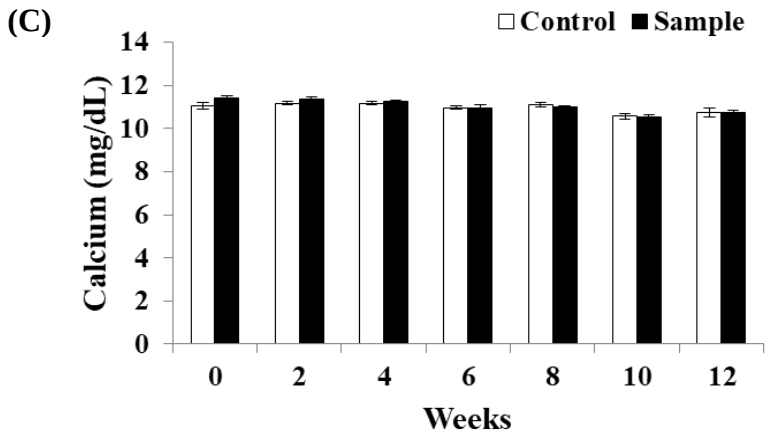

Fig. 42. Effect of diet containing PCE on kidney function in beagle dogs.

After every 2 weeks of sample treatment, functional parameters of kidney including BUN (A), creatinine (B), and calcium (C) levels were evaluated in the serum of both the control and sample groups. Data are presented as the mean ± SE. **p < 0.005 compared to those at week 0.

3.4.7. Amylase

The effect of PCE on pancreas function was evaluated by analyzing serum amylase levels in beagle dogs for 12 weeks (Fig. 43). At week 4, the sample-treated group showed significantly decreased ($p < 0.05$) serum levels of amylase compared with those in the control group. However, at week 12, neither the control nor sample treated group showed changes in the serum level of amylase compared with those at week 0. These results show that PCE-supplemented diet feeding did not change the serum level of amylase in beagle dogs.

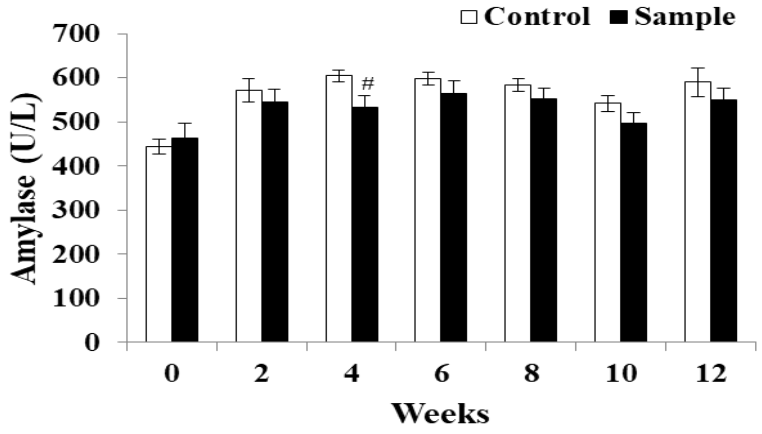

Fig. 43. Effect of diet containing PCE on serum amylase level in beagle dogs.

At every 2 weeks of sample treatment, the amylase level was determined in the serum of both the control and sample groups. Data are presented as the mean ± SE. $^{\#}p < 0.05$ compared to control group.

3.4.8. Serum proteins

The effect of PCE on serum proteins was evaluated by analyzing total protein, albumin, and globulin levels in the serum of beagle dogs for 12 weeks (Fig. 44). The sample-treated groups did not show alterations in the serum total protein and albumin levels at week 12 compared with those at week 0 (Fig. 44A and B). Furthermore, the sample-treated groups showed significantly increased ($p < 0.05$) the serum globulin levels at week 12 compared with those at week 0 (Fig. 44C). However, sample treatment did not significantly alter serum globulin levels compared with those in the control group at week 12. These results show that PCE-supplemented diet feeding did not alter the serum levels of total protein, albumin, and globulin in beagle dogs.

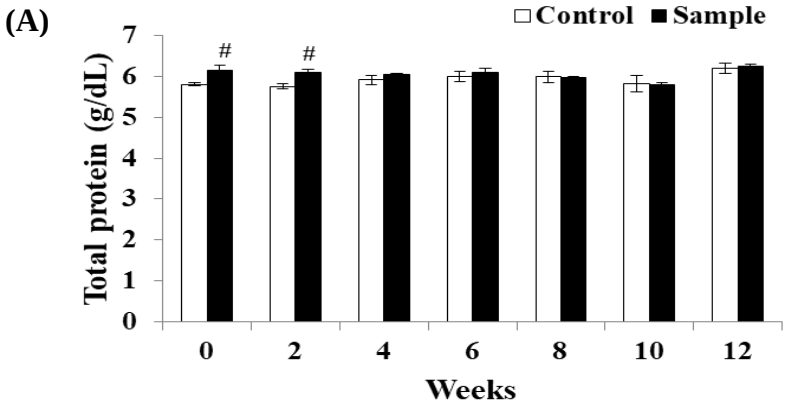

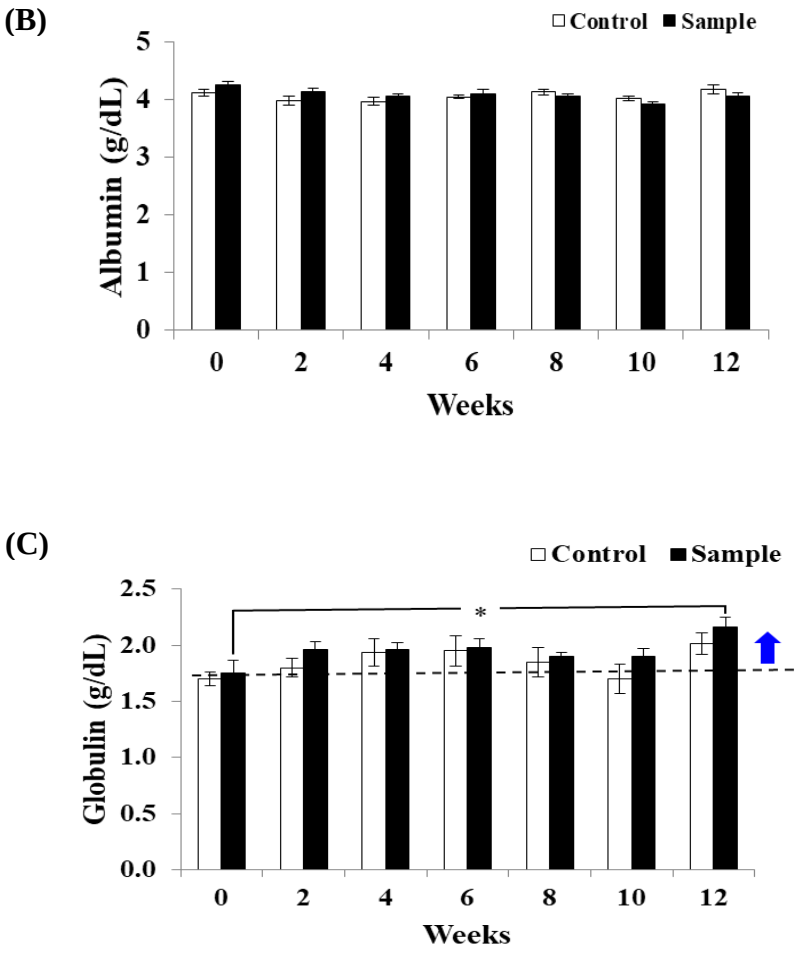

Fig. 44. Effect of diet containing PCE on serum protein levels in beagle dogs.

At every 2 weeks of sample treatment, total protein (A), albumin (B), and globulin (C) levels were measured in the serum of both the control and sample groups. Data are presented as the mean ± SE. $^{\#}p < 0.05$ compared to control group. *$p < 0.05$ compared to group at week 0.

3.5. Discussion

The present study investigated the effect of diet containing PCE on serum parameters in beagle dogs. The results showed that the body weight of the group fed the diet containing PCE did not significantly differ from that in the control group throughout the experiment. PCE-containing diet feeding decreased the TG, LDL-C, and glucose levels, whereas it beneficially increased HDL-C level in the serum of beagle dogs at week 12. Furthermore, serological tests revealed that PCE did not alter functional parameters of liver, kidney, and pancreas in the serum of beagle dogs over 12 weeks.

The current study evidenced that the group supplemented with diet containing PCE did not show significant difference of the body weight compared with control group throughout the experiment. A previous study reported that administration of flavonoids did not prevent body weight gain but increased fatty acid oxidation in obese mice [135]. In addition, a previous study showed that supplementation with flavonoids did not affect body weight, yet it affects adipogenesis and basal metabolism in humans [136, 137]. Similarly, the present study observed that the flavonoid-enriched PCE did not alter the body weight gain but it may have affected basal metabolism in beagle dogs.

In the present study, the group supplemented with PCE showed significantly decreased serum TG levels compared with those in the control group at week 12. Previous studies showed that polyphenols and flavonoids prevented increases in plasma TG levels in mice [138, 139]. Similarly, the present findings showed that flavonoid-enriched PCE decreased TG levels in the serum of beagle dogs.

The current study evidenced that the diet containing PCE decreased the serum LDL-C, whereas it increased serum HDL-C levels in beagle dogs at week 12. Studies have shown that polyphenols and flavonoids reduced plasma LDL-C levels and effectively increased HDL-C

levels in mice [138, 139]. Similarly, the present findings observed that flavonoid-enriched PCE decreased serum LDL-C levels, whereas it beneficially increased HDL-C levels in the serum of beagle dogs.

Furthermore, the present study observed that the diet containing PCE significantly decreased the glucose levels in the serum of beagle dogs. Diabetes is associated with hyperglycemia in dogs [140]. In addition, flavonoids prevent hyperglycemia in rats [141]. The finding of the present study suggests that the flavonoids in PCE may reduce glucose levels in the serum of beagle dogs.

The present investigation confirmed that the treatment of a diet containing PCE did not significantly alter functional parameters of liver, including ALT, ALP, and total bilirubin in the serum of beagle dogs. Previously, researchers showed that ALT and ALP levels are elevated in hepatic disease as a consequence of hepatocellular necrosis and cholestasis [142]. In addition, total bilirubin is increased in hepatobiliary disease [143]. The results of the present study showed that feeding of a diet containing PCE for 12 weeks did not affect liver function in beagle dogs.

The present study showed that PCE decreased BUN levels but did not affect creatinine and calcium levels in the serum of beagle dogs. Previous studies showed that BUN is a waste product of protein catabolism, and creatinine is formed through normal muscle metabolism [144]. These two substances are normally cleared from the bloodstream by the kidneys and therefore are used as biomarkers to evaluate and monitor kidney function in dogs [145, 146]. In addition, calcium homeostasis is altered in chronic kidney disease and used to predict the progression of kidney dysfunction in dogs [147, 148]. The present study showed that 12 weeks treatment of PCE did not cause kidney dysfunction in beagle dogs.

The current investigation revealed that PCE did not affect amylase levels in the serum of beagle dogs. A previous study illustrated that pancreatic amylase digests starch for energy acquisition, and its serum level is increased in dogs with pancreatitis [149, 150]. The present study confirmed that 12 weeks of treatment with PCE did not affect pancreas function in beagle dogs.

The current study showed that PCE did not alter the total protein, albumin, and globulin levels in the serum of beagle dogs. A previous study showed that chronic inflammation increased the serum level of total protein and globulin and decreased the serum level of albumin in dogs [151]. The present study denoted that 12 weeks supplementation of PCE did not cause chronic inflammation in beagle dogs.

In conclusion, the diet supplemented with PCE appeared to have anti-obesity and anti-diabetic effects by decreasing TG, LDL-C, and glucose levels while beneficially increasing HDL-C levels without affecting functional parameters of liver, kidney, and pancreas in the serum of beagle dogs (Fig. 45).

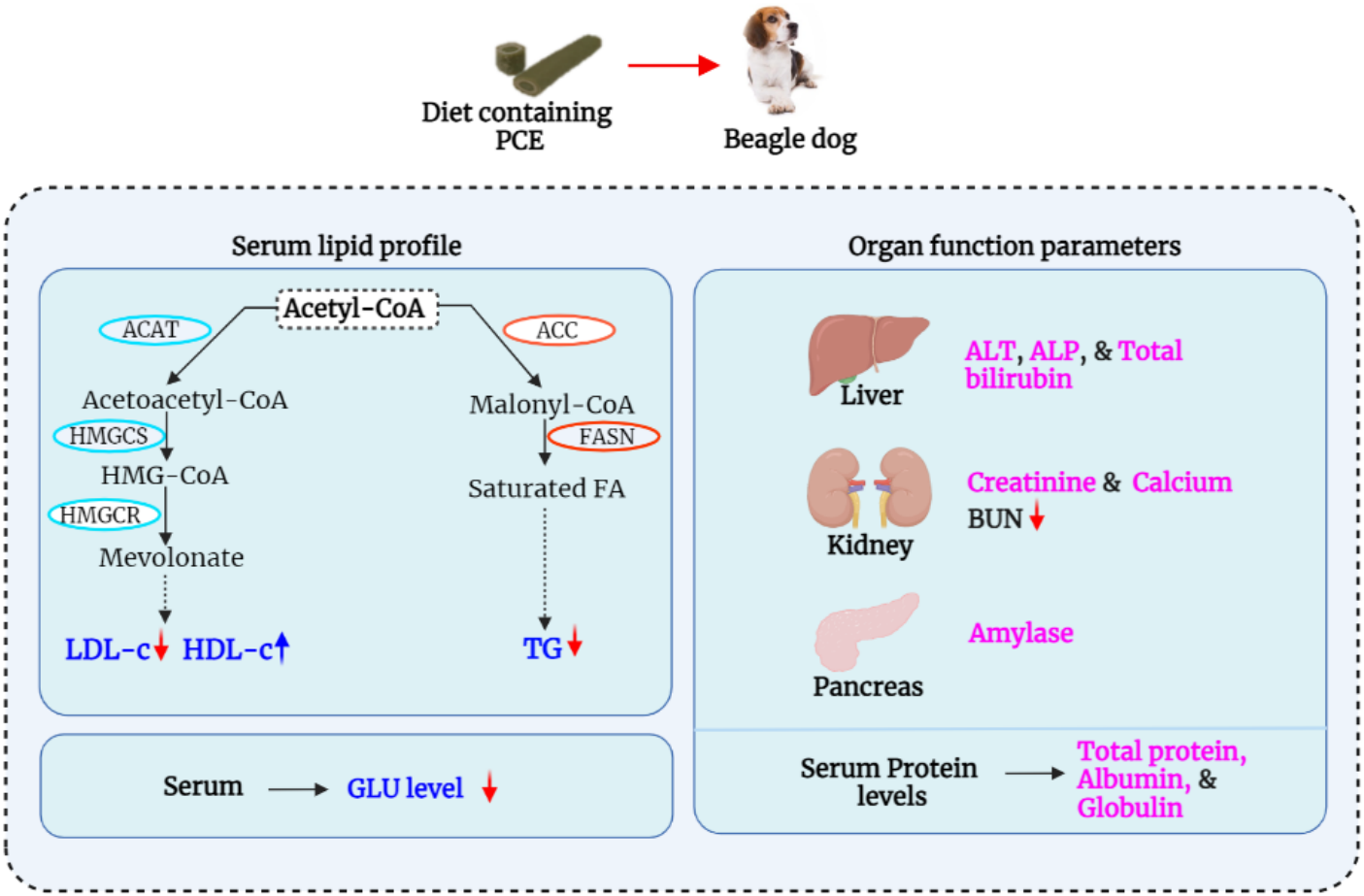

Fig. 45. Effect of diet containing PCE on serum parameters in beagle dog

General Conclusion

This study supports that flavonoids present in PCE has anti-adipogenic and anti-diabetic effects by activating AMPK and normalizing the expression of genes related to insulin signaling and glucose metabolism in PA-treated HepG2 cells and HFD-induced obese mice. Furthermore, PCE exerts anti-obesity and anti-diabetic effects by reducing TG, cholesterol, and glucose levels in the serum of beagle dogs.

Conclusion 1: Flavonoids exert anti-adipogenic effects on PA-treated HepG2 cells via activating AMPK signaling pathway

Analysis of anti-adipogenic effects in PA-treated HepG2 cells indicated that flavonoids significantly reduced both the intracellular lipid accumulation and TG content and enhanced glucose uptake in an insulin-independent manner in PA-treated HepG2 cells. In addition, flavonoid-mediated AMPK activation increased the phosphorylation level of ACC and decreased the expression levels of SREBP-2 and HMGCR, which are crucial for lipogenesis and cholesterol biosynthesis. Furthermore, flavonoids increased the phosphorylation levels of GSK3β, which is a key enzyme in glycogen synthesis. Molecular docking analysis revealed that the flavonoids bind to the CBS domain in the regulatory γ-subunit with high binding affinities, suggesting that flavonoids positively modulate AMPK activation. Overall, these results suggest that citrus flavonoids have anti-adipogenic effects on PA-treated HepG2 cells via activating AMPK signaling pathway (Fig. 46).

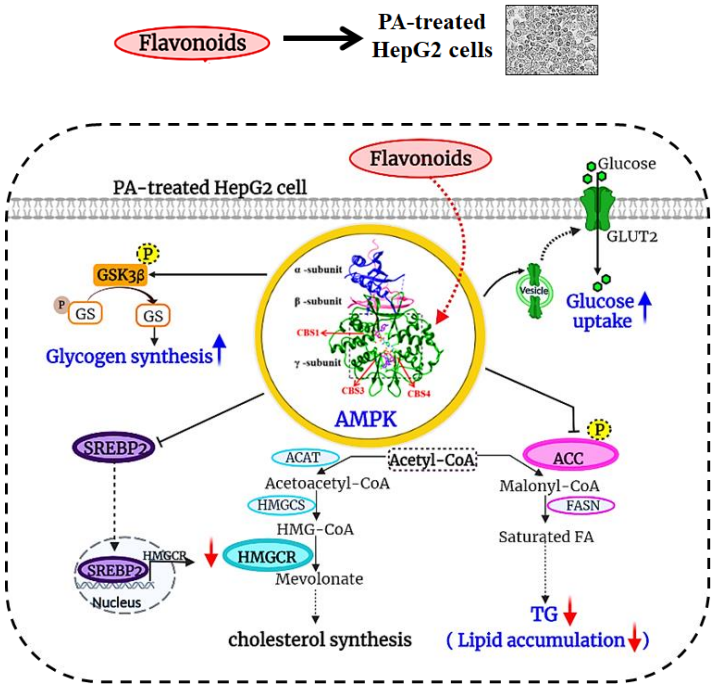

Fig. 46. Flavonoids exert anti-adipogenic effects on PA-treated HepG2 cells via activating AMPK signaling pathway

Conclusion 2: Hesperidin exhibits anti-diabetic effect by normalizing the expressions of genes and proteins related to insulin signaling and glucose metabolism, which were perturbed in HFD-induced obese mice

Analysis of anti-diabetic study effects in PA-treated HepG2 cells and HFD-induced obese mice suggested that HES improved glucose uptake in an insulin-independent manner and exerted an insulin-sensitizing effect by increasing insulin-mediated phosphorylation of Akt and GSK3β in PA-treated HepG2 cells. Furthermore, supplementation of HES to HFD-induced obese mice improved insulin sensitivity by reducing blood glucose, and serum insulin levels and HOMA-IR values and improved both glucose tolerance and insulin sensitivity. Particularly, treatment with HES restored insulin sensitivity and glucose tolerance by normalizing the expression of genes including *Eno1*, *Pik3cd*, *Hk2*, *Trib3*, *Myc*, *Nos3*, *Ppargc1a*, and *Igf2* in the liver of HFD-induced obese mice. In addition, insulin sensitivity and glucose clearance were improved by HES via normalizing the expression of proteins including hexokinase-II, enolase-1, and PI3 kinase p110δ in HFD-induced obese mice. These results show that HES is a promising therapeutic solution for diabetes to normalize the expressions of genes and proteins related to insulin signaling and glucose metabolism, which were perturbed in HFD-induced obese mice (Fig. 47).

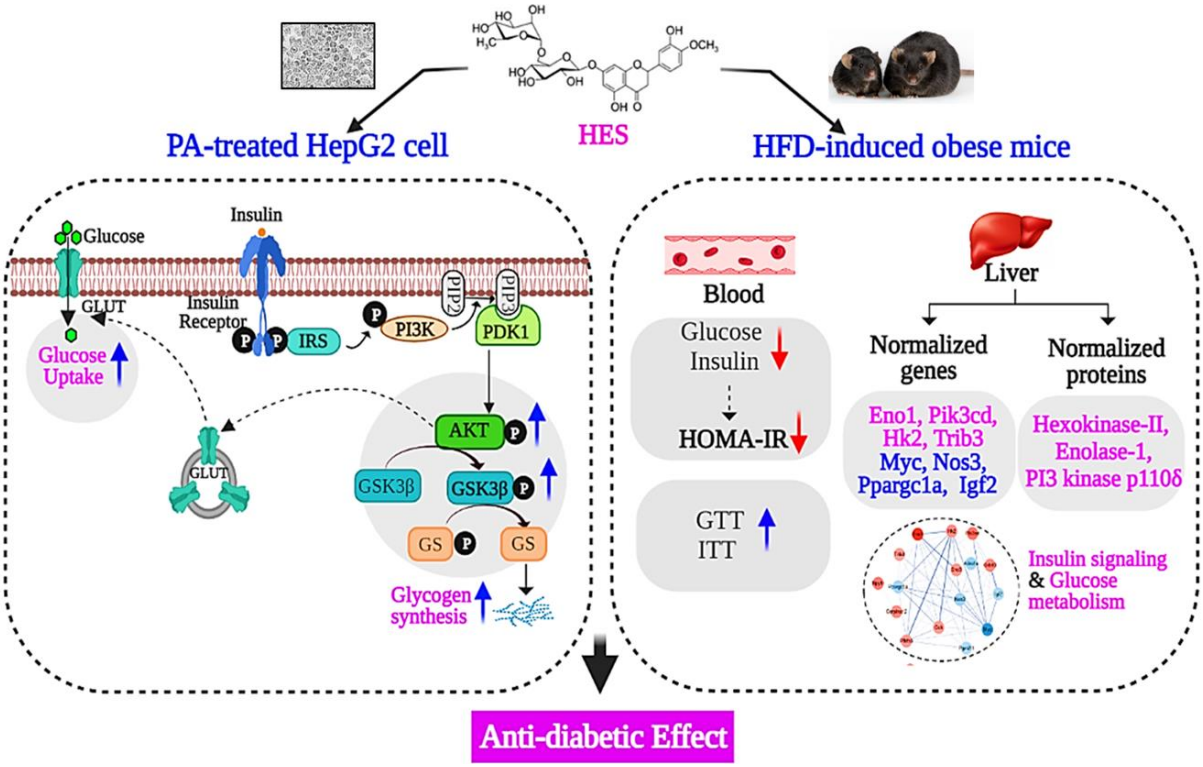

Fig. 47. Hesperidin exhibits anti-diabetic effect by normalizing the expressions of genes and proteins related to insulin signaling and glucose metabolism, which were perturbed in HFD-induced obese mice

Conclusion 3: Diet containing PCE had anti-obesity and anti-diabetic effects by reducing TG, cholesterol, and glucose levels in the serum of beagle dogs

The diet supplemented with PCE had anti-obesity and anti-diabetic effects in beagle dogs by decreasing TG, LDL-C, and glucose levels while beneficially increasing HDL-C levels without affecting functional parameters of liver, kidney, and pancreas in the serum (Fig.48).

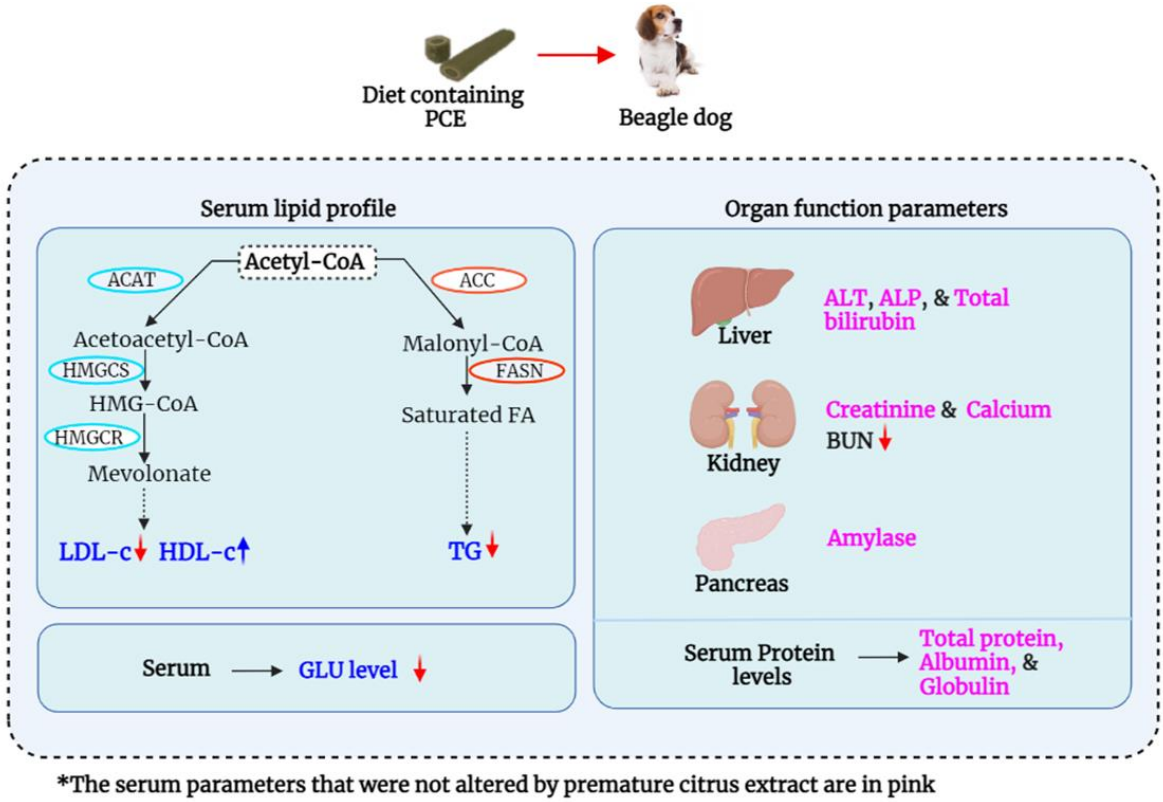

Fig. 48. Diet containing premature citrus extract shows anti-obesity and anti-diabetic effects by reducing TG, cholesterols, and glucose levels in the serum of beagle dogs

References

1. **Ros Pérez M, Medina-Gómez G**. Obesity, adipogenesis and insulin resistance. Endocrinol Nutr Engl Ed 2011, **58**, 360–369.

2. **Hafidi ME, Buelna-Chontal M, Sánchez-Muñoz F, Carbó R**. Adipogenesis: A Necessary but Harmful Strategy. Int J Mol Sci 2019, **20**, 3657.

3. **Zhao Y, Zhao MF, Jiang S, Wu J, Liu J, Yuan XW, et al**. Liver governs adipose remodelling via extracellular vesicles in response to lipid overload. Nat Commun 2020, **11**, 719.

4. **Strissel KJ, Stancheva Z, Miyoshi H, Perfield JW, DeFuria J, Jick Z, et al**. Adipocyte Death, Adipose Tissue Remodeling, and Obesity Complications. Diabetes 2007, **56**, 2910–2918.

5. **Ahmad B, Serpell CJ, Fong IL, Wong EH**. Molecular Mechanisms of Adipogenesis: The Anti-adipogenic Role of AMP-Activated Protein Kinase. Front Mol Biosci 2020, **7**, 76.

6. **Jiménez-Sánchez C, Olivares-Vicente M, Rodríguez-Pérez C, Herranz-López M, Lozano-Sánchez J, Segura-Carretero A, et al**. AMPK modulatory activity of olive–tree leaves phenolic compounds: Bioassay-guided isolation on adipocyte model and in silico approach. PLOS ONE 2017,**12**, e0173074.

7. **Wang Q, Liu S, Zhai A, Zhang B, Tian G**. AMPK-Mediated Regulation of Lipid Metabolism by Phosphorylation. Biol Pharm Bull 2018,**41**, 985–993.

8. **Zhu D, Zhang N, Zhou X, Zhang M, Liu Z, Liu X**. Cichoric acid regulates the hepatic glucose homeostasis via AMPK pathway and activates the antioxidant response in high glucose-induced hepatocyte injury. RSC Adv 2017, **7**, 1363–1375.

9. **Yuan HD, Kim DY, Quan HY, Kim SJ, Jung MS, Chung SH**. Ginsenoside Rg2 induces orphan nuclear receptor SHP gene expression and inactivates GSK3β via AMP-activated protein kinase to inhibit hepatic glucose production in HepG2 cells. Chem Biol Interact 2012, **195**, 35–42.

10. **Alam W, Rocca C, Khan H, Hussain Y, Aschner M, De Bartolo A, et al**. Current Status and Future Perspectives on Therapeutic Potential of Apigenin: Focus on Metabolic-Syndrome-Dependent Organ Dysfunction. Antioxidants 2021, **10**, 1643.

11. **Weyer C, Bogardus C, Mott DM, Pratley RE**. The natural history of insulin secretory dysfunction and insulin resistance in the pathogenesis of type 2 diabetes mellitus. J Clin Invest 1999, **104**, 787–794.

12. **Goldstein BJ**. Insulin resistance as the core defect in type 2 diabetes mellitus. Am J Cardiol 2002, **90**, 3–10.

13. **Fujimoto WY**. The importance of insulin resistance in the pathogenesis of type 2 diabetes mellitus. Am J Med 2000, **108**, 9–14.

14. **Saini V**. Molecular mechanisms of insulin resistance in type 2 diabetes mellitus. World J Diabetes 2010, **1**, 68.

15. **Whiteman EL, Cho H, Birnbaum MJ**. Role of Akt/protein kinase B in metabolism. Trends Endocrinol Metab 2002, **13**, 444–451.

16. **Samuel VT, Petersen KF, Shulman GI**. Lipid-induced insulin resistance: unravelling the mechanism. The Lancet 2010, **375**, 2267–2277.

17. **Han HS, Kang G, Kim JS, Choi BH, Koo SH**. Regulation of glucose metabolism from a liver-centric perspective. Exp Mol Med 2016, **48**, e218.

18. **Xuguang H, Aofei T, Tao L, Longyan Z, Weijian B, Jiao G**. Hesperidin ameliorates insulin resistance by regulating the IRS1-GLUT2 pathway via TLR4 in HepG2 cells. Phytother Res 2019, **33**, 1697–1705.

19. **Panche AN, Diwan AD, Chandra SR**. Flavonoids: an overview. J Nutr Sci 2016, **5**, e47.

20. **Perez-Vizcaino F, Fraga CG**. Research trends in flavonoids and health. Arch Biochem Biophys 2018, **646**, 107–112.

21. **Kim DS, Lim SB**. Extraction of flavanones from immature Citrus unshiu pomace: process optimization and antioxidant evaluation. Sci Rep 2020, **10**, 19950.

22. **Garg A, Garg S, Zaneveld LJD, Singla AK**. Chemistry and pharmacology of the citrus bioflavonoid hesperidin. Phytother Res 2001, **15**, 655–669.

23. **Jeon HJ, Seo MJ, Choi HS, Lee OH, Lee BY**. *Gelidium elegans* , an Edible Red Seaweed, and Hesperidin Inhibit Lipid Accumulation and Production of Reactive Oxygen Species and Reactive Nitrogen Species in 3T3-L1 and RAW264.7 Cells. Phytother Res 2014, **28**, 1701–1709.

24. **Yoshida H, Tsuhako R, Sugita C, Kurokawa M**. Glucosyl Hesperidin Has an Anti-diabetic Effect in High-Fat Diet-Induced Obese Mice. Biol Pharm Bull 2021, **44**, 422–430.

25. **Jung UJ, Lee MK, Jeong KS, Choi MS**. The Hypoglycemic Effects of Hesperidin and Naringin Are Partly Mediated by Hepatic Glucose-Regulating Enzymes in C57BL/KsJ-db/db Mice. J Nutr 2004, **134**, 2499–2503.

26. **Akiyama S, Katsumata S, Suzuki K, Ishimi Y, Wu J, Uehara M**. Dietary hesperidin exerts hypoglycemic and hypolipidemic effects in streptozotocin-induced marginal type 1 diabetic rats. J Clin Biochem Nutr 2010, **46**, 87-92.

27. **Amiot MJ, Riva C, Vinet A**. Effects of dietary polyphenols on metabolic syndrome features in humans: a systematic review. Obes Rev 2016, **17**, 573–586.

28. **Wang X, Hasegawa J, Kitamura Y, Wang Z, Matsuda A, Shinoda W, et al**. Effects of Hesperidin on the Progression of Hypercholesterolemia and Fatty Liver Induced by High-Cholesterol Diet in Rats. J Pharmacol Sci 2011, **117**, 129–138.

29. **Qurtam AA, Mechchate H, Es-safi I, Al-zharani M, Nasr FA, Noman OM, et al**. Citrus Flavanone Narirutin, In Vitro and In Silico Mechanistic Antidiabetic Potential. Pharmaceutics 2021, **13**, 1818.

30. **Park HY, Ha SK, Eom H, Choi I**. Narirutin fraction from citrus peels attenuates alcoholic liver disease in mice. Food Chem Toxicol 2013, **55**, 637–644.

31. **Lee YC, Cheng TH, Lee JS, Chen JH, Liao YC, Fong Y, et al**. Nobiletin, a citrus flavonoid, suppresses invasion and migration involving FAK/PI3K/Akt and small GTPase signals in human gastric adenocarcinoma AGS cells. Mol Cell Biochem 2011, **347**, 103–115.

32. **Kim YJ, Choi MS, Woo JT, Jeong MJ, Kim SR, Jung UJ**. Long-term dietary supplementation with low-dose nobiletin ameliorates hepatic steatosis, insulin

resistance, and inflammation without altering fat mass in diet-induced obesity. Mol Nutr Food Res 2017, **61**, 1600889.

33. **Lee YS, Cha BY, Saito K, Yamakawa H, Choi SS, Yamaguchi K, et al**. Nobiletin improves hyperglycemia and insulin resistance in obese diabetic ob/ob mice. Biochem Pharmacol 2010, **79**, 1674–1683.

34. **Han Jie L, Jantan I, Yusoff SD, Jalil J, Husain K**. Sinensetin: An Insight on Its Pharmacological Activities, Mechanisms of Action and Toxicity. Front Pharmacol 2021, **11**, 553404.

35. **Mohamed EA, Siddiqui MJ, Ang LF, et al**. Potent α-glucosidase and α-amylase inhibitory activities of standardized 50% ethanolic extracts and sinensetin from Orthosiphon stamineus Benth as anti-diabetic mechanism. BMC Complement Altern Med 2012, **12**, 176.

36. **Kang SI, Shin HS, Ko HC, Kim SJ**. Effects of Sinensetin on Lipid Metabolism in Mature 3T3-L1 Adipocytes. Phytother Res 2013, **27**, 131–134.

37. **Kang SI, Shin HS, Kim SJ**. Sinensetin Enhances Adipogenesis and Lipolysis by Increasing Cyclic Adenosine Monophosphate Levels in 3T3-L1 Adipocytes. Biol Pharm Bull 2015, **38**, 552–558.

38. **Vaiyapuri S, Ali MS, Moraes LA, Sage T, Lewis KR, Jones CI, et al**. Tangeretin Regulates Platelet Function Through Inhibition of Phosphoinositide 3-Kinase and Cyclic Nucleotide Signaling. Arterioscler Thromb Vasc Biol 2013, **33**, 2740–2749.

39. **Kim MS, Hur HJ, Kwon DY, Hwang JT**. Tangeretin stimulates glucose uptake via regulation of AMPK signaling pathways in C2C12 myotubes and improves glucose tolerance in high-fat diet-induced obese mice. Mol Cell Endocrinol 2012, **358**, 127–134.

40. **Sundaram R, Shanthi P, Sachdanandam P**. Effect of tangeretin, a polymethoxylated flavone on glucose metabolism in streptozotocin-induced diabetic rats. Phytomedicine 2014, **21**, 793–799.

41. **McConkey BJ, Sobolev V, Edelman M**. The performance of current methods in ligand–protein docking. Curr sci 2002, **10**, 845-856.

42. **Gohlke H, Klebe G**. Approaches to the Description and Prediction of the Binding Affinity of Small-Molecule Ligands to Macromolecular Receptors. Angew Chem Int Ed 2002, **41**, 2644–2676.

43. **Meng XY, Zhang HX, Mezei M, Cui M**. Molecular Docking: A Powerful Approach for Structure-Based Drug Discovery. Curr Comput Aided-Drug Des 2011, **7**, 146–157.

44. **McDermaid A, Monier B, Zhao J, Liu B, Ma Q**. Interpretation of differential gene expression results of RNA-seq data: review and integration. Brief Bioinform 2019, **20**, 2044–2054.

45. **Lamb J, Crawford ED, Peck D, Modell JW, Blat IC, Wrobel MJ, et al**. The Connectivity Map: Using Gene-Expression Signatures to Connect Small Molecules, Genes, and Disease. Science 2006, **313**, 1929–1935.

46. **Kukurba KR, Montgomery SB**. RNA Sequencing and Analysis. Cold Spring Harb Protoc 2015, **11**, 951-969.

47. **Liu X, Yang X, Chen X, Zhang Y, Pan X, Wang G, et al**. Expression Profiling Identifies Bezafibrate as Potential Therapeutic Drug for Lung Adenocarcinoma. J Cancer 2015, **6**, 1214–1221.

48. **Sirota M, Dudley JT, Kim J, Chiang AP, Morgan AA, Sweet-Cordero A, et al**. Discovery and Preclinical Validation of Drug Indications Using Compendia of Public Gene Expression Data. Sci Transl Med 2011, **3**, 96ra77.

49. **Piehler J**. New methodologies for measuring protein interactions in vivo and in vitro. Curr Opin Struct Biol 2005, **15**, 4–14.

50. **Jaeger S, Aloy P**. From protein interaction networks to novel therapeutic strategies. IUBMB Life 2012, **64**, 529–537.

51. **Yu D, Lim J, Wang X, Liang F, Xiao G**. Enhanced construction of gene regulatory networks using hub gene information. BMC Bioinformatics 2017, **18**, 186.

52. **Mahdi T, Hänzelmann S, Salehi A, Muhammed SJ, Reinbothe TM, Tang Y, et al**. Secreted Frizzled-Related Protein 4 Reduces Insulin Secretion and Is Overexpressed in Type 2 Diabetes. Cell Metab 2012, **16**, 625–633.

53. **Xin FJ, Wang J, Zhao RQ, Wang ZX, Wu JW**. Coordinated regulation of AMPK activity by multiple elements in the α-subunit. Cell Res 2013, **23**, 1237–1240.

54. **Ross FA, MacKintosh C, Hardie DG**. AMP-activated protein kinase: a cellular energy sensor that comes in 12 flavours. FEBS J 2016, **283**, 2987–3001.

55. **Yong Y, Shin SY, Jung Y, Jung H, Ahn S, Chong Y, et al**. Flavonoids activating adenosine monophosphate-activated protein kinase. J Korean Soc Appl Biol Chem 2015, **58**, 13–19.

56. **Yang Y, Wu Y, Zou J, Wang YH, Xu MX, Huang W, et al**. Naringenin Attenuates Non-Alcoholic Fatty Liver Disease by Enhancing Energy Expenditure and Regulating Autophagy via AMPK. Front Pharmacol 2021, **12**, 687095.

57. **Kim DS, Lim SB**. Extraction of flavanones from immature Citrus unshiu pomace: process optimization and antioxidant evaluation. Sci Rep 2020, **10**, 19950.

58. **Qi G, Guo R, Tian H, Li L, Liu H, Mi Y, et al**. Nobiletin protects against insulin resistance and disorders of lipid metabolism by reprogramming of circadian clock in hepatocytes. Biochim Biophys Acta BBA - Mol Cell Biol Lipids 2018, **1863**, 549–562.

59. **Su D, Liu H, Qi X, Dong L, Zhang R, Zhang J**. Citrus peel flavonoids improve lipid metabolism by inhibiting miR-33 and miR-122 expression in HepG2 cells. Biosci Biotechnol Biochem 2019, **83**, 1747–1755.

60. **Xiong H, Wang J, Ran Q, Lou G, Peng C, Gan Q, et al**. Hesperidin: A Therapeutic Agent For Obesity. Drug Des Devel Ther 2019, **13**, 3855–3866.

61. **Zhao NQ, Li XY, Wang L, Feng ZL, Li XF, Wen YF, et al**. Palmitate induces fat accumulation by activating C/EBPβ-mediated G0S2 expression in HepG2 cells. World J Gastroenterol 2017, **23**, 7705–7715.

62. **Malik SA, Acharya JD, Mehendale NK, Kamat SS, Ghaskadbi SS**. Pterostilbene reverses palmitic acid mediated insulin resistance in HepG2 cells by reducing oxidative stress and triglyceride accumulation. Free Radic Res 2019, **53**, 815–827.

63. **Liu JY, Zhang YC, Song LN, Zhang L, Yang FY, Zhu XR, et al**. Nifuroxazide ameliorates lipid and glucose metabolism in palmitate-induced HepG2 cells. RSC Adv 2019, **9**, 39394–39404.

64. **Kramer B, Rarey M, Lengauer T**. Evaluation of the FLEXX incremental construction algorithm for protein–ligand docking. Proteins 1999, **37**, 228-241.

65. **Su D, Liu H, Qi X, Dong L, Zhang R, Zhang J**. Citrus peel flavonoids improve lipid metabolism by inhibiting miR-33 and miR-122 expression in HepG2 cells. Biosci Biotechnol Biochem 2019, **83**, 1747–1755.

66. **Kim MS, Hur HJ, Kwon DY, Hwang JT**. Tangeretin stimulates glucose uptake via regulation of AMPK signaling pathways in C2C12 myotubes and improves glucose tolerance in high-fat diet-induced obese mice. Mol Cell Endocrinol 2012, **358**, 127–134.

67. **Kahn BB, Alquier T, Carling D, Hardie DG**. AMP-activated protein kinase: Ancient energy gauge provides clues to modern understanding of metabolism. Cell Metab 2005, **1**, 15–25.

68. **Carling D**. The AMP-activated protein kinase cascade – a unifying system for energy control. Trends Biochem Sci 2004, **29**, 18–24.

69. **Chen L, Duan Y, Wei H, Ning H, Bi C, Zhao Y, et al**. Acetyl-CoA carboxylase (ACC) as a therapeutic target for metabolic syndrome and recent developments in ACC1/2 inhibitors. Expert Opin Investig Drugs 2019, **28**, 917–930.

70. **Foretz M, Viollet B**. Activation of AMPK for a Break in Hepatic Lipid Accumulation and Circulating Cholesterol. EBioMedicine 2018, **31**, 15–16.

71. **Yuk T, Kim Y, Yang J, Sung J, Jeong HS, Lee J**. Nobiletin Inhibits Hepatic Lipogenesis via Activation of AMP-Activated Protein Kinase. Evid Based Complement Alternat Med 2018, **2018**, 1–8.

72. **Luo J, Yang H, Song BL**. Mechanisms and regulation of cholesterol homeostasis. Nat Rev Mol Cell Biol 2020, **21**, 225–245.

73. **Sakakura Y, Shimano H, Sone H, Takahashi A, Inoue K, Toyoshima H, et al**. Sterol Regulatory Element-Binding Proteins Induce an Entire Pathway of Cholesterol Synthesis. Biochem Biophys Res Commun 2001, **286**,176–183.

74. **Lu J, Meng Z, Cheng B, Liu M, Tao S, Guan S**. Apigenin reduces the excessive accumulation of lipids induced by palmitic acid via the AMPK signaling pathway in HepG2 cells. Exp Ther Med 2019, **18**, 2965-2971.

75. **Ha DT, Trung TN, Hien TT, Dao TT, Yim N, Ngoc TM, et al**. Selected compounds derived from Moutan Cortex stimulated glucose uptake and glycogen synthesis via AMPK activation in human HepG2 cells. J Ethnopharmacol 2010, **131**, 417–424.

76. **Zhu D, Zhang N, Zhou X, Zhang M, Liu Z, Liu X**. Cichoric acid regulates the hepatic glucose homeostasis via AMPK pathway and activates the antioxidant response in high glucose-induced hepatocyte injury. RSC Adv 2017, **7**, 1363–1375.

77. **Xiao B, Heath R, Saiu P, Leiper FC, Leone P, Jing C, et al**. Structural basis for AMP binding to mammalian AMP-activated protein kinase. Nature 2007, **449**, 496–500.

78. C**arling D, Mayer FV, Sanders MJ, Gamblin SJ**. AMP-activated protein kinase: nature's energy sensor. Nat Chem Biol 2011, **7**, 512–518.

79. **Jeon SM**. Regulation and function of AMPK in physiology and diseases. Exp Mol Med 2016, **48**, e245.

80. **Saltiel AR**. Insulin Signaling in the Control of Glucose and Lipid Homeostasis. Metabolic Control 2015, **1**, 51-71.

81. **Hay N**. Akt isoforms and glucose homeostasis – the leptin connection. Trends Endocrinol Metab 2011, **22**, 66–73.

82. **Samuel VT, Petersen KF, Shulman GI**. Lipid-induced insulin resistance: unravelling the mechanism. The Lancet 2010, **375**, 2267–2277.

83. **Han HS, Kang G, Kim JS, Choi BH, Koo SH**. Regulation of glucose metabolism from a liver-centric perspective. Exp Mol Med 2016, **48**, e218.

84. **Zhang Z, Liu H, Liu J**. Akt activation: A potential strategy to ameliorate insulin resistance. Diabetes Res Clin Pract 2019, **156**, 107092.

85. **Huang X, Liu G, Guo J, Su Z**. The PI3K/AKT pathway in obesity and type 2 diabetes. Int J Biol Sci 2018, **14**, 1483–1496.

86. **Qatanani M, Lazar MA**. Mechanisms of obesity-associated insulin resistance: many choices on the menu. Genes Dev 2007, **21**, 1443–1455.

87. **Wondmkun YT**. Obesity, Insulin Resistance, and Type 2 Diabetes: Associations and Therapeutic Implications. Diabetes Metab Syndr Obes Targets Ther 2020, **13**, 3611–3616.

88. **Saltiel AR, Kahn CR**. Insulin signalling and the regulation of glucose and lipid metabolism. Nature 2001, **414**, 799–806.

89. **Lee J young, Cho HK, Kwon YH**. Palmitate induces insulin resistance without significant intracellular triglyceride accumulation in HepG2 cells. Metabolism 2010, **59**, 927–934.

90. **Martyn JAJ, Kaneki M, Yasuhara S, Warner DS, Warner MA**. Obesity-induced Insulin Resistance and Hyperglycemia. Anesthesiology 2008, **109**, 137–148.

91. **Hajialyani M, Hosein Farzaei M, Echeverría J, Nabavi S, Uriarte E, Sobarzo-Sánchez E**. Hesperidin as a Neuroprotective Agent: A Review of Animal and Clinical Evidence. Molecules 2019, **24**, 648.

92. **Xiong H, Wang J, Ran Q, Lou G, Peng C, Gan Q, et al**. Hesperidin: A Therapeutic Agent For Obesity. Drug Des Devel Ther 2019, **13**, 3855–3866.

93. A**kiyama S, Katsumata S ichi, Suzuki K, Nakaya Y, Ishimi Y, Uehara M**. Hypoglycemic and Hypolipidemic Effects of Hesperidin and Cyclodextrin-Clathrated Hesperetin in Goto-Kakizaki Rats with Type 2 Diabetes. Biosci Biotechnol Biochem 2009, **73**, 2779–2782.

94. **Peng P, Jin J, Zou G, Sui Y, Han Y, Zhao D, et al**. Hesperidin prevents hyperglycemia in diabetic rats by activating the insulin receptor pathway. Exp Ther Med 2020, **21**, 53.

95. **Rajan P, Natraj P, Ranaweera SS, Dayarathne LA, Lee YJ, Han CH**. Anti-adipogenic effect of the flavonoids through the activation of AMPK in palmitate (PA)-treated HepG2 cells. J Vet Sci 2022, **23**, e4.

96. **Dayarathne LA, Ranaweera SS, Natraj P, Rajan P, Lee YJ, Han CH**. The effects of naringenin and naringin on the glucose uptake and AMPK phosphorylation in high glucose treated HepG2 cells. J Vet Sci 2021, **22**, e92.

97. **Dayarathne LA, Ranaweera SS, Natraj P, Rajan P, Lee YJ, Han CH**. Restoration of the adipogenic gene expression by naringenin and naringin in 3T3-L1 adipocytes. J Vet Sci 2021, **22**, e55.

98. **Ranaweera SS, Dissanayake CY, Natraj P, Lee YJ, Han CH**. Anti-inflammatory effect of sulforaphane on LPS-stimulated RAW 264.7 cells and ob/ob mice. J Vet Sci 2020, **21**, e91.

99. **Ranaweera SS, Natraj P, Rajan P, Dayarathne LA, Mihindukulasooriya SP, Dinh DTT, et al**. Anti-obesity effect of sulforaphane in broccoli leaf extract on 3T3-L1 adipocytes and ob/ob mice. J Nutr Biochem 2022, **100**, 108885.

100. **Langmead B, Salzberg SL**. Fast gapped-read alignment with Bowtie 2. Nat Methods 2012, **9**, 357-359.

101. **Gentleman RC, Carey VJ, Bates DM, et al**. Bioconductor: open software development for computational biology and bioinformatics. Genome Biol 2004, **5**, R80.

102. **Rojas JM, Schwartz MW**. Control of hepatic glucose metabolism by islet and brain. Diabetes Obes Metab 2014, **16**, 33–40.

103. **Karim S**. Hepatic expression and cellular distribution of the glucose transporter family. World J Gastroenterol 2012, **18**, 6771.

104. **Xuguang H, Aofei T, Tao L, Longyan Z, Weijian B, Jiao G**. Hesperidin ameliorates insulin resistance by regulating the IRS1-GLUT2 pathway via TLR4 in HepG2 cells. Phytother Res 2019, **33**, 1697–1705.

105. **Ždychová J, Komers R**. Emerging Role of Akt Kinase/Protein Kinase B Signaling in Pathophysiology of Diabetes and Its Complications. Physiol Res 2005, **54**, 16.

106. **Mackenzie R, Elliott B**. Akt/PKB activation and insulin signaling: a novel insulin signaling pathway in the treatment of type 2 diabetes. Diabetes Metab Syndr Obes Targets Ther 2014, **7**, 55-64.

107. **Qi G, Guo R, Tian H, Li L, Liu H, Mi Y, et al**. Nobiletin protects against insulin resistance and disorders of lipid metabolism by reprogramming of circadian clock in hepatocytes. Biochim Biophys Acta BBA - Mol Cell Biol Lipids 2018, **1863**, 549–562.

108. **Huang H, Tang S, Ji M, Tang Z, Shimada M, Liu X, et al**. p300-Mediated Lysine 2-Hydroxyisobutyrylation Regulates Glycolysis. Mol Cell 2018, **70**, 663-678.

109. **Cho H, Um J, Lee JH, Kim WH, Kang WS, Kim SH, et al**. ENOblock, a unique small molecule inhibitor of the non-glycolytic functions of enolase, alleviates the symptoms of type 2 diabetes. Sci Rep 2017, **7**, 44186.

110. **Durand CA, Richer MJ, Brenker K, Graves M, Shanina I, Choi K, et al**. Selective pharmacological inhibition of phosphoinositide 3-kinase p110delta opposes the progression of autoimmune diabetes in non-obese diabetic (NOD) mice. Autoimmunity 2013, **46**, 62–73.

111. **Zhai X, Qian G, Wang Y, Chen X, Lu J, Zhang Y, et al**. Elevated B Cell Activation is Associated with Type 2 Diabetes Development in Obese Subjects. Cell Physiol Biochem 2016, **38**, 1257–1266.

112. **Rabbani N, Thornalley PJ**. Hexokinase-2 Glycolytic Overload in Diabetes and Ischemia–Reperfusion Injury. Trends Endocrinol Metab 2019, **30**, 419–431.

113. **Simoneau JA, Kelley DE**. Altered glycolytic and oxidative capacities of skeletal muscle contribute to insulin resistance in NIDDM. J Appl Physiol 1997, **83**, 166–171.

114. **Du K, Herzig S, Kulkarni RN, Montminy M**. TRB3: A *tribbles* Homolog That Inhibits Akt/PKB Activation by Insulin in Liver. Science 2003, **300**, 1574–1577.

115. **Riu E, Ferre T, Hidalgo A, Mas A, Franckhauser S, Otaegui P, et al**. Overexpression of c *-myc* in the liver prevents obesity and insulin resistance. FASEB J 2003, **17**, 1715–1717.

116. **Peterson C W**. An extended Myc network contributes to glucose homeostasis in cancer and diabetes. Front Biosci 2011, **16**, 2206.

117. **Tessari P, Cecchet D, Cosma A, Vettore M, Coracina A, Millioni R, et al**. Nitric Oxide Synthesis Is Reduced in Subjects With Type 2 Diabetes and Nephropathy. Diabetes 2010, **59**, 2152–2159.

118. **Bahadoran Z, Mirmiran P, Ghasemi A**. Role of Nitric Oxide in Insulin Secretion and Glucose Metabolism. Trends Endocrinol Metab 2020, **31**, 118–130.

119. **Tian L, Nikolic-Paterson DJ, Tesch GH**. Establishing equivalent diabetes in male and female Nos3-deficient mice results in a comparable onset of diabetic kidney injury. Physiol Rep 2019, **7**, e14197.

120. B**esse-Patin A, Jeromson S, Levesque-Damphousse P, Secco B, Laplante M, Estall JL**. PGC1A regulates the IRS1:IRS2 ratio during fasting to influence hepatic metabolism downstream of insulin. Proc Natl Acad Sci 2019, **116**, 4285–4290.

121. **Gillberg L, Jacobsen S, Ribel-Madsen R, Gjesing AP, Boesgaard TW, Ling C, et al**. Does DNA Methylation of PPARGC1A Influence Insulin Action in First Degree Relatives of Patients with Type 2 Diabetes? PLoS ONE 2013, **8**, e58384.

122. **Boughanem H, Yubero-Serrano EM, López-Miranda J, Tinahones FJ, Macias-Gonzalez M**. Potential Role of Insulin Growth-Factor-Binding Protein 2 as Therapeutic Target for Obesity-Related Insulin Resistance. Int J Mol Sci 2021, **22**, 1133.

123. **Irshad Z, Xue M, Ashour A, Larkin JR, Thornalley PJ, Rabbani N**. Activation of the unfolded protein response in high glucose treated endothelial cells is mediated by methylglyoxal. Sci Rep 2019, **9**, 7889.

124. **Gossellin J, Wren JA, Sunderland SJ**. Canine obesity ? an overview. J Vet Pharmacol Ther 2007, **30**, 1–10.

125. **Cruz PMR, Mo H, McConathy WJ, Sabnis N, Lacko AG**. The role of cholesterol metabolism and cholesterol transport in carcinogenesis: a review of scientific findings, relevant to future cancer therapeutics. Front Pharmacol 2013, **4**, 119.

126. **Kersten S**. Mechanisms of nutritional and hormonal regulation of lipogenesis. EMBO Rep 2001, **2**, 282–286.

127. **Mc Auley MT**. Effects of obesity on cholesterol metabolism and its implications for healthy ageing. Nutr Res Rev 2020, **33**, 121–133.

128. **Nakajima VM, Macedo GA, Macedo JA**. Citrus bioactive phenolics: Role in the obesity treatment. LWT - Food Sci Technol 2014, **59**, 1205–1212.

129. **Abad-García B, Garmón-Lobato S, Sánchez-Ilárduya MB, Berrueta LA, Gallo B, Vicente F, et al**. Polyphenolic contents in Citrus fruit juices: authenticity assessment. Eur Food Res Technol 2014, **238**, 803–818.

130. **Kim DS, Lim SB**. Extraction of flavanones from immature Citrus unshiu pomace: process optimization and antioxidant evaluation. Sci Rep 2020, **10**, 19950.

131. **Kim JH, Kim MY**. Phytochemical and antioxidant characterization of thinned immature citrus unshiu fruits. Int J Pharm Pharm Sci 2017, **9**, 293.

132. P**arhiz H, Roohbakhsh A, Soltani F, Rezaee R, Iranshahi M**. Antioxidant and Anti-Inflammatory Properties of the Citrus Flavonoids Hesperidin and Hesperetin: An Updated Review of their Molecular Mechanisms and Experimental Models. Phytother Res 2015, **29**, 323–331.

133. **Yoshida H, Tsuhako R, Sugita C, Kurokawa M**. Glucosyl Hesperidin Has an Anti-diabetic Effect in High-Fat Diet-Induced Obese Mice. Biol Pharm Bull 2021, **44**, 422–430.

134. **Xiong H, Wang J, Ran Q, Lou G, Peng C, Gan Q, et al**. Hesperidin: A Therapeutic Agent For Obesity. Drug Des Devel Ther 2019, **13**, 3855–3866.

135. **Goto T, Teraminami A, Lee JY, Ohyama K, Funakoshi K, Kim YI, et al**. Tiliroside, a glycosidic flavonoid, ameliorates obesity-induced metabolic disorders via activation of adiponectin signaling followed by enhancement of fatty acid oxidation in liver and skeletal muscle in obese–diabetic mice. J Nutr Biochem 2012, **23**, 768–776.

136. **Bell ZW, Canale RE, Bloomer RJ**. A dual investigation of the effect of dietary supplementation with licorice flavonoid oil on anthropometric and biochemical markers of health and adiposity. Lipids Health Dis 2011, **10**, 29.

137. **Knab AM, Shanely RA, Jin F, Austin MD, Sha W, Nieman DC**. Quercetin with vitamin C and niacin does not affect body mass or composition. Appl Physiol Nutr Metab 2011, **36**, 331–338.

138. **Ramchoun M, Khouya T, Harnafi H, Alem C, Benlyas M, Simmet T, et al**. Effect of polyphenol, flavonoid, and saponin fractions from Thymus atlanticus on acute and chronic hyperlipidemia in mice. Future J Pharm Sci 2020, **6**, 69.

139. **Morrow NM, Burke AC, Samsoondar JP, Seigel KE, Wang A, Telford DE, et al**. The citrus flavonoid nobiletin confers protection from metabolic dysregulation in high-fat-fed mice independent of AMPK. J Lipid Res 2020, **61**, 387–402.

140. **Rand JS**. Diabetes Mellitus in Dogs and Cats. Clinical Small Animal Internal Medicine 2020, **30**, 93–102.

141. **Peng P, Jin J, Zou G, Sui Y, Han Y, Zhao D, et al**. Hesperidin prevents hyperglycemia in diabetic rats by activating the insulin receptor pathway. Exp Ther Med 2020, **21**, 53.

142. **Center SA**. Interpretation of Liver Enzymes. Vet Clin North Am Small Anim Pract 2007, **37**, 297–333.

143. **Rothuizen J, van den Brom WE, Fevery J**. The origins and kinetics of bilirubin in dogs with hepatobiliary and haemolytic diseases. J Hepatol 1992, **15**, 17-24.

144. **Baum N, Dichoso CC, Carlton CE**. Blood urea nitrogen and serum creatinine. Physiology and interpretations. Urology 1975, **5**, 583-588.

145. **Pardo-Marín L, Martínez-Subiela S, Pastor J, Tvarijonaviciute A, Garcia-Martinez JD, Segarra S, et al**. Evaluation of various biomarkers for kidney monitoring during canine leishmaniosis treatment. BMC Vet Res 2016, **13**, 31.

146. **Kim J, Lee CM, Kim HJ**. Biomarkers for chronic kidney disease in dogs: a comparison study. J Vet Med Sci 2020, **82**, 1130–1137.

147. **Lippi I, Guidi G, Marchetti V, Tognetti R, Meucci V**. Prognostic role of the product of serum calcium and phosphorus concentrations in dogs with chronic kidney disease: 31 cases (2008–2010). J Am Vet Med Assoc 2014, **245**, 1135–1140.

148. **Felsenfeld AJ, Levine BS, Rodriguez M**. Pathophysiology of Calcium, Phosphorus, and Magnesium Dysregulation in Chronic Kidney Disease. Semin Dial 2015, **28**, 564–577.

149. **Eddine RD**. Analytical Study of Pancreatitis in Dogs. J Dairy Vet Sci 2018, **6**, 2.

150. **Date K, Satoh A, Iida K, Ogawa H**. Pancreatic α-Amylase Controls Glucose Assimilation by Duodenal Retrieval through N-Glycan-specific Binding, Endocytosis, and Degradation. J Biol Chem 2015, **290**, 17439–17450.

151. **Keenan CM, Hendricks LD, Lightner L, Webster HK, Johnson AJ**. Visceral Leishmaniasis in the German Shepherd Dog. Vet Pathol 1984, **21**, 74–79.

Acknowledgements

First and foremost, I would like to thank the God, the Almighty, for his showers of blessings throughout my research work to complete the research successfully.

I would like to express my deep and sincere gratitude to my research advisor, Prof. Chang-Hoon Han for all of his guidance and wisdom throughout my PhD study, from inception to completion, as well as his incredible and unwavering patience in working with me over the past four years. He gives me a lifetime unforgettable memory of his benevolence, patience, intelligence, diligence, and erudition.

I would also like to thank and acknowledge my thesis committee members, Prof. Young Jae Lee, Prof. Jae Hoon Kim, Prof. Se Jae Kim, and Prof. Chang-Hwan Ahn for investing time and providing interesting and valuable feedbacks. I feel proud and honored that you have accepted to be on my committee.

This thesis and project would not have been possible without the funding support from Ministry of Agriculture, Food and Rural Affairs (MAFRA) and Vetcom Korea. I would like to extend my sincere thanks to the CEO of Vetcom Korea, Mr. Chan Soo Kim for funding my research.

I would like to thank my current and former lab members Mrs. Gyung Hye Yang, Mrs. Sachithra, Miss. Lakshi, Mr. Kyung-Jun, and Mr. Sang-Jae for their valuable suggestions, constructive criticism, and word of encouragement at all times during my research in Veterinary Biochemistry Lab. I am also grateful to my friends in JNU for their moral support during the study.

I will forever be indebted to my parents, Mr. K. T. Rajan Babu and Mrs. R. Kasthuri Rajan, my brother Mr. R. Tharun Prakash as well as my in-laws for the endless love and

constant support they have given me throughout this journey. Thanks should also go to my best friends for their positive distraction and motivation to complete this thesis.

Finally, words cannot express my gratitude to my husband (who is also my lab senior), Mr. N. Premkumar for supporting my dream. Without his continued support, encouragement, and love I would not be where I am today. The last word goes for my baby boy, Chris Raziel who has given me the extra strength and motivation to get things done. Thank you for your patience on the evenings when playtimes were missed because I had to work in lab.

I thank all who in one way or another contributed in the completion of this thesis. I could not have completed this thesis without the support of you all. Thanks for everything that helped me get to this day.